Environmental Research 236 (2023) 116850

Contents lists available at ScienceDirect

Environmental Research

journal homepage: www.elsevier.com/locate/envres

Drug permeation enhancement, efficacy, and safety assessment of azelaic acid loaded SNEDDS hydrogel to overcome the treatment barriers of atopic dermatitis

Neha Parveen [a], Afsana Sheikh [a], Nagashekhara Molugulu [b], Sivakumar Annadurai [c], Shadma Wahab [c], Prashant Kesharwani [a,d,*,1]

[a] Department of Pharmaceutics, School of Pharmaceutical Education and Research, Jamia Hamdard, New Delhi, 110062, India
[b] School of Pharmacy, Monash University, Bandar Sunway, Jalan Lagoon Selatan, 47500, Malaysia
[c] Department of Pharmacognosy, College of Pharmacy, King Khalid University, Abha, 62529, Saudi Arabia
[d] Department of Pharmacology, Saveetha Dental College, Saveetha Institute of Medical and Technical Sciences, Saveetha University, Chennai, India

ARTICLE INFO

Keywords:
Atopic dermatitis
Azelaic acid
Inflammation
Topical delivery
Snedds
Nanomedicine
Skin permeation

ABSTRACT

Atopic dermatitis is one of the most widespread chronic inflammatory skin conditions that can occur at any age, though the prevalence is highest in children. The purpose of the current study was to prepare and optimize the azelaic acid (AzA) loaded SNEDDS using Pseudo ternary phase diagram, which was subsequently incorporated into the Carbopol 940 hydrogel for the treatment of atopic dermatitis. The composition was evaluated for size, entrapment efficiency, *in vitro*, *ex vivo*, and *in vivo* studies. The polydispersity index of the optimized preparation was found to be less than 0.5, and the size of the distributed globules was found to be 151.20 ± 3.67 nm. The SNEDDS hydrogel was characterized for pH, viscosity, spreadability, and texture analysis. When compared to the marketed formulation, SNEDDS hydrogel was found to have a higher rate of permeation through the rat skin. In addition, a skin irritation test carried out on experimental animals showed that the SNEDDS formulation did not exhibit any erythematous symptoms after a 24-h exposure. In conclusion, the topical delivery of AzA through the skin using SNEDDS hydrogel could prove to be an effective approach for the treatment of atopic dermatitis.

1. Introduction

Atopic dermatitis (AD), commonly known as atopic eczema, is a chronic inflammatory skin disease marked by severe itching and recurring eczematous lesions (Cláudia Paiva-Santos et al., 2022). It is one of the most widespread chronic inflammatory skin conditions that can occur at any age, though the prevalence is highest in children (Akhtar et al., 2017). In developed nations, there is a 20% chance that someone will acquire AD at some point (Souto et al., 2019). Specifically, it appears to be more prevalent in women during adolescence or maturity (Zhuo et al., 2018). Although the pathological mechanism of the disease is not completely known, it seems to be a consequence of an intricate relationship between immune dysregulation and skin barrier dysfunction, exhibiting underlying infectious, environmental, and genetic factors (Silverberg, 2020). With a wide range of clinical features, including various lesions morphologies, and a pattern of distribution that changes depending on the patient's age (Zhang et al., 2022), AD is known to be an extremely heterogeneous disease (Hu et al., 2021). Patients with AD frequently experience skin pain, xerosis, and sleep problems, which significantly reduce their quality of life. In addition, it has a strong correlation with non-atopic comorbid conditions, specifically mental health issues like anxiety and melancholy, as well as other atopic comorbidities like allergic rhinitis and asthma (Pople and Singh, 2010). Adopting non-pharmacological measures, such as avoiding contact with allergens that cause disease, everyday skincare, and routine bathing, is crucial when considering disease prevention. AD treatment calls for a multistep strategy with various interventions aimed at enhancing the skin barrier and minimizing inflammation (Zheng et al., 2022).

The skin barrier is repaired as part of AD therapy, along with itch control, inflammation reduction, and infection prevention or reduction (Damiani et al., 2019; Hasan et al., 2023; Jain et al., 2022; Kaur and

* Corresponding author. Department of Pharmaceutics, School of Pharmaceutical Education and Research, Jamia Hamdard, New Delhi, India, 110062.
E-mail address: prashantdops@gmail.com (P. Kesharwani).
[1] https://scholar.google.co.in/citations?user=DJkvOAQAAAAJ&hl=en.

https://doi.org/10.1016/j.envres.2023.116850
Received 10 June 2023; Received in revised form 4 August 2023; Accepted 6 August 2023
Available online 7 August 2023
0013-9351/© 2023 Published by Elsevier Inc.

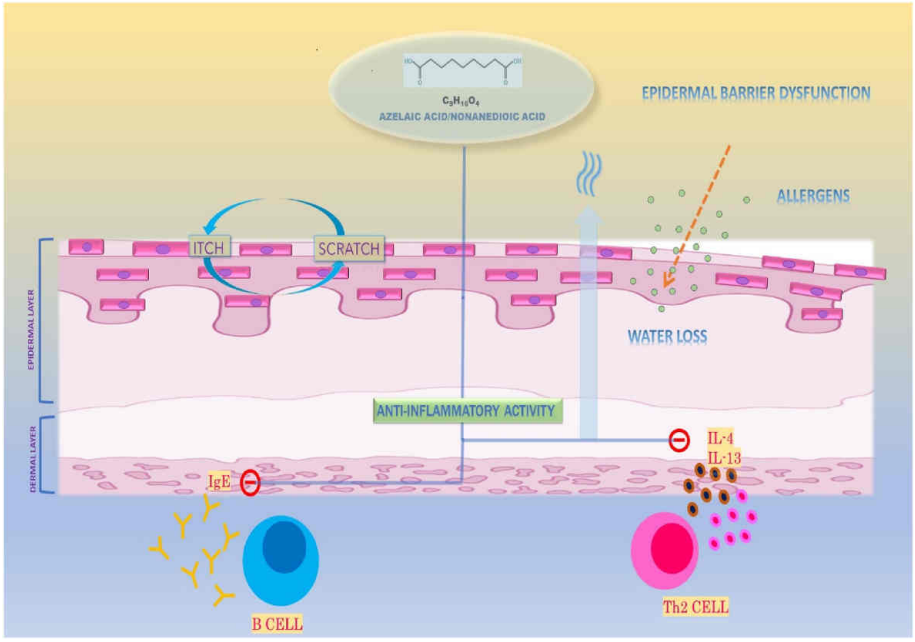

Fig. 1. Schematic diagram of the mechanism of action of Azelaic Acid in treating Atopic Dermatitis.

Kesharwani, 2021; Kumari et al., 2022; Tiwari et al., 2023; Zeng et al., 2023). Thus, in addition to anti-inflammatory treatments such as glucocorticoids and topical calcineurin inhibitors, people with AD needed topical therapy with emollients to provide moisturizing and soothing effects. Systemic therapy using mycophenolate mofetil, azathioprine, cyclosporine A, and glucocorticoids may be necessary for severe instances (Schäkel et al., 2014). But systemic therapy has limited efficacy and causes severe side effects in many patients, whose symptoms frequently return after treatment is stopped (Boguniewicz et al., 2017). Lotions, ointments, and creams used in traditional topical therapies have a restricted penetration depth into the skin (Akhtar et al., 2017). To address AD more effectively, there is a need for innovative topical formulations that penetrate deeply into the epidermis (Try et al., 2016).

Nanotechnology has numerous uses in several skin diseases, including creating drug-loaded nanostructured materials such as nanoparticles and nanoemulsions (Chandra et al., 2023; Kesharwani et al., 2023a; Mohammadpour et al., 2023; Qin et al., 2023). Due to their distinctive physicochemical features, nanostructured materials have attracted significant research in a variety of fields (Ahamed et al., 2023; Aziz Hazari et al., 2023; Dongsar et al., 2023; Karimi-Maleh et al., 2022; Kesharwani et al., 2014, 2023b; Parveen et al., 2023a, 2023b). The delivery of drugs to particular cell types is increasingly accomplished using nanoparticles as a carrier (Nodehi et al., 2021). Drugs could be incorporated into a nanoformulation as an approach to facilitating topical application and enhancing drug penetration into the epidermis. Self-nano emulsifying drug delivery systems (SNEDDS) are isotropic mixtures of nanoformulation of an active drug in a blend of hydrophilic solubilizers/co-solvent, surfactants, and lipids that spontaneously form ultrafine emulsions in the aqueous phase (usually less than 200 nm in size) after gentle agitation (Kazi et al., 2023). High lipophilic chemical solubilizing ability, thermodynamic stability, simplicity of fabrication, and attractive look are all characteristics of SNEDDS (van Staden et al., 2020). It has been demonstrated that they improve the skin's ability to absorb lipophilic compounds like azelaic acid and curcumin (Khan et al., 2019). When a SNEDDS is applied externally, an aqueous phase that is already present at the skin's surface as a result of trans-epidermal water loss or sweat secretion may be diluted, resulting in an occlusive dermal formulation with a potent thermodynamic force that allow for topical drug delivery system. ("Self-microemulsifying and microemulsion systems for transdermal delivery of indomethacin: Effect of phase transition - ScienceDirect," n.d.). The highly lipophilic drugs can be delivered into the skin using the SNEDDS method to specifically target melanocytes in the epidermis basal layer, fibroblasts in the dermis, and UV-induced inflammation mechanisms that take place in the dermis and epidermal layers (Imokawa et al., 2015). The exclusion of aqueous phase during assembling and storing decreases the chance that dissolved oxygen in an emulsion's aqueous phase will harm drugs, which suggests that SNEDDS may have benefits for drug stability.

Azelaic acid (AzA), also known as nonanedioic acid or 1,7 heptane dicarboxylic acid, is a naturally discovered, saturated, straight-chained dicarboxylic acid that is efficacious for topical therapy of several skin diseases that are associated with abnormal or hyperactive melanocyte function, including erythema, itching, inflammation (Dall'Oglio et al., 2021), lentigo maligna (Kasprzak and Xu, 2015), rosacea (Thiboutot, 2008), and photochemical and physical hyperpigmentation (Fitton and Goa, 1991). AzA also exhibits antiproliferative and cytotoxic actions against cancerous melanocytes both *in vivo* and *in vitro*, as well as on tumor cells without tyrosinase (Fitton and Goa, 1991). AzA appears to help AD, but the exact cause is unclear ("Azelaic Acid: Evidence-based Update on Mechanism of Action and Clinical Application - JDDonline - Journal of Drugs in Dermatology," n.d.). AzA may influence the microflora directly or by changing the composition of skin secretions if microorganisms are a factor in the etiology of AD (Takiwaki et al., 2003). Additionally, research conducted *ex vivo* and *in vitro* suggests that AzA may have a specific anti-inflammatory impact by preventing neutrophils from producing or releasing proinflammatory reactive oxygen species (Summarized in Fig. 1) (Akamatsu et al., 1991). AzA's anti-inflammatory and antibacterial properties may therefore help reduce inflammatory sores and erythema in AD and rosacea (Passi et al., 1991). The effectiveness of 20% AzA cream formulation in treating dermatitis (erythema, itching, and inflammation) has been demonstrated, but the therapeutic benefits may not become apparent for up to 4 weeks after application. The patient should maintain treatment for at least 6 months (NGUYEN and BUI, 1995). Following topical administration of 1 g of 20% AzA cream, a plasma concentration of 0.038 g/mL and a percutaneous absorption of about 3% were calculated. Consequently, poor dermal penetration reduces its therapeutic efficacy (Bladon et al., 1986). AzA has a pilosebaceous unit as its site of action, and its buildup in this region can enhance the therapy of AD. Because of its poor solubility in water, which is approximately 2.4 mg/ml at 25 °C, and

restricted permeation throughout the outermost skin layer several nanoformulations have been suggested to improve the permeability and solubility of AzA via the stratum corneum and to decrease the quantity of drug utilized in the preparations (Schaller et al., 2016). The selection of a suitable dosage form in the pharmaceutical industry is affected by different types of factors, such as manufacturing method, patient compliance, cost, and therapeutic effect. To create adequate formulations, selecting suitable excipients and ingredients is a vital first step (Aytekin et al., 2013). The self-nanoemulsifying drug delivery system (SNEDDS) is an intriguing nanocarrier for the topical administration of hydrophobic therapeutic substances (Pratiwi et al., 2017). The composition is uncomplicated, containing merely the water phase, the oil phase, cosurfactant, and surfactants, and it is simple to produce a homogenous fine oil-in-water SNEDDS formulation. The formulation is less greasy and simple to remove from the applied areas because the continuous phase is water. As a result, O/W SNEDDS formulation was investigated in this research as a drug carrier to concurrently improve AzA solubilization and skin permeability (Ponto et al., 2021). Azelaic Acid can cause hypopigmentation, burning, tingling, stinging, etc, but these effects are overcome by loading the drug into the Carbopol 940 hydrogel. SNEDDS do not inherently possess any properties that are harmful to the human body. Their administration does not elicit any adverse reactions. As Azelaic Acid has anti-inflammatory and anti-bacterial activity, it is used to treat a number of skin conditions. It does not have any contraindications.

Hydrogels are 3D networks that can absorb a huge quantity of water and swell in the presence of water due to hydrophilic groups such as $–SO_3H$, –CONH, $–CONH_2$, –OH, –COOH, and -NH2 (Cong and Fu, 2022). Its network is often made up of crosslinked polymer chains, though occasionally crosslinked colloidal clusters can also form this network (Xu et al., 2022). Because of their capacity to absorb water, they can be soft and flexible. The hydrogels can be created by physically or chemically crosslinking natural or synthetic polymer strands. Hydrogels closely mimic live tissue due to their high-water content, supple shape, and porosity (Huang et al., 2022). Carbopol is a polymer made of acrylic. Carbopol is suitable for hydrogel preparations because it is non-irritating and non-toxic (Song et al., 2022). In hydrogel preparations, Carbopol 940 is frequently employed as a gelling agent. To create a high-quality gel preparation, Carbopol 940 concentration must be taken into consideration (Safitri et al., 2021). It was shown that Carbopol 940 hydrogel could perhaps be used to treat skin inflammation. Carbopol 940 hydrogel is known for its anti-inflammatory properties and hence can be used in the treatment of skin diseases that cause inflammation like psoriasis, rosacea, full-thickness wound, etc (Song et al., 2022).

Therefore, the current research endeavored to develop and optimize AzA-loaded SNEDDS hydrogel to enhance effectiveness against AD by increasing permeability and solubility across the skin barrier. Consequently, is predicted that the finished SNEDDS hydrogel of AzA would offer a better anti-inflammatory effect. Pseudo ternary phase diagram was utilized in order to optimize and characterize the creation of SNEDDS formulation. To further demonstrate the supremacy of AzA-loaded SNEDDS hydrogel over commercial preparation, experiments on skin irritability and permeation across rat skin were performed.

2. Materials and methods

2.1. Materials

AzA was procured from Sigma-Aldrich, Bangalore, India. Tween 80, Acetonitrile, Tween 20Propylene, PEG 200, PEG 400, Methanol, and Ethanol were bought from SD fine chemicals limited, Mumbai, India. Labrasol, Kolliphor RH40, Kolliphor EL, and Lauroglycol were procured from Loba Chemie Private Limited, Mumbai, India.

2.2. Formulation development and characterization of SNEDDS formulation

2.2.1. Screening of excipients

2.2.1.1. Screening and selection of oil. The solubility of AzA in several oils (Transcutol-P, oleic acid, castor oil, labrasol, capryol 90, isopropyl myristate, and olive oil) was assessed by putting excessive quantities of the drug separately in 1 ml oils in vials. To achieve proper mixing, the vials were firmly closed and mechanically shaken constantly for 72 h at 25.0 ± 0.5 °C. A high-speed centrifuge was used to centrifuge the mixture for 30 min after 72 h at 12,000 rpm. Using a UV spectrophotometer, the supernatant was separated and diluted with methanol (because it was used as a blank), and the absorbance was measured in triplicate at λ_{max} 213 nm for AzA (Date and Nagarsenker, 2007).

2.2.1.2. Screening and selection of surfactant. The emulsifying power of different surfactants in the chosen oily phase was tested, including Tween 80, Tween 40, Tween 20, Cremophor S9, and Cremophor RH 40. The degree of clarity and simplicity of emulsification were taken into account when selecting the surfactant. Briefly, 500 μL of the chosen oil and 500 μL of each surfactant were mixed. For optimal homogeneity, the mixes were gradually heated for 2 min at 50 °C. Each mixture was subsequently mixed with distilled water up to a maximum of 50 mL in a flask with a glass stopper. The stoppered flasks were repeatedly inverted to determine how many inversions were necessary to create homogenous nanoemulsions (devoid of phase separation turbidity). The generated emulsions were additionally left to remain for 2 h while the percentage transmittance was measured at 650 nm (using a UV–Vis Spectrophotometer) with distilled water as the control. For each emulsion, the transmittance percentage has been determined three times, and the average values and standard deviation were computed. The transparent emulsion with minimal inversions and a larger percentage of transmittance was created by the surfactant that was selected (Patel and Vavia, 2007).

2.2.1.3. Screening and selection of Co-surfactant. The chosen surfactant and oily phase were utilized to subsequently test the effectiveness of emulsification of the various cosurfactants (PEG 400, Propylene glycol, PEG 600, PEG 200, and Glycerol). Preliminary screening of surfactants was used to generate and assess mixtures of cosurfactant, surfactant, and oil at volumes of 200 μL, 400 μL, and 600 μL respectively (Bahadur et al., 2020).

2.2.1.4. Construction of pseudoternary phase diagram. A pseudo-ternary phase diagram was built at ambient temperature utilizing a water titration approach to ascertain the component concentrations for the current spectrum of the SNEDDS (Shafiq et al., 2007). For phase experiments, cosurfactant, surfactant, and oil were grouped in various ways. Each group received a different weight ratio (1:1, 2:1, 3:1, and 4:1) of surfactant and cosurfactant (Smix). These Smix ratios were set to increase surfactant concentration relative to co-surfactant. For each phase diagram, the oil and a certain Smix ratio were fully mixed in several glass vials at various weight ratios (9:1, 8:2, 7:3, 6:4, 5:5, 4:6, 3:7, 2:8, and 1:9). To properly define the limits of each phase, several oil and Smix ratios were created (Atef and Belmonte, 2008). To achieve an aqueous phase concentration of 5%–95% of the total, the amount of water phase was increased by 5%. The vial mixtures had been vortexed for 2 min before being allowed to equilibrate after each addition of the aqueous phase. The three-component ternary phase diagram, in which the water, Smix, and oil were each represented by one axis, was used to visually examine and mark the shift from transparent to turbid and vice versa in terms of physical conditions. The software Tri Draw was used to draw the various phase diagrams.

2.2.2. Preparation of drug-loaded SNEDDS formulation

According to Hong et al.'s method, the SNEDDS was developed utilizing a spontaneous emulsification technique and high-energy input (Hong et al., 2017). SNEDDS formulations were created with the necessary component ratios after the self-nano emulsifying region was found. Using pseudo ternary phase diagrams, the ratio of surfactant to cosurfactant (Smix) was also optimized. In a nutshell, 4 ml of surfactant was mixed with 3 mg of AzA using magnetic stirring at a speed of 1000 rpm for 10 min. The mixture was then thoroughly mixed in 1 ml of the oil phase while being magnetically stirred for 10 min at 1000 rpm. This mixture was then mixed with 1 ml of co-surfactant utilizing magnetic stirring for 10 min, followed by 1 h at room temperature of sonication in a water bath. The preliminary AzA solubility analysis of each vehicle component served as the basis for the formulation vehicle addition sequence. The system was then filled with distilled water drop by drop until the self-nanoemulsions were created. There were numerous further tests conducted utilizing various concentrations of oil, surfactant, and different sonication time settings. The resulting SNEDDS formulations were put through evaluation testing.

2.2.3. Characterization of AzA-loaded SNEDDS formulation

2.2.3.1. Particle size and polydispersity index (PDI). Droplet size is a significant component in self-emulsification efficiency because it affects the degree and rate of drug release. One mL of each SNEDDS formulation was neutralized with distilled water ten times before measurement. Dynamic light scattering (DLS) was employed to determine the polydispersity index and particle size of the synthesized nanoemulsions using a photon correlation spectrometer (Zetasizer, Malvern Instruments LTD, Malvern, UK), which examines variations in the dispersion of light caused by particles of Brownian motion. At 25 °C and a 90° scattering angle, light scattering was observed ("(Chudasama et al.,) A novel lipid-based oral drug delivery system of nevirapine," n. d.). Three measurements were taken for each, and the mean and standard deviation were calculated.

2.2.3.2. Zeta potential. Zetasizer (Malvern Instruments) was used to calculate the zeta potential of the diluted SNEDDS formulation. Results were recorded after samples were put in clean disposable cuvettes. We assessed the zeta potential and charge of emulsion droplets (Nasr et al., 2016).

2.2.3.3. Transmission electron microscopy (TEM). Transmission electron microscopy was used to determine the SNEDDS formulae's surface appearance and globule size. Distilled water was used to dilute the SNEDDS samples ten times before examination. On a copper grid with a film coating, a drop of the resulting nanoemulsion was applied, forming a thin liquid film. After that, 2% (w/v) phosphotungstic acid solution was used to adversely stain the films. The stained films were air-dried before being imaged by transmission electron microscopy (Balakumar et al., 2013).

2.2.3.4. FTIR analysis. The infrared spectrum of optimized AzA SNEDDS formulation was obtained by combining potassium bromide (KBr) and sample in a (100:1) ratio and then forming pellets. To examine any chemical interactions between the drug, oil, and surfactant, FTIR spectra of the sample were acquired utilizing an FTIR spectrometer (Bruker).

2.2.3.5. Entrapment efficiency and drug loading. Any insoluble compound that was present in the produced SNEDDS was removed by passing it through 0.22 μm Millex filters (EMD Millipore Corporation, MA, US). In methanol (9 vol), one volume of SNEDDS formulation was mixed. Quantifying the concentration or amount of AzA in SNEDDS (C_{total}) was done using the established and validated UV method. To separate the non-encapsulated (free) drug from the encapsulated drug, the SNEDDS was vortexed for 5 min, then centrifuged at 12,000 rpm for 30 min. Through the use of the UV technique, the supernatant was analyzed to determine the concentration (C_{free}) of the free drug (Elnaggar et al., 2009). The drug loading and entrapment efficiency of AzA were determined using one volume of dried and weighed SNEDDS and the following equation:

$$\text{Drug loading } (\%) = \left(C_{total} - C_{free}\right) / \text{Total SNEDDS particle} \times {}^{100}$$

$$\text{Entrapmentefficiency}(\%) = {}^{(Ctotal-Cfree)/Ctotal\times} 100$$

2.3. Development and characterization of SNEDDS Carbopol hydrogel

2.3.1. Preparation of SNEDDS-loaded Carbopol 940 hydrogel

SNEDDS hydrogel containing AzA was created utilizing Carbopol 940 as a gelling agent in 1.0% concentrations for topical application. The gelling agent concentration must be chosen carefully because it's one of the factors that can alter the nature and physical stability of the gel since it may impact the penetration of drug-like substances on the skin. Firstly, 1 g of Carbopol 940 was dissolved in 100 mL of distilled water using a magnetic stirrer to create a Carbopol solution (1%), which was then allowed to sit overnight to swell. Then, SNEDDS formulation and other excipients propylparaben and methylparaben were mixed with Carbopol solution. Finally, triethanolamine was added and mixed into the mixture using a magnetic stirrer. Propylparaben and methylparaben was added as the preservatives (Indrati et al., 2020).

2.3.2. Characterization of hydrogel

2.3.2.1. Determination of pH. Precisely weighed 5 ± 0.01 g of the gel, dissolved in 45 ml of water, and the pH of the solution was assessed at 27 °C using the pH meter (Bajaj and Sharma, 2015).

2.3.2.2. Determination of viscosity. We used a cone and plate viscometer to evaluate the viscosity of SNEDDS-based hydrogels (0.5 g), a spindle 52 at 50 rpm and room temperature (Brookfield, Middleborough, USA) (Ojha et al., 2022).

2.3.2.3. Determination of spreadability. The term "spreadability" is used to indicate the extent to which a topical treatment penetrates the skin when administered to the afflicted areas. The formulation's spreadability has an impact on how effective it is as a treatment. As a result, figuring out spreadability is essential for evaluating the qualities of topical treatments The excess sample (3 g) was put between two glass slides to test spreadability, and it was compacted to a uniform thickness for 5 min using a weight of 1000 gm. After that, the pan was given additional weight (50 g), and the top plate was pulled with the aid of a line tied to the hook. The amount of time required for the upper glass slide to move the lower plate 10 cm is recorded. Better spreadability is indicated by a shortened interval (Bajaj and Sharma, 2015; Bajaj and Sharma, 2015). The following formula was utilized for calculating the spreadability (S):

$$S = \frac{M \times L}{T}$$

where, S – Spreadability, L - Length moved on a glass slide, M -Weight tied to the upper glass slide, T - Time taken.

2.3.2.4. Determination of homogeneity. Visual inspection was used to examine the SNEDDS hydrogel homogeneity test to determine whether any lumps or particles were present. We classified the scores as follows: A: Good, B: Fair, and C: Poor. Additionally, a small quantity of SNEDDS hydrogel was pressed between the thumb and index finger to test whether the hydrogel was homogenous or non-homogenous (Ahmad

et al., 2019).

2.3.2.5. Determination of stability. The created compound underwent 8 weeks of room temperature storage. Phase separation and homogeneity, as well as any other physical appearance alterations, were noticed. The outcomes were carefully noted and evaluated (Ahad et al., 2017).

2.3.2.6. Texture analysis. The texture characteristics of the hydrogels were ascertained using a Texture Analyser. A standard 100 mL beaker was loaded with roughly 50 mL of the gel preparation to guarantee the production of a smooth top surface and to keep air out of the sample. A 40-mm disc was pushed into the gel and then drawn once again. The technique parameters, such as depth of insertion and speed rate were dependent on the hydrogel type. As we prepared the Carbopol hydrogel so the speed rate was 1 mm/s and the distance was 15 mm from the above surface of the hydrogel. For SNEDDS formulation hydrogel, five identical analyses were performed in the same manner at room temperature for every reading. The resulting force-time plot was used to calculate gel characteristics like adhesiveness, cohesiveness, and hardness (Hurler et al., 2012).

2.4. In vitro drug release study

To test *in vitro* release, Franz diffusion cells were employed. 10 mL was the size of the receptor compartment, and the diffusion area was 2.5 cm^2. The partition across the receptor and donor compartments was a dialysate membrane. The donor compartment of a diffusion cell held 750 μL of the formulation. The receptor compartment received phosphate-buffered saline (PBS) with 5% SDS (pH 6.5) and was continuously agitated at 600 rpm. At certain intervals, samples were taken out, and to keep the sink condition, an equal amount of PBS solution was supplied. AzA concentration in the collected samples was calculated using UV analysis (Ugur Kaplan et al., 2019).

2.5. Skin permeation enhancement study

DSC and FTIR were used to analyze a rat skin permeation study using the prepared formulation. The SNEDDS hydrogel was applied on top of the excised skin to compare it to untreated skin. On Franz diffusion cells, epidermis samples were placed, and they were left there for 8 h. Following a normal saline wash, the samples were divided into tiny pieces and drained at a constant 60 °C in a hot air oven. According to the previously published research, the dried samples were then examined using DSC and FTIR (Iqubal et al., 2021).

2.6. HET-CAM assay

The Hen's Egg Test was conducted to gauge the formulation irritant potential. Ten days were spent incubating fertilized chicken eggs at a temperature of 37 °C and 65% relative humidity for the test. After that, the white membrane and the outermost shell were taken off, and samples were applied to the chorioallantoic membrane in amounts of 300 μL for a SNEDDS formulation and 0.300 g for formed hydrogels. A physiological solution was added to the CAM after 20 s in consideration of the opaqueness of the SNEDDS formulation. The CAM was watched for 300 s sequentially. Further changes to the membrane (such as coagulation, haemorrhage, and vasoconstriction) were observed during this time, and the length of time it took for each alteration to take place was noted. The SNEDDS formulations were tried without AzA to see if the ingredients had any irritating effects. The negative (saline solution) and positive (0.1 N sodium hydroxide-NaOH) controls were assessed for the goal of experimental validation. The preparations were categorized as non-irritating (0–0.9), somewhat irritating (1–4.9), moderately irritating (5–8.9), and severely irritating (9–21) based on the acquired IS values. The equation was used to calculate the irritation score (IS):

$$IS = \frac{301 - TIME\ H}{300} \times 5 + \frac{301 - TIME\ V}{300} \times 7 + \frac{301 - TIME\ C}{300} \times 9$$

where H is the period of haemorrhage, V is the time of vasoconstriction, and C is the time of coagulation.

2.7. Ex vivo studies

2.7.1. Ex vivo permeation studies on rat skin

Ex vivo permeation experiments have been carried out utilizing the Franz diffusion cell, which has a 1.76 cm^2 surface area and 10 ml volume, to find out how well AzA-loaded SNEDDS hydrogel permeates across epidermal rat skin (Salimi et al., 2020). 10 mL of PBS solution was placed inside the receptor chambers. The epidermal skin of the rat was freshly excised and subcutaneous fat was removed, cut to the proper size, and installed in the Franz diffusion cell across the receptor and donor compartments with the corneum layer spreading towards the compartment of the donor. To prevent diffusion media leakage, the donor compartment of the diffusion cell was positioned over the rat skin mounting and clamped to the rim of the receptor compartment. Permeation studies of AzA-loaded SNEDDS hydrogel and AzA solution were performed by placing 2 ml in the donor compartment of a Franz diffusion cell and magnetically stirring constantly at 200 rpm. A sample (0.5 ml) from the receptor compartment was taken out at present intervals (0.5, 1, 2, 4, 6, 8, 12, and 24 h) and then subjected to UV spectrophotometer analysis at 213 nm. Each sample that was withdrawn was promptly swapped with an equivalent volume of fresh PBS diffusion medium that was kept at 32 ± 0.5 °C. At each sampling site, the amount of AzA that had crossed the epidermal skin was calculated using the UV technique. Plotting the quantity of drug permeated per unit epidermal skin surface area (g/cm^2) versus time (h) allowed for the creation of the permeation profile. By analyzing the slope of the plot using linear regression, the steady state flux (Jss, μ/cm^2/h) was calculated. The results of each test were performed three times.

2.7.2. Ex-vivo confocal laser scanning microscopy (CLSM) visualization

Rhodamine B dye stacked AzA suspension and an optimized AzA loaded SNEDDS formulation was created. The epidermal rat skin with PBS (pH 6.5) was installed in a Franz diffusion cell and exposed to rhodamine-loaded SNEDDS and a methanolic solution of rhodamine was utilized as the control for 12 h. The cleaned rat skin was then sliced into small segments and rinsed with distilled water to create a microscopic slide. To monitor the penetration of optimized SNEDDS and suspension over the entire epidermal layers, CLSM was used to inspect the produced slides. In this study, rhodamine fluorescence was optically excited using a 488 nm Argon laser beam, and fluorescence emission above 532 nm was analyzed. CLSM was used to measure the extent of SNEDDS and suspension penetration (Bağcı et al., 2019).

2.8. In vivo studies

2.8.1. Animals and study protocol

According to a previously approved by the Institutional Animal Ethics Committee (IAEC) of the Central Animal House Facility, Hamdard University (Protocol no. 1981, date 21/12/22), the *in vivo* tests were conducted on female Wistar rats that were 6–8 weeks old. These animals were kept in a typical dark-light cycle at room temperature and ranged in weight from 120 to 150 g. The rats had unhindered access to water and food. The hair on the upper back of rats was clipped and shaved while they were under the effects of ether anesthesia (Alam et al., 2013).

2.8.2. Induction of AD: erythema score and scratching score

Following a published procedure, calcipotriol, a low-calcaemic vitamin D3 analog (bought from Sigma, 2 nM dissolving in ethanol), was topically treated to the upper back of rats to create an AD rat model

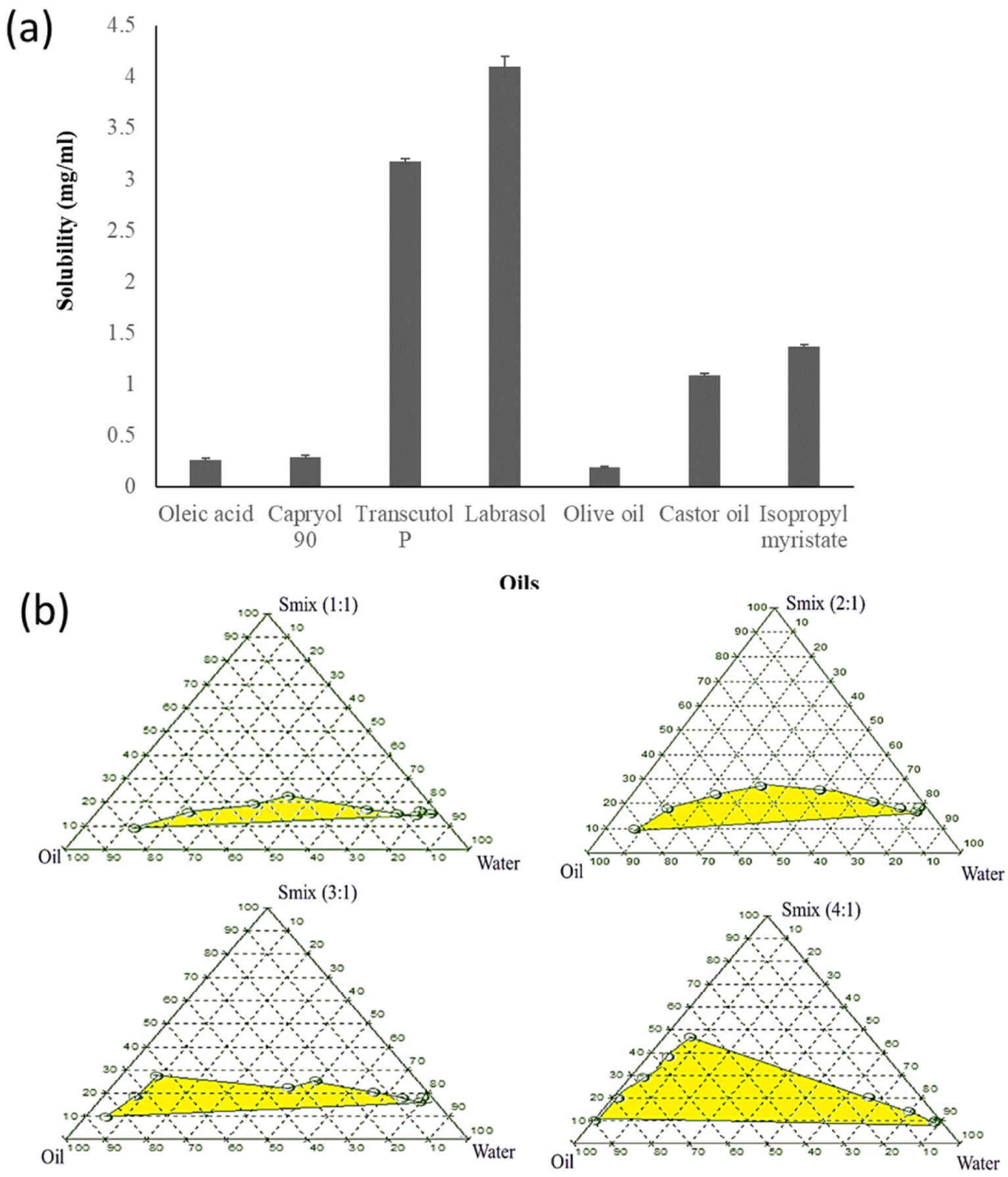

Fig. 2. (a) Equilibrium solubility of azelaic acid in various oils in mg/ml, data represented as mean ± SD; (n = 3); (b) The Pseudoternary phase diagrams of the Oil-Smix–Water system at the 1:1, 2:1, 3:1 and 4:1 wt ratio of Labrasol -Tween 80/PEG 400 at ambient temperature, shaded area show nanoemulsions zone.

(Chu et al., 2021). The animals have been divided into five groups. After trichotomization, all groups were induced with calcipotriol dissolved in ethanol on the upper back, except the first group, which got only 20 μL ethanol and maintained under the same feeding and environmental conditions as the remaining groups, serving as the control group (C). Dermatitis was induced 7 days after induction with calcipotriol in ethanol (10 treatments with 24-h intervals) on the abdomen after trichotomization. The first group, that got only ethanol, was euthanized 72 h immediately following the final application of the induction agent. The rats in the second group, which served as the positive control, were euthanized following their final administration of calcipotriol. The AzA hydrogel was applied topically on the abdomen of the third group, the fourth group got marketed cream (Aziderm), while the fifth received topical administration of the AzA-loaded SNEDDS hydrogel on the abdomen. One milligram of AzA was the dosage for applying the SNEDDS hydrogel and commercial cream. On days 7, 14, and 21, groups 3, 4, and 5 were given 0.5 ml of the AzA hydrogel, drug-loaded SNEDDS hydrogel, and marketed cream for 15 days. To achieve greater drug permeation, all formulations were massaged evenly throughout the abdomen. After that, a digital camera was used to take a 30-min snapshot of the scratching score and erythema scores thrice a week. After the conclusion of each treatment, the rats were euthanized (Alam et al., 2013).

2.8.3. *Skin irritation test*

All of the ingredients used to make SNEDDS formulation are in the

generally recognized as safe (GRAS) group. The concentration of all the ingredients is a crucial factor in this composition. Surfactants in large quantities typically irritate the epidermis. To prove that the material concentration used to prepare SNEDDS is safe, a skin irritancy test was conducted. Therefore, a skin sensitivity analysis was done to validate the safety of the AzA-loaded SNEDDS that had been optimized. Histological microscopy was used to assess the amount of skin irritation brought on by the formulations under evaluation. The female Wistar rats were split into four groups: the tested groups (treated with drug-loaded and drug-free SNEDDS hydrogel, and a commercial product), the water-treated group serving as the negative control, and the 0.8% paraformaldehyde-treated group serving as the positive control. For testing, 2.54 cm^2 of shaved abdominal skin was covered with 0.5 mL of the formulation and parafilm for 24 h. The applied skin tissue was then removed from the rats after they were sacrificed, put in a 10% buffered solution of formaldehyde for not fewer than 24 h, and used for histological analysis. Tissue samples were prepared by fixing, rinsing under flowing distilled water, dehydrating with a progressive series of ethanol solutions, and embedding in paraffin. For histological analysis, the tissue samples were divided into 20 μm slices, rehydrated, and stained with eosin and haematoxylin. A light microscope was employed to inspect each sample (Hung et al., 2021).

2.8.4. Histological observation of skin

Dorsal skin sections were preserved with 10% neutral formalin, sectioned at a 4 μm, and encased in paraffin. Haematoxylin-eosin was used to stain the sections. To identify the eosinophils and mast cells, sections were also labeled with direct first scarlet and toluidine blue, respectively. Under a light microscope with a magnification of about 200, the number of mast cells was counted in five arbitrarily chosen fields of view (Espinoza et al., 2020).

3. Results and discussion

3.1. Selection of SNEDDS components

3.1.1. Screening of oil phase

The solubility of the drug in various formulation components determines how self-nanoemulsion systems for poorly soluble pharmaceuticals can be created, and drug loading per formulation is a crucial design element. To give the drug in a form that is encapsulated at the recommended dosage, the formulation's volume should be kept to a minimum. An essential factor in choosing oils is the drug's solubility in the oil phase. This is crucial when developing topical formulations because the solubility of the drug in the oil phase has a substantial effect on the self-nanoemulsion capacity to keep the solubilized form of the drug. There may be a chance of precipitation if the cosurfactant or surfactant is helping to solubilize the drug. For this reason, it's crucial to comprehend the variables affecting drug capacity for loading while preserving the system's ability to endure monophasic dispersion via water and reducing the risk of precipitation of drugs or crystallization in diluted systems are important considerations when constructing robust and appropriate low-volume self-nanoemulsion systems for the delivery of drugs. Recently, amphiphilic compounds with surfactant characteristics, such as novel semisynthetic medium chain derivatives, have gained favor. Additionally, creating a self-nanoemulsion with oil that has inadequate drug solubility would necessitate adding more oil to reach the desired drug dose, which would then necessitate adding more surfactant to accomplish oil solubilization, potentially making the system more toxic. New semi-synthetic medium-chain compounds with surfactant characteristics are gradually and successfully replacing conventional medium-chain triglyceride oils. The comparative solubility studies of the AzA in different oils are depicted in Fig. 2a. According to Fig. 2a, labrasol (4.09 ± 0.2 mg/mL) demonstrated the highest solubility for AzA among the oils. To build pseudo-ternary phase diagrams, the labrasol was chosen as an oil phase for phase titration experiments.

Table 1
(a) Emulsification efficiency of different surfactants in Labrasol oil; (b) Emulsification efficiency of different cosurfactants in Labrasol oil and Tween 80 surfactant.

(a) Emulsification efficiency of different surfactants in Labrasol oil

Surfactants	% Transmittance	No. of inversion
Tween 80	99.67 ± 0.17	3
Cremophor RH40	98.72 ± 0.34	7
Tween 40	83.98 ± 0.12	11
Tween 20	91.66 ± 0.89	6
Cremophor S9	19.90 ± 0.87	13

(b) Emulsification efficiency of different cosurfactants in Labrasol oil and Tween 80 surfactant

Cosurfactants	**% Transmittance**	**No. of inversions**
PEG 400	99.43 ± 0.09	4
PEG 200	99.33 ± 0.13	7
PEG 600	96.89 ± 0.04	9
Glycerol	92.78 ± 0.19	11

3.1.2. Screening of surfactant

The toxicity of the constituents is the most serious issue with systems built on self-nanoemulsions. When applied topically, excessive surfactants may irritate the skin. As a result, careful surfactant selection is required. Thus, it's crucial to accurately calculate the surfactant concentration and apply the formulation's lowest concentration. Non-ionic surfactants usually have low CMCs and are less harmful than their ionic counterparts. Additionally, non-ionic surfactant-based o/w nanoemulsion dosage forms for topical use are expected to provide *in vivo* stability. Consequently, choosing the right surfactant becomes essential. After labrasol was chosen as the oil phase, the objective was to determine the surfactant with the greatest ability to solubilize the oil. Five non-ionic surfactants—Tween 80, Tween 40, Tween 20, Cremophor S9, and Cremophor RH40—were selected for screening in the current research.

The certain number of flask inversions are necessary to make a SNEDDS was used to gauge the surfactant's emulsion-forming capacity, and 2 h after preparation, the percentage UV transmittance of the emulsion was used to assess its stability. A high transmittance is correlated with optical clarity because clear dispersions are less effective at scattering incident light than opalescent dispersions. When optical homogeneities are absent in the medium, scattering of light that results cause the light intensity traveling by dispersion to occur. Therefore, the relative droplet size of the emulsion could be accurately predicted using percentage transmittance. Based on this idea, droplets of oil were assumed to be in a condition of nanodispersion, and high transmittance (means absorbance is lower) aqueous dispersions were regarded as optically transparent. Table 1a contains the total no. of flask inversions and values of % for different dispersions. Cremophor S9 had the highest reported number of flask inversions (11 inversions) among all screened surfactants, suggesting the most challenging emulsion formation. Cremophor S9 emulsions also had the least stability, as shown by the lowest recorded percentage of UV transmission (19.90 ± 0.87%). However, using Tween 80 as the emulsifying agent, only three flask inversions were necessary to create an emulsion. Further evidence of the formed nanoemulsion's durability came from the fact that their UV transmission percentage (2 h after preparation) nearly reached 100%. Due to its improved nanoemulsification effectiveness, Tween 80 was chosen as the surfactant for further research.

3.1.3. Screening of cosurfactants

To create nanoemulsion systems at low surfactant concentrations, cosurfactants are introduced. Cosurfactants with short to medium chains are widely used to progressively decrease interfacial tension and enhance interface fluidity. Additionally, they make the hydrocarbon tail more mobile and let more oil get into this area. Because of its partitioning between oil and aqueous phases, alcohols can improve the

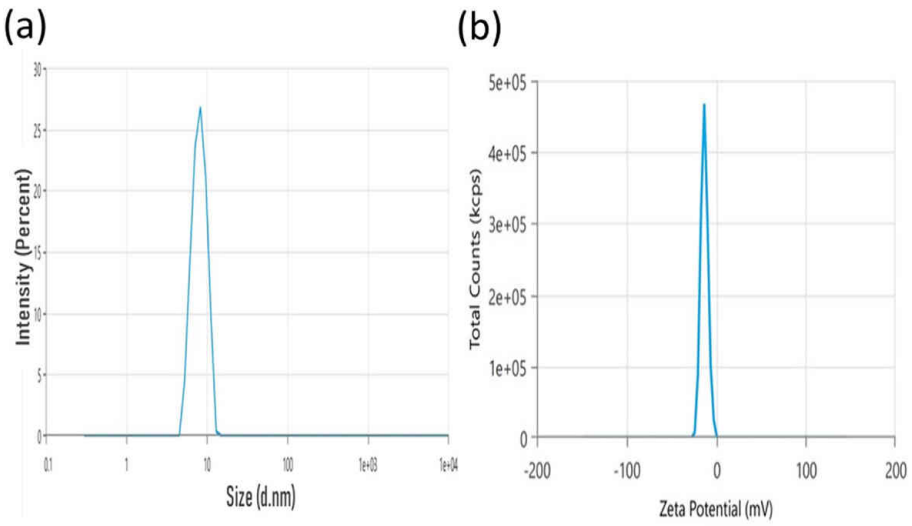

Fig. 3. (a) Mean particle size and PDI of optimized azelaic acid loaded SNEDDS formulation; (b) Zeta potential of optimized azelaic acid loaded SNEDDS formulation.

miscibility of both phases. As a result, the cosurfactants propylene glycol, glycerol, PEG 400, PEG 200, PEG 600 was chosen. Additionally, PEG 400 was chosen because they exhibit greater permeation in formulations and are generally tolerable. PEG 400 used in this research seemed to enhance Labrasol and Tween 80 capacity to emulsify. The drug absorption and dispersibility from formulations containing surfactants were said to be improved by the addition of a cosurfactant. In contrast to other used cosurfactants, PEG 400 demonstrated high emulsification efficiency with Tween 80 and Labrasol mixture, demonstrating the highest transmittance (99.43 ± 0.09%) and only 4 inversions as shown in Table 1b.

3.1.4. Construction of pseudo ternary phase diagram

The change that occurs if the system is diluted is one of the key characteristics of SNEDDS, as this could result in the precipitation of drugs because of the decrease in solvent capacity. For the development of SNEDDS, pseudo-ternary phase diagrams were made to identify the self-nano emulsifying regions and determine the ideal ratios of cosurfactant, surfactant, and oil. At certain ratios of surfactant to cosurfactant (1:1, 2:1, 3:1, and 4:1) the phase diagrams were plotted. A comparison was made between the sizes of the nanoemulsion regions in the diagrams; the bigger the size, the more effectively the sample self-nano emulsified. Based on a visual examination of the material, the

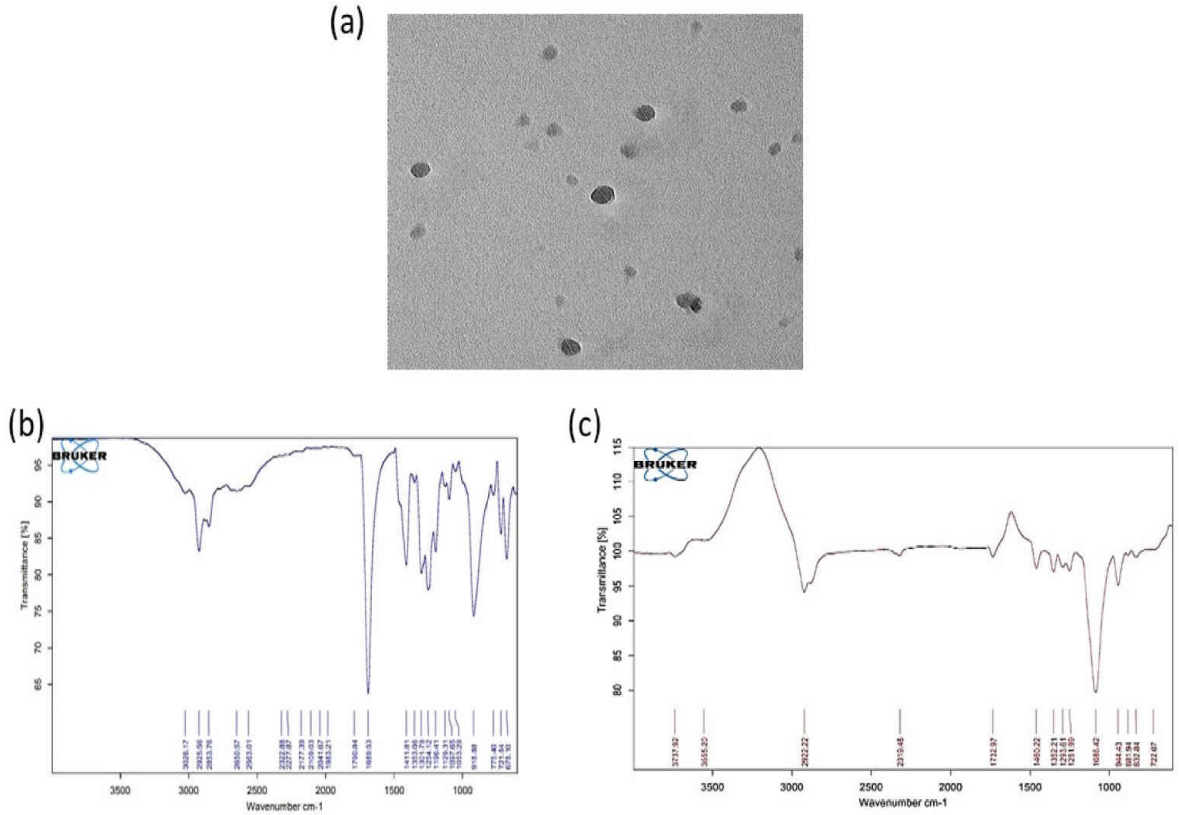

Fig. 4. (a) TEM image of optimized AzA-SNEDDS formulation; (b) FTIR spectra of Azelaic acid c) FTIR spectra ofAzelaic acid loaded SNEDDS.

nanoemulsion phase was found to be the region where transparent and clear formulations have been achieved on dilutions. According to pseudo ternary phase diagrams, as shown in Fig. 2b, a formulation made with a 4:1 ratio of Tween 80-PEG 400 mixture (Smix) had the largest nanoemulsion zone. So, from the perspective of stability, setting the surfactant/cosurfactant mixture at 4:1 is preferable. When the water concentration was greater than 69% of the SNEDDS formulation, it was found that emulsification efficiency was high. The largest nanoemulsion region was seen at Smix 4:1, possibly as a result of the interface's enhanced fluidity and further lowering of interfacial tension.

3.2. Characterization of AzA-loaded SNEDDS formulation

3.2.1. Particle size and polydispersity index (PDI)

The mean diameter and PDI of optimized AzA-loaded SNEDDS was found to be 151.20 ± 3.67 nm and 0.2278 ± 0.011, respectively (Fig. 3a). The size of the distributed globules, a crucial self-nanoemulsion characterizing measure, contributes to the formulation's stability while the nanometric lipid globules facilitate simple permeation via the stratum corneum. The drug's capacity to be permeated is based on the self-nanoemulsion particle size. Small particle size generates a large surface area, which increases drug release and boosts drug permeation. In particular, if the drugs show a lipophilic characteristic, it could be speculated that the incorporation of drug particulates allows particles to come into contact with the microstructure of the system, decreasing globule size. PDI guarantees globule size consistency within the formulation. A homogeneous and consistent globule size characterizes the formulation if the PDI value is less than 0.5. Since it promotes skin permeability, a smaller globule size is crucial for the topical application of the formulation. The optimized drug measurements show that our drug-loaded SNEDDS formulation is suitable for topical administration. The PDI in the current study was 0.22, indicating a monodisperse system, as it has been cited in the literature for different nanoformulations such as nanoemulsion, ethosomes, cubosomes, and so on. A PDI of 0.40 or less is regarded as appropriate because it indicates a homogenous population of phospholipid-containing vesicles (Marzuki et al., 2019).

3.2.2. Zeta potential

Zeta potential is a measure of colloidal dispersions' physical stability that can usually be estimated by the magnitude of the charge surface, which reveals the electrostatic mobility of nanoparticles which is dispersed. The ideal zeta potential of the AzA-loaded SNEDDS formulation was −13.18 ± 0.152 mV (Fig. 3b), showing the system's physical stability. Zeta values serve as an indicator of electrostatic attraction between particles. From the literature, values of zeta potential more than +30 mV or low than −30 mV guarantee the stability of the formulations with no aggregation (Sharifi et al., 2021). The negative charge provides repulsive interactions within the globules and so inhibits aggregation or coagulation of the dispersed globules. The non-ionic surfactant used in the formulation is responsible for the low zeta potential. These globules can be added to the polymeric matrix to prevent them from moving around, which will increase the formulation's stability. Additionally, the dispersed drug-loaded oil globules' negative charge may be due to the anionic moieties in the oil core and cosurfactant.

3.2.3. Transmission electron microscopy (TEM)

The SNEDDS particles are roughly spherical with a dark globule, as illustrated in Fig. 4a, according to the results of the exterior morphological investigation of the optimized AzA-loaded SNEDDS conducted using TEM. The results of particle size analysis using Zetasizer and the TEM were well correlated. The observation from the TEM image closely resembles the information previously provided by Rathore et al. (2023).

3.2.4. FTIR analysis

FT-IR spectrum of the AzA displays characteristic bands coming from the stretching of the carboxylic acid O–H atom at 2933 cm^{-1}, the stretching of the carboxylic acid C=O atom at 1683 cm^{-1}, the plane bend of the C–O–H atom at 1409 cm^{-1}, the stretching of the carboxylic acid C–O atom at 1251 cm^{-1}, and the out-of-plane bending of bound OH at 914 cm^{-1} (Fig. 4b). FTIR spectra of AzA loaded SNEDDS formulation revealed that the typical peak of azelaic acid at 1683 cm^{-1} disappeared and the peak shifted from 1251 cm^{-1} to a lower wavenumber whereas the band at 1409 cm^{-1} and 914 cm^{-1} shifted towards a higher wavenumber (Fig. 4c). As a result, the proof that AzA has been effectively incorporated into the SNEDDS formulation is supported by the FT-IR data. The observation data of FTIR analysis closely resembles the information previously provided by Berlitz et al. (Jacobus Berlitz et al., 2019).

3.2.5. Entrapment efficiency and drug loading

The developed AzA-loaded SNEDDS formulation calculated entrapment efficiency for the drug AzA was 92.85% and the drug loading was reported to be 9.07 ± 0.09%. AzA solubility in oil phase and disarranged structure of SNEDDS formulation are responsible for the high drug loading and entrapment efficiency.

3.3. Characterization of SNEDDS hydrogel

3.3.1. Determination of pH

The produced SNEDDS hydrogel pH was discovered to be 6.71 ± 0.22. The pH of the prepared hydrogel was within the range of healthy skin, making them suitable for applying topically without causing any skin irritation. The developed SNEDDS hydrogel formulation's pH value was determined to be 6.7, which is in acceptance with the pH value (6.67) cited in the literature and lies within an acceptable range to prevent skin irritation. As a result, the developed SNEDDS hydrogel is suitable for dermal application (Al-Suwayeh et al., 2014).

3.3.2. Determination of viscosity

The viscosity of the AzA-SNEDDS hydrogel was discovered to be 9.12 ± 0.03 Pa s, at a shear rate of 6 s^{-1} and shear stress of 60 Pa. It was discovered that incorporating optimized nanoemulsion into a blank hydrogel did not change the formulation's rheological characteristics. The results we obtained are consistent with previous literature (Md et al., 2020), which indicates that the formulation's viscosity would be at a point where it may spread easily throughout the skin.

3.3.3. Determination of spreadability

It was discovered that the spreadability was 5.18 ± 0.12 g-cm/sec. The spreading of gels affects their therapeutic efficacy. The prepared gels must be well spreadable and meet the ideal requirements for topical application to aid in the uniform administration of the gel to the skin. Additionally, this is thought to be a key element in patient adherence to therapy. One of the most essential characteristics of anti-inflammatory and analgesic topical preparations is their consistency. The gel's spreadability characteristics demonstrated a very short spreading time as well as consistency. The gel's ability to be ejected from the tube in a consistent and desirable amount depends on its consistency. The distance covered by a falling cone is inversely correlated with its consistency. In this investigation, optimized AzA-SNEDDS-Hydrogel was discovered to have a very good spreadability which is also reported in the literature provided by Ahmed (2015).

3.3.4. Homogeneity

The developed SNEEDS hydrogel was created to look pleasant and well-homogenized. As well as no phase separation or coarse particles were seen.

3.3.5. Stability testing

The hydrogel organoleptic properties remained unchanged for the first 30 days of storage at ambient temperature and in a refrigerator,

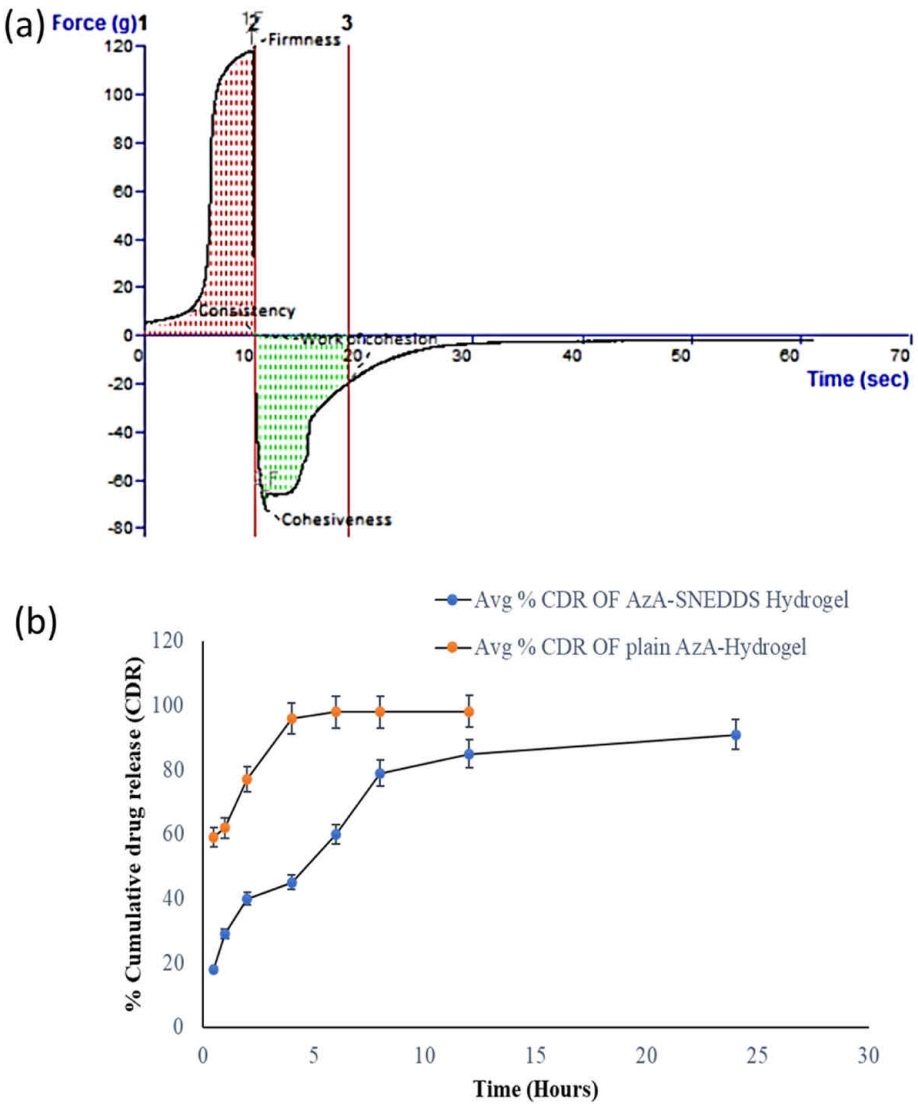

Fig. 5. (a) Representative force versus time curve of a backward extrusion assessment of SNEDDS Carbopol hydrogels. (b) *In vitro* drug release curve for AzA plain hydrogel and AzA-SNEDDS hydrogel.

indicating that their physical stability was adequate for the time frame suggested by the US pharmacopoeia. To assure the hydrogel formulation's security and quality during the shelf life, stability testing was done at a temperature of 25 °C/60% RH. After the investigation was finished, or after one month, no changes in the hydrogels' appearance, color, viscosity, homogeneity, or pH were noticed. There was never any skin irritation.

3.3.6. Texture analysis

When hydrogels are placed on dermis, they ought to develop a microgel network that can withstand the physiological stress brought on by the body's mobility while also allowing for closer and more sustained contact with the skin. A balance between gel cohesiveness and gel adhesiveness must be kept while creating the ideal topical formulation, especially about extended retention duration at the site of application for hydrogels intended for the management of AD. A trustworthy summary of those qualities might be offered through texture analysis. Gel properties like adhesiveness, cohesiveness, and hardness were calculated by the demonstrated force-time plot (Fig. 5a). The hardness of the hydrogel formulation is demonstrated by the maximal force. The amount of effort necessary to distort the hydrogel during the probe's downward motion is referred to as cohesiveness. The hydrogel's ability to adhere to the probe is demonstrated in the second area. These characteristics of hydrogels will also impact how quickly the drug integrated into them is released from the delivery system.

3.4. In vitro drug release study

In-vitro drug release tests have been employed to assess the drug release patterns to meet the requirement. A UV spectrophotometer with a 213 nm wavelength was used to achieve this. The Franz diffusion cell was employed to analyze the *in vitro* release characteristics of AzA formulations. Under circumstances that mimicked physiological skin conditions, the *in vitro* drug release was calculated. In this investigation, phosphate buffer with a pH of 6.5 and maintained at a temperature of 32 °C ± 0.5 °C was used as the receptor media. The results of the comparative study between AzA plain hydrogel and AzA SNEDDS hydrogel are shown in Fig. 5b. The first drug release from AzA plain hydrogel was rapid in the first 2 h, followed by a sustained release that lasted for 20 h. The drug's immediate burst expulsion from the simple hydrogel could be caused by the superficial trapping of the drug. The prolonged and sustained release of drug behaviour that has been observed in nano dermatology is really interesting. Therefore, it may be assumed that this kind of drug release behaviour can be used to identify

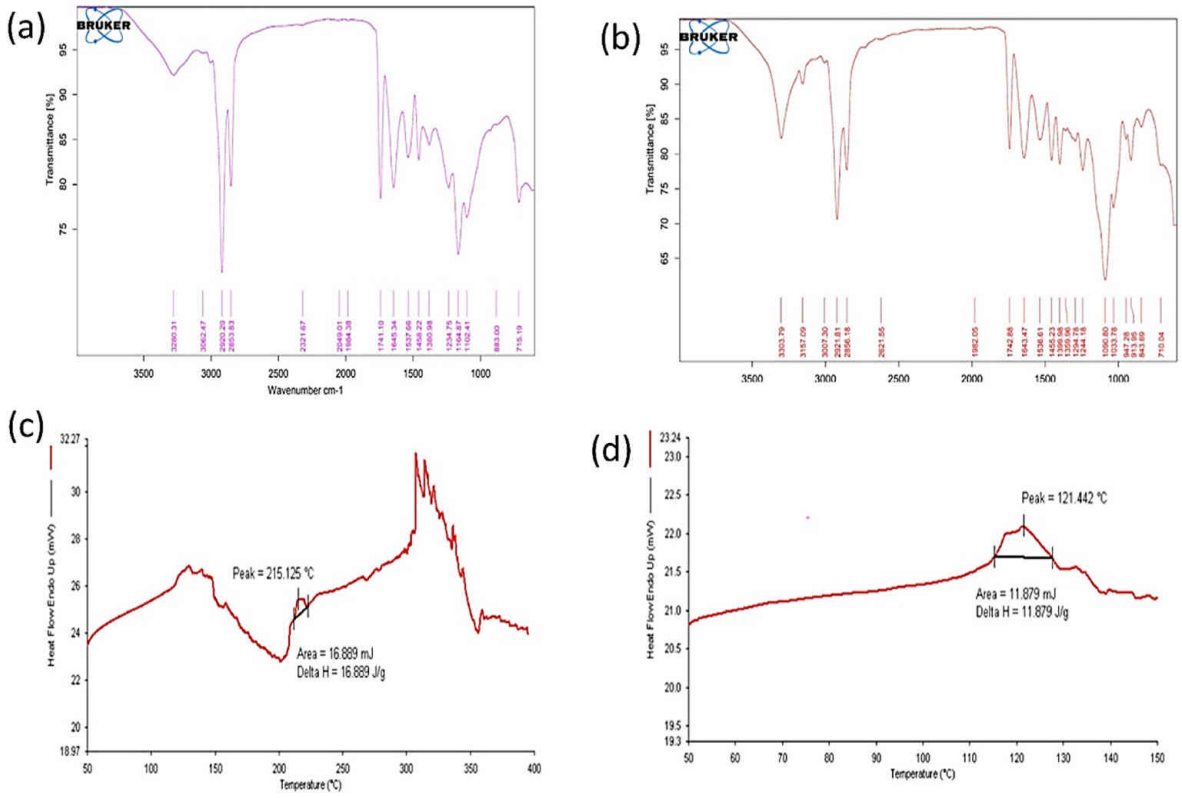

Fig. 6. Skin permeation enhancement study evaluated by FTIR and DSC: (a) FTIR of normal skin (b) FTIR of AzA-SNEDDS hydrogel treated skin (c) DSC of normal skin and (d) DSC OF AzA-SNEDDS hydrogel treated skin.

the intended topical delivery of the drug. As an outcome, the first quick and then gradual release lessens the AzA possibility of drug loss due to routine activities. Sweating and changing clothes are two instances of actions. Because of the occlusive/moisturizing qualities of the nano-emulsions and maintained effectively delayed and sustained drug release, this encourages enhanced skin administration. After 12 h, AzA plain gel at pH 6.5 releases approximately 98.63 ± 0.97% of the drug. The order of the drug release characteristics was AzA plain hydrogel greater than the AzA-SNEDDS hydrogel (ANOVA, $p < 0.05$). The drug partitioning between the oil and aqueous phases as well as interactions with surfactants are all controlling factors for the release of drugs. To effectively release the medicine from the SNEDDS hydrogel, the particles need to be smaller in size and have a larger surface area. The formulation's nanosize accelerates AzA solubility into the aqueous phase. The solubility and medication release are both enhanced. The release takes place in a controlled way. The AzA plain gel formulation does not exhibit a burst release pattern, except an immediate rapid release within the initial 2 h. In contrast to a rapid or burst release, a steady release is the best parameter for long-term disorders like dermatitis. However, the drug is absorbed and released rapidly in inflammatory dermatitis lesions, and a burst delivery also results in toxic effects. The optimized SNEDDS formulation was converted into hydrogel form to provide a sustained release of the active ingredient and superior retention of drug properties.

3.5. Skin permeation enhancement study

DSC and FTIR were used to analyze the mechanism of AzA-SNEDDS hydrogel permeation into the skin from the hydrogel (Fig. 6). The band of absorption in the region of 3000 to 2700 cm^{-1} in FTIR of healthy skin is caused mostly by the C–H stretching motion of alkyl groups found in lipids and proteins. Peaks in the absorption bands 2853.81 and 2926.14 cm^{-1} are caused by symmetric and asymmetric C–H stretching in lipids, respectively. The stretching vibrations of the proteins amide I and amide II are the primary cause of the values of 1639.56 and 1550.83 cm^{-1}. The amide – I band and the amide II band are produced by the vibration of the atoms C=O and C–N, respectively. Component bands that indicate different keratin structural variants make form the amide I band. In contrast, the FTIR spectra of the treated skin showed an absorption band at 3062.13, 3421.87, and 3576.18 cm^{-1}. Stretching of alkenes is illustrated by the band at 1665.60 cm^{-1}, stretching of C=O by the band at 1750.48 cm^{-1}, and stretching of C–H by the band at 2855.73 cm^{-1}. Alkane C–H bending, as well as O–H bending and C=C bending, may be seen in the absorption band at 1462.11 cm^{-1}, 1426.42 cm^{-1}, and 971.20 cm^{-1} respectively. Both the AzA spectrum and the rat skin undergoing the preparation exhibits comparable features with slight variations. The chemical reaction between skin and AzA-SNEDDS hydrogel is the cause of this variance in peak. The results show that AzA-SNEDDS hydrogel effectively fluidized the skin's protein and lipid by increasing the permeability of the membrane, leading to enhanced formulation retention and permeation. According to FTIR research, skin dermis treated with AzA-SNEDDS hydrogel changed to higher wavenumbers at 3303.04 cm^{-1} and 3344.03 cm^{-1}, which are representative of N–H or O–H bonds in lipids, keratin, or ceramide. Furthermore, compared to the dermis that had not been treated, skin that had been exposed to the formulation showed a greater wavenumber of the FTIR band at 2852 cm^{-1} and 2920 cm^{-1}. The hydrogen bond strength of the skin is said to be lowered by interactions between AzA SNEDDS hydrogel and keratin or polar ceramide areas, as well as lipid components in the stratum corneum, leading to effective skin fluidization. The results show that the improved AzA SNEDDS formulation fluidized the skin's epidermis and dermis efficiently, possibly enhancing drug retention and permeability. On the other hand, the addition of PEG 400 and tween 80 considerably increased these effects.

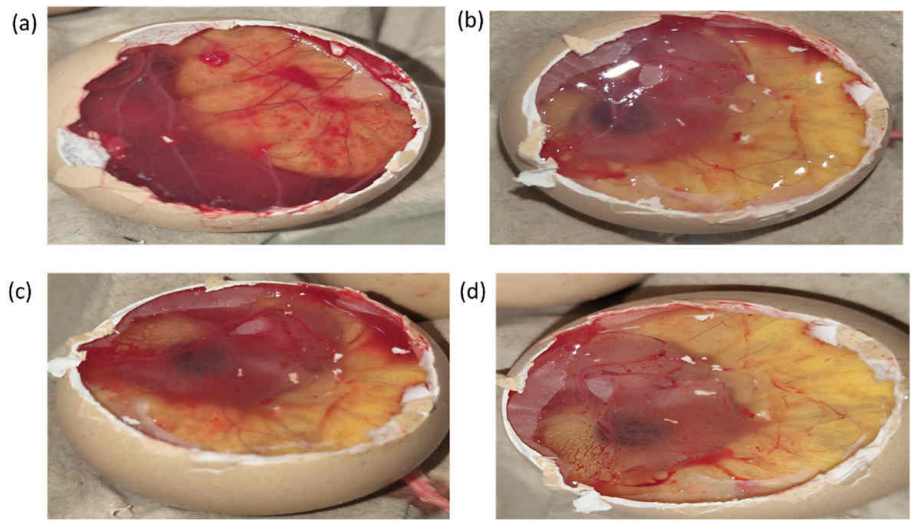

Fig. 7. Representative pictures of HET-CAM study after the administration of (a) Positive control- 0.1 M NaOH; (b) Negative control- 0.9% NaCl; (c) SNEDDS Hydrogel; (d) Azelaic acid SNEDDS hydrogel.

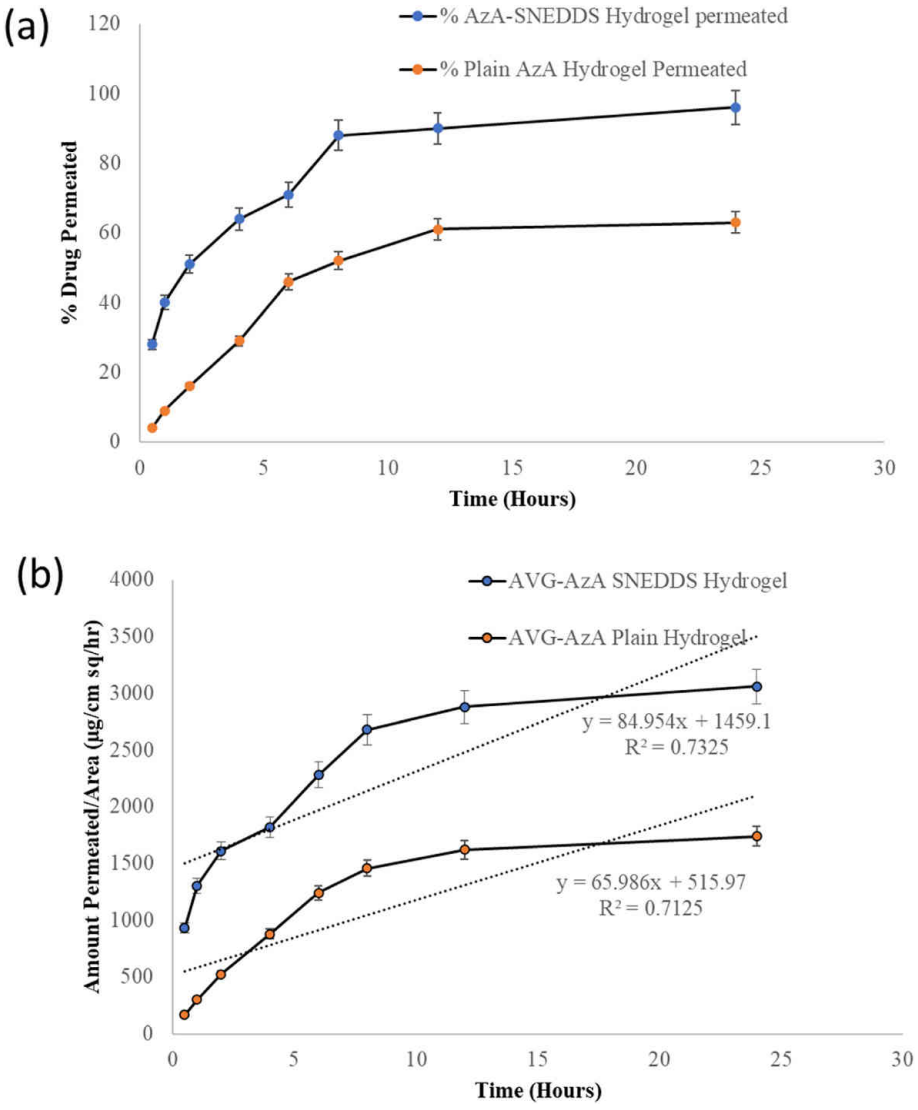

Fig. 8. (a) *Ex vivo* permeation of AzA from SNEDDS hydrogel and plain hydrogel. (b) Flux for AzA-SNEDDS hydrogel and Plain AzA.

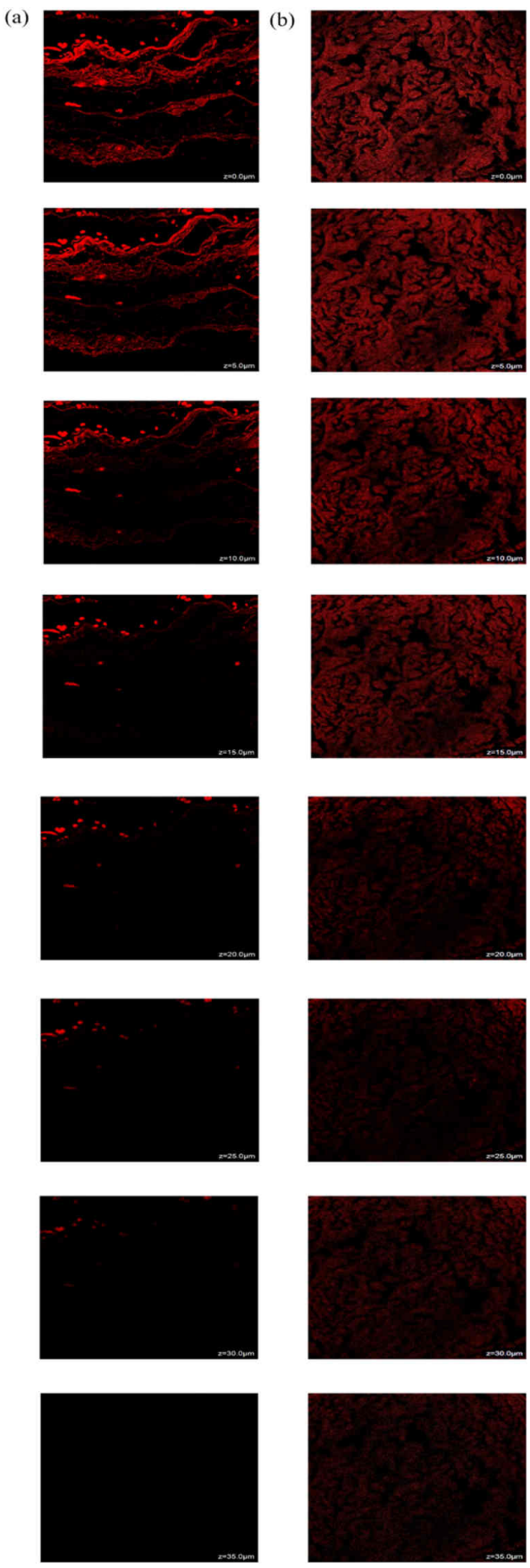

Fig. 9. (a) CLSM penetration for AzA Hydrogel (b) CLSM penetration for AzA-SNEDDS Hydrogel.

3.6. HET-CAM assay

After applying all of the test groups, no haemorrhage, lysis, or coagulation was seen in the HET-CAM study (IS = 0). The positive control was categorized as harsh irritants as predicted (IS = 19.9 ± 0.0). After the test was performed, the HET-CAM study is depicted in typical images in Fig. 7.

3.7. Ex vivo studies

3.7.1. Ex vivo permeation studies on rat skin

The *ex vivo* drug permeation response of AzA-SNEDDS hydrogel and AzA hydrogel was discovered utilizing rat skin. Fig. 8 displays the outcomes of the *ex vivo* permeation of AzA from the AzA-SNEDDS hydrogel and AzA hydrogel preparations at pH 6.5. As can be seen from a comparison of the permeation patterns of the two products, the percentage cumulative drug permeated of AzA from the produced SNEDDS hydrogel formulation is 96.09 ± 1.21% whereas in the case of plain AzA hydrogel formulation only 60.18 ± 0.29% drug was permeated (Fig. 8a). This accelerated permeation may be caused by an abundance of AzA-containing nanosized oil globules, which may accelerate the rate at which the drug permeates through the skin's lipophilic layers and allow for immediate passage of the drug through the skin. The permeation flux was substantially increased ($P < 0.05$) with AzA-SNEDDS hydrogel (84.954 ± 1.19 μg cm^{-2} h^{-1}) as contrasted to the hydrogel formulation (65.986 ± 0.21 μg cm^{-2} h^{-1}) when the permeation characteristics were compared simultaneously (Fig. 8b). This may be caused by the enhanced skin permeation brought on by PEG 400 presence, while the nanometric lipophilic globules also contributed to this permeation. The optimized SNEDDS formulation increased the amount of drug permeated as compared to plain AzA hydrogel indicating that the drug will be able to effectively permeate from epidermal layers.

3.7.2. Ex-vivo confocal laser scanning microscopy (CLSM) visualization

Confocal microscopic analysis was done to assess the permeation of AzA-SNEDDS hydrogel and regular AzA hydrogel. The intensity of the red color depicts the amount of medication deposited on the skin of the rats. The results of the CLSM investigation showed that, in comparison to the AzA hydrogel which could only permeate the rat skin up to 25 μm, AzA-SNEDDS hydrogel was highly permeable (up to 35 μm) through the epidermal layer of the rat skin (Fig. 9). The findings thus demonstrate that the drug may effectively cross the epidermal-dermal barrier, which is necessary for the treatment of AD.

3.8. In vivo studies

3.8.1. In vivo study of scratching score and erythema score

A calcipotriol-induced AD model of Wistar female rats was developed to study scratching, scabs, edema, and erythema behavior. After that, rats in groups 3, 4, and 5 received treatments from AzA hydrogel, market formulations, and AzA-SNEDDS hydrogel. Every time they used their hind paws to massage their dorsal skin, the scratching score and erythema score were observed and quantified as shown in Fig. 10a and b. After 2 weeks of AzA-SNEDDS hydrogel treatment, the inflammatory skin began to heal and developed a scab. Scabs developed into healing skin throughout this process, and the injured stratum corneum began to sprout new hairs. Scratching scores for the control and the plain AzA hydrogel-based group were 55.01 ± 0.09 and 15.01 ± 0.16, respectively. In the second week of the experiment with calcipotriol-induced AD Wistar rats, the scratching score considerably decreased after a dose of AzA-SNEDDS hydrogel (from 30.43 ± 0.34 to 6.57 ± 1.83) as shown in Fig. 9b. However, after receiving a high dose of plain AzA hydrogel, the scratching score went up. This demonstrates that, when compared to the dose of AzA hydrogel, the dose of AzA-SNEDDDS hydrogel maintained AzA in various skin layers and had an immediate effect. As seen in Fig. 10a and b, low-dose of plain AzA hydrogel can

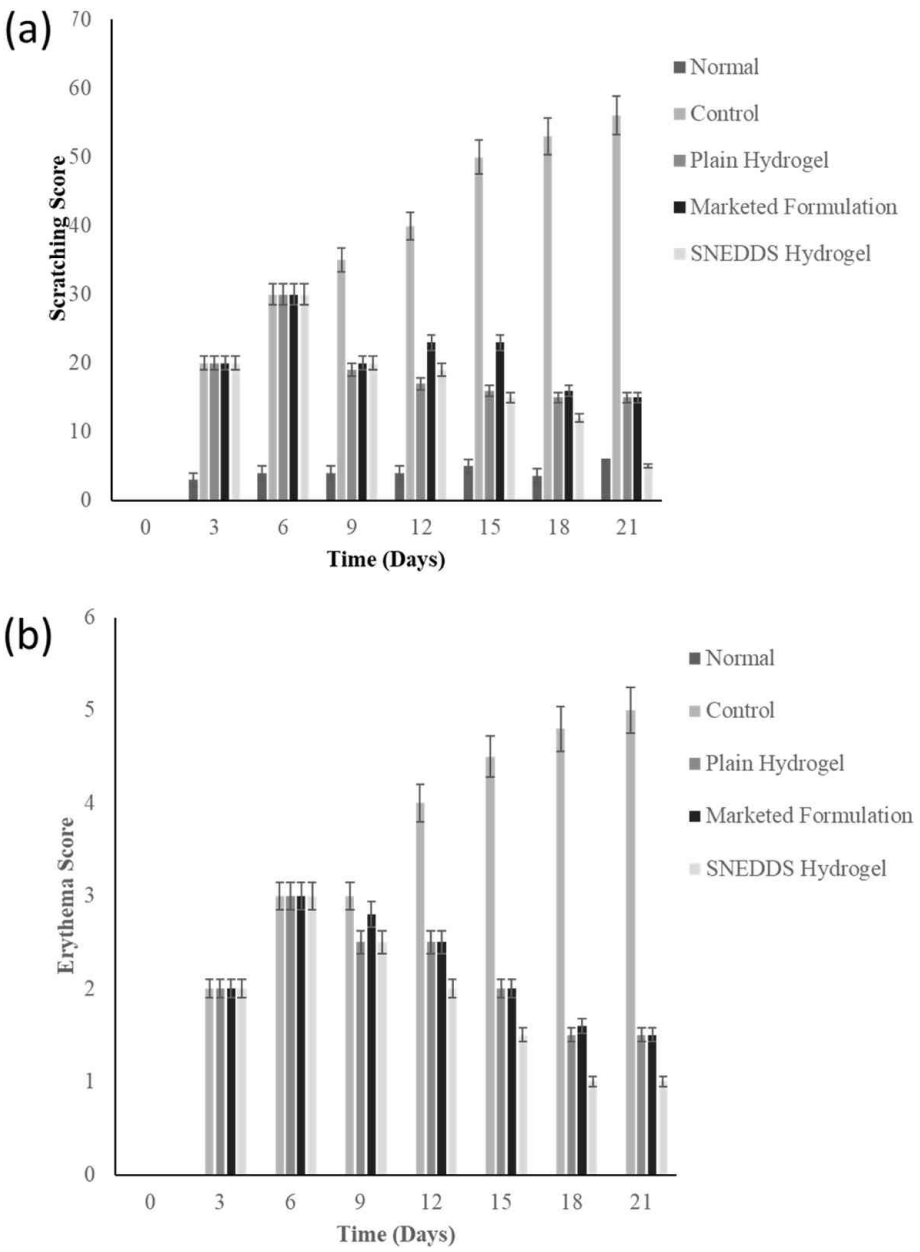

Fig. 10. Two weeks of treatment with AzA-SNEDDS hydrogel showed considerable skin recovery when compared to the marketed formulation, as demonstrated by reduced (a) Erythema score and (b) Scratching score (±SD, n = 3, $p < 0.5$).

reduce erythema and scratching scores to the same extent as the marketed formulation. Fig. 11 demonstrates how the clinical characteristics of the Wistar rat skin are covered.

3.8.2. Skin irritation study

Skin irritation is a significant problem for preparations that are administered topically. In this study, a histological examination of the skin after 24 h of administration was done to determine whether the intended formulations may irritate. As a positive control and negative control, the skin samples were exposed to 0.8% paraformaldehyde aqueous solution and distilled water, respectively. Fig. 12 shows the histological representation of the treated rat skin segment. The epidermal and dermal layers were delineated in the negative control (Fig. 12a), whereas the positive control displayed erythema, itching, minor edematous exfoliating subcutaneous layer (disruption and swelling in the inner layer of skin), the epidermal and dermal layer was even and lose texture of collagen in dermis layer (reduce thickness and stiffness of skin) (Fig. 12b). The marketed product showed a mild edematous exfoliation of the subcutaneous layer (Fig. 12c). Negligible erythema and edema were observed in the blank (Fig. 12d) and drug-loaded SNEDDS formulation-treated skin segments (Fig. 12e), when compared to the skin sections treated with distilled water in Fig. 12b. Based on the findings, it seemed that the developed SNEDDS formulation was a secure vehicle for the topical application of AzA.

3.8.3. Histopathological examination

According to a negative control group (Fig. 13a), the histological analysis of healthy Wistar rat skin revealed a homogenous epidermis and dermis along with a healthy capillary loop. The literature states that AD is thought to develop when the body's immune system sets off aberrant or excessively active inflammatory reactions in the epidermis and dermis. The histological skin segment from the positive control group that received calcipotriol treatment showed all of these alterations. The positive control group (Fig. 13b) depicts the localized haemorrhage,

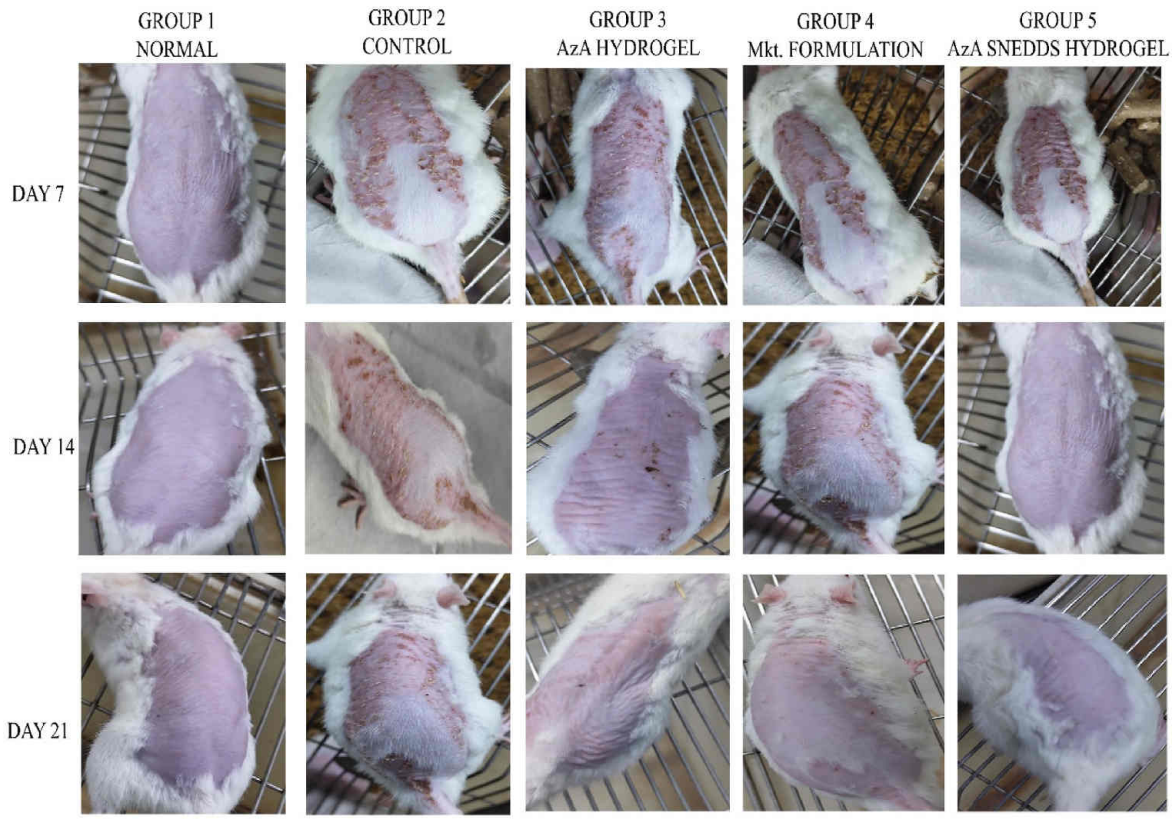

Fig. 11. Clinical characteristics of Wistar rat skin following topical administration of AzA-hydrogel, marketed formulation and AzA-SNEDDS hydrogel on calcipotriol-induced atopic dermatitis.

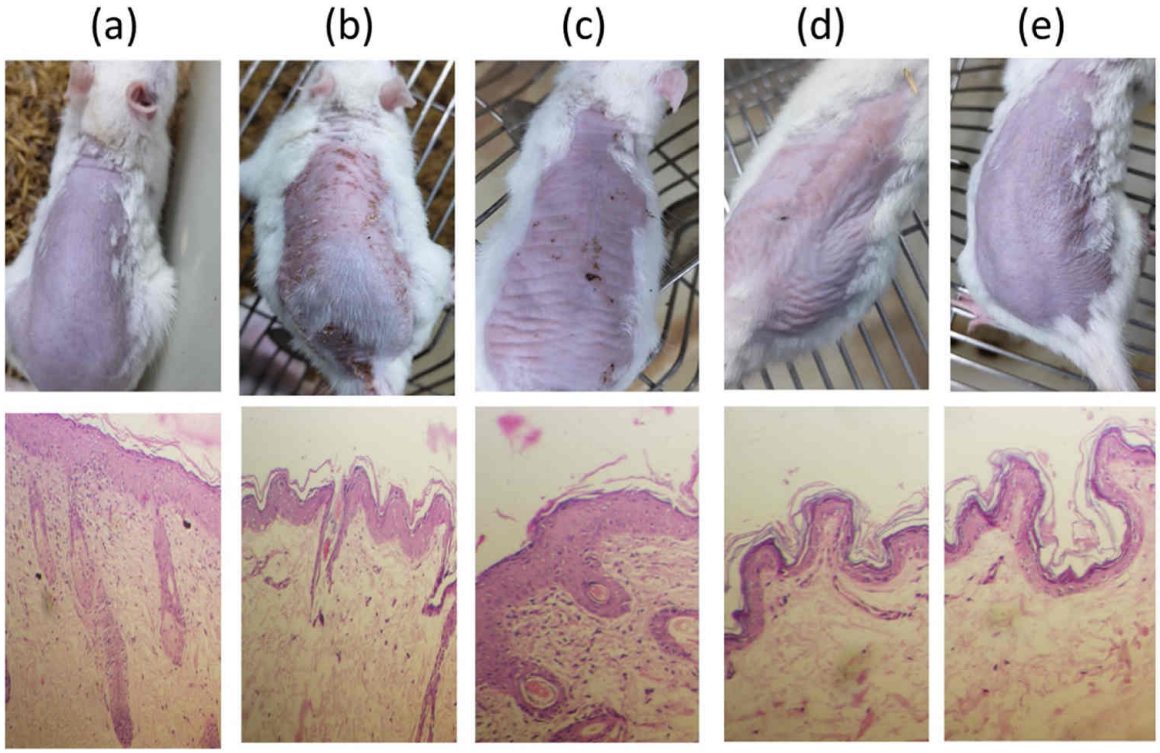

Fig. 12. The pictures of rat skin sections treated in various ways and seen below a light microscope (a) Negative control group demonstrating intact skin and integrity; (b) Positive control group that had been exposed to paraformaldehyde showed slightly exfoliated skin and the dermis' collagen had a looser texture; (c) Marketed formulation treated group skin showed minor exfoliation of edema; (d) SNEDDS hydrogel treated group showed negligible erythema and edema; (e) AzA-SNEDDS hydrogel treated group displaying well delineated epidermal and dermal layers.

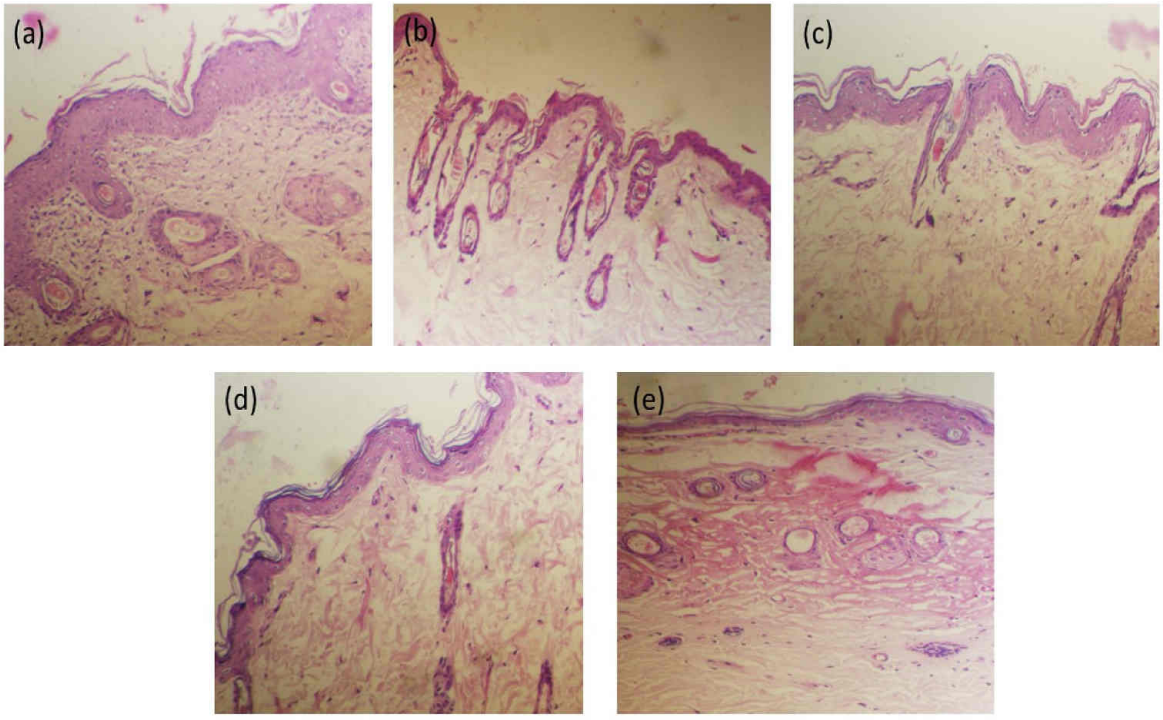

Fig. 13. Histopathology of (a) Negative control group; (b) Positive control group (induced by calcipotriol); (c) Plain AzA-hydrogel treated group; (d) Marketed formulation treated group; (e) AzA-SNEDDS hydrogel treated group.

leukocytes in the muscle and dermis, inflammatory cell infiltration, and a modest layer of compact hyperkeratosis. The control group likewise displayed focal interface dermatitis with persistent inflammation and a thick dermal layer. As seen in Fig. 13c, the AzA hydrogel-treated group displayed recovered epidermis and dermis cell structure, but no change was seen in the skin appendages or focal acanthosis, and leukocytes were not seen. Concurrently, AzA hydrogel-treated group (Fig. 13c) from the histological section demonstrates that the epidermal layer grew noticeably thinner and that the number of inflammatory cell nuclei also decreased. Similar skin healing improvements and substantially enhanced hair growth are shown in Fig. 13c. Rats were given a marketed formulation and exhibited minor infiltration of inflammatory cells and the presence of leukocytes in subcutaneous adipose tissue. Additionally, a foreign body granuloma was visible in the skin's dermis (Fig. 13d). The epidermal and dermal layers were even and uninterrupted in the Wistar rat's skin that had received the AzA-SNEDDS hydrogel. In addition, as shown in Fig. 13e, the group resulted in a thinner epidermis and reduced infiltration of inflammatory cells in subcutaneous adipose tissue. The scratching and erythema scores shown in Fig. 10 were supported by the histology data that were seen.

4. Conclusion

In this research, AzA-loaded SNEDDS hydrogel was successfully developed for the topical delivery of drugs in the management of AD. AzA is an anti-inflammatory drug with low skin penetration, which reduces its therapeutic efficacy and raises the intensity of skin irritants. The SNEDDS formulations are effective in treating various skin diseases. They provide higher skin permeation, which enhances the topical action and skin retention. The development of SNEDDS formulation was optimized using a pseudoternary phase diagram. The ideal SNEDDS formulation included labrasol as an optimized oil phase, PEG 400 as a cosurfactant, and Tween 80 as a surfactant. The polydispersity index of the optimized preparation was found to be less than 0.5, and the size of the distributed globules was found to be 151.20 ± 3.67 nm. AzA-SNEDDS containing hydrogel for topical administration was developed using Carbopol 940 as a gelling agent. The prepared SNEDDS hydrogel's texture analysis, spreadability, viscosity, and pH were all deemed acceptable and suited for topical application. Additionally, it was discovered that the produced SNEDDS hydrogel of AzA activity is better than the plain hydrogel of AzA and marketed formulation in terms of *in vitro* release rate and anti-inflammatory action. Comparatively to the plain AzA hydrogel, the SNEDDS improved AzA penetration into the epidermal layers. When compared to the marketed formulation, the *ex vivo* skin permeability of AzA from the produced SNEDDS was shown to be greater; as a result, there was a 35.91 ± 0.19% increased flux with AzA-SNEDDS hydrogel. Additionally, the histological examination showed that the skin of the experimental animals had no signs of toxicity, indicating that the formulation could be administered topically safely, and effectively. In conclusion, the developed AzA-SNEDDS hydrogel formulation can be employed as a potential carrier for the treatment of inflammation and AD.

Credit author statement

N.P., and A.S. performed the experiment. N.M. S.A. and S.W. help in the revision of the manuscript. P.K. develop the concept, proofread the article and supervise to complete it.

Declaration of competing interest

The authors declare that they have no known competing financial interests or personal relationships that could have appeared to influence the work reported in this paper.

Data availability

The data that has been used is confidential.

Acknowledgement

The authors (Sivakumar Annadurai and Shadma Wahab) extend

their appreciation to the Deanship of Scientific Research at King Khalid University for funding this work through Small group Research Project under grant number RGP1/220/44. The author (Prashant Kesharwani) acknowledges financial support from the Indian Council of Medical Research (ICMR), New Delhi, India, through Extramural Research Grants.

References

Ahad, A., Al-Saleh, A.A., Al-Mohizea, A.M., Al-Jenoobi, F.I., Raish, M., Yassin, A.E.B., Alam, M.A., 2017. Pharmacodynamic study of eprosartan mesylate-loaded transfersomes Carbopol® gel under Dermaroller® on rats with methyl prednisolone acetate-induced hypertension. Biomed. Pharmacother. 89, 177–184. https://doi.org/10.1016/j.biopha.2017.01.164.

Ahamed, J., Jaswanth Gowda, B.H., Almalki, W.H., Gupta, N., Sahebkar, A., Kesharwani, P., 2023. Recent advances in nanoparticle-based approaches for the treatment of brain tumors: opportunities and challenges. Eur. Polym. J. 193, 112111 https://doi.org/10.1016/J.EURPOLYMJ.2023.112111.

Ahmad, N., Ahmad, F.J., Bedi, S., Sharma, S., Umar, S., Ansari, M.A., 2019. A novel Nanoformulation Development of Eugenol and their treatment in inflammation and periodontitis. Saudi Pharm. J. SPJ Off. Publ. Saudi Pharm. Soc. 27, 778–790. https://doi.org/10.1016/J.JSPS.2019.04.014.

Ahmed, E.M., 2015. Hydrogel: preparation, characterization, and applications: a review. J. Adv. Res. 6, 105–121. https://doi.org/10.1016/J.JARE.2013.07.006.

Akamatsu, H., Komura, J., Asada, Y., Miyachi, Y., Niwa, Y., 1991. Inhibitory effect of azelaic acid on neutrophil functions: a possible cause for its efficacy in treating pathogenetically unrelated diseases. Arch. Dermatol. Res. 283, 162–166. https://doi.org/10.1007/BF00372056.

Akhtar, N., Verma, A., Pathak, K., 2017. Exploring preclinical and clinical effectiveness of nanoformulations in the treatment of atopic dermatitis: safety aspects and patent reviews. Bull. Fac. Pharmacy, Cairo Univ. 55, 1–10. https://doi.org/10.1016/J.BFOPCU.2016.12.003.

Al-Suwayeh, S.A., Taha, E.I., Al-Qahtani, F.M., Ahmed, M.O., Badran, M.M., 2014. Evaluation of skin permeation and analgesic activity effects of carbopol lornoxicam topical gels containing penetration enhancer. Sci. World J. https://doi.org/10.1155/2014/127495, 2014.

Alam, M.S., Ali, M.S., Alam, N., Siddiqui, M.R., Shamim, M., Safhi, M.M., 2013. In vivo study of clobetasol propionate loaded nanoemulsion for topical application in psoriasis and atopic dermatitis. Drug Invent. Today 5, 8–12. https://doi.org/10.1016/J.DIT.2013.02.001.

Atef, E., Belmonte, A.A., 2008. Formulation and in vitro and in vivo characterization of a phenytoin self-emulsifying drug delivery system (SEDDS). Eur. J. Pharm. Sci. 35, 257–263. https://doi.org/10.1016/J.EJPS.2008.07.004.

Aytekin, M., Gursoy, R.N., Ide, S., Soylu, E.H., Hekimoglu, S., 2013. Formulation and Characterization of Liquid Crystal Systems Containing Azelaic Acid for Topical Delivery, pp. 228–239. https://doi.org/10.3109/03639045.2012.671829.

Azelaic Acid: Evidence-based Update on Mechanism of Action and Clinical Application - JDDonline - Journal of Drugs in Dermatology [WWW Document], (n.d).

Aziz Hazari, S., Kaur, H., Karwasra, R., Abourehab, M.A.S., Ali Khan, A., Kesharwani, P., 2023. An overview of topical lipid-based and polymer-based nanocarriers for treatment of psoriasis. Int. J. Pharm. 638, 122938 https://doi.org/10.1016/J.IJPHARM.2023.122938.

Bağcı, I.S., Aoki, R., Krammer, S., Ruzicka, T., Sárdy, M., Hartmann, D., 2019. Ex vivo confocal laser scanning microscopy: an innovative method for direct immunofluorescence of cutaneous vasculitis. J. Biophot. 12 https://doi.org/10.1002/JBIO.201800425.

Bahadur, S., Yadu, K., Baghel, P., Naurange, T., Sahu, M., 2020. Review of formulation and evaluation of self-micro emulsifying drug delivery system (Smedds). Sci. Pharm. Sci. 26, 25–35. https://doi.org/10.15587/2519-4852.2020.210825.

Bajaj, J., Sharma, D., 2015. Formulation and evaluation of topical azelaic acid gel. Available online Pharm. Res. (N. Y.) 7, 616–620. J. Chem.

Balakumar, K., Raghavan, C.V., selvan, N.T., prasad, R.H., Abdu, S., 2013. Self nanoemulsifying drug delivery system (SNEDDS) of rosuvastatin calcium: design, formulation, bioavailability and pharmacokinetic evaluation. Colloids Surf. B Biointerfaces 112, 337–343. https://doi.org/10.1016/J.COLSURFB.2013.08.025.

Bladon, P.T., Burke, B.M., Cunliffe, W.J., Forster, R.A., Holland, K.T., King, K., 1986. Topical azelaic acid and the treatment of acne: a clinical and laboratory comparison with oral tetracycline. Br. J. Dermatol. 114, 493–499. https://doi.org/10.1111/J.1365-2133.1986.TB02856.X.

Boguniewicz, M., Alexis, A.F., Beck, L.A., Block, J., Eichenfield, L.F., Fonacier, L., Guttman-Yassky, E., Paller, A.S., Pariser, D., Silverberg, J.I., Lebwohl, M., 2017. Expert perspectives on management of moderate-to-severe atopic dermatitis: a multidisciplinary consensus addressing current and emerging therapies. J. Allergy Clin. Immunol. Pract. 5, 1519–1531. https://doi.org/10.1016/J.JAIP.2017.08.005.

Chandra, J., Molugulu, N., Annadurai, S., Wahab, S., Karwasra, R., Singh, S., Shukla, R., Kesharwani, P., 2023. Hyaluronic acid-functionalized lipoplexes and polyplexes as emerging nanocarriers for receptor-targeted cancer therapy. Environ. Res. 233, 116506 https://doi.org/10.1016/J.ENVRES.2023.116506.

Chu, Z., Xu, Q., Zhu, Q., Ma, X., Mo, J., Lin, G., Zhao, Y., Gu, Y., Bian, L., Shao, L., Guo, J., Ye, W., Li, J., He, G., Xu, Y., 2021. Design, synthesis and biological evaluation of novel benzoxaborole derivatives as potent PDE4 inhibitors for topical treatment of atopic dermatitis. Eur. J. Med. Chem. 213 https://doi.org/10.1016/J.EJMECH.2021.113171.

Chudasama, A, Patel, V, Nivsarkar, M, Vasu, K, Shishoo, C, n.d.. A Novel Lipid-based Oral Drug Delivery System of Nevirapine. Int. J. PharmTech Res. 3 (2), 1159–1168.

Cláudia Paiva-Santos, A., Gama, M., Peixoto, D., Sousa-Oliveira, I., Ferreira-Faria, I., Zeinali, M., Abbaspour-Ravasjani, S., Mascarenhas-Melo, F., Hamishehkar, H., Veiga, F., 2022. Nanocarrier-based dermopharmaceutical formulations for the topical management of atopic dermatitis. Int. J. Pharm. 618 https://doi.org/10.1016/J.IJPHARM.2022.121656.

Cong, Y., Fu, J., 2022. Hydrogel-tissue interface interactions for implantable flexible bioelectronics. Langmuir 38, 11503–11513. https://doi.org/10.1021/ACS.LANGMUIR.2C01674.

Dall'Oglio, F., Tedeschi, A., Lacarrubba, F., Fabbrocini, G., Skroza, N., Chiodini, P., Micali, G., 2021. A novel azelaic acid formulation for the topical treatment of inflammatory rosacea: a multicentre, prospective clinical trial. J. Cosmet. Dermatol. 20, 28. https://doi.org/10.1111/JOCD.14098.

Damiani, G., Eggenhöffner, R., Pigatto, P.D.M., Bragazzi, N.L., 2019. Nanotechnology meets atopic dermatitis: current solutions, challenges and future prospects. Insights and implications from a systematic review of the literature. Bioact. Mater. 4, 380–386. https://doi.org/10.1016/J.BIOACTMAT.2019.11.003.

Date, A.A., Nagarsenker, M.S., 2007. Design and evaluation of self-nanoemulsifying drug delivery systems (SNEDDS) for cefpodoxime proxetil. Int. J. Pharm. 329, 166–172. https://doi.org/10.1016/J.IJPHARM.2006.08.038.

Dongsar, T.T., Dongsar, T.S., Gupta, N., Almalki, W.H., Sahebkar, A., Kesharwani, P., 2023. Emerging potential of 5-Fluorouracil-loaded chitosan nanoparticles in cancer therapy. J. Drug Deliv. Sci. Technol. 82, 104371 https://doi.org/10.1016/J.JDDST.2023.104371.

Elnaggar, Y.S.R., El-Massik, M.A., Abdallah, O.Y., 2009. Self-nanoemulsifying drug delivery systems of tamoxifen citrate: design and optimization. Int. J. Pharm. 380, 133–141. https://doi.org/10.1016/J.IJPHARM.2009.07.015.

Espinoza, L.C., Vera-García, R., Silva-Abreu, M., Domènech, Ò., Badia, J., Rodríguez-Lagunas, M.J., Clares, B., Calpena, A.C., 2020. Topical pioglitazone nanoformulation for the treatment of atopic dermatitis: design, characterization and efficacy in hairless mouse model. Pharm. Times 12 (255 12), 255. https://doi.org/10.3390/PHARMACEUTICS12030255, 2020.

Fitton, A., Goa, K.L., 1991. Azelaic acid. A review of its pharmacological properties and therapeutic efficacy in acne and hyperpigmentary skin disorders. Drugs 41, 780–798. https://doi.org/10.2165/00003495-199141050-00007.

Hasan, N., Imran, M., Sheikh, A., Tiwari, N., Jaimini, A., Kesharwani, P., Jain, G.K., Ahmad, F.J., 2023. Advanced multifunctional nano-lipid carrier loaded gel for targeted delivery of 5-flurouracil and cannabidiol against non-melanoma skin cancer. Environ. Res. 233, 116454 https://doi.org/10.1016/J.ENVRES.2023.116454.

Hong, L., Zhou, C.L., Chen, F.P., Han, D., Wang, C.Y., Li, J.X., Chi, Z., Liu, C.G., 2017. Development of a Carboxymethyl Chitosan Functionalized Nanoemulsion Formulation for Increasing Aqueous Solubility, Stability and Skin Permeability of Astaxanthin Using Low-Energy Method, pp. 707–721. https://doi.org/10.1080/02652048.2017.1373154.

Hu, F., Shi, X., Wang, H., Nan, N., Wang, K., Wei, S., Li, Z., Jiang, S., Hu, H., Zhao, S., 2021. Is health contagious?—based on empirical evidence from China family panel studies' data. Front. Public Heal. 9, 691746 https://doi.org/10.3389/FPUBH.2021.691746/BIBTEX.

Huang, C., Dong, L., Zhao, B., Lu, Y., Huang, S., Yuan, Z., Luo, G., Xu, Y., Qian, W., 2022. Anti-inflammatory hydrogel dressings and skin wound healing. Clin. Transl. Med. 12 https://doi.org/10.1002/CTM2.1094.

Hung, W.H., Chen, P.K., Fang, C.W., Lin, Y.C., Wu, P.C., 2021. Preparation and evaluation of azelaic acid topical microemulsion formulation: in vitro and in vivo study. Pharmaceutics 13. https://doi.org/10.3390/PHARMACEUTICS13030410.

Hurler, J., Engesland, A., Poorahmary Kermany, B., Škalko-Basnet, N., 2012. Improved texture analysis for hydrogel characterization: gel cohesiveness, adhesiveness, and hardness. J. Appl. Polym. Sci. 125, 180–188. https://doi.org/10.1002/APP.35414.

Imokawa, G., Nakajima, H., Ishida, K., 2015. Biological mechanisms underlying the ultraviolet radiation-induced formation of skin wrinkling and sagging II: over-expression of neprilysin plays an essential role. Int. J. Mol. Sci. 16, 7776–7795. https://doi.org/10.3390/ijms16047776.

Indrati, O., Martien, R., Rohman, A., Nugroho, A.K., 2020. Development of nanoemulsion-based hydrogel containing andrographolide: physical properties and stability evaluation. J. Pharm. BioAllied Sci. 12, S816–S820. https://doi.org/10.4103/JPBS.JPBS_174_20.

Iqubal, M.K., Iqubal, A., Imtiyaz, K., Rizvi, M.M.A., Gupta, M.M., Ali, J., Baboota, S., 2021. Combinatorial lipid-nanosystem for dermal delivery of 5-fluorouracil and resveratrol against skin cancer: delineation of improved dermatokinetics and epidermal drug deposition enhancement analysis. Eur. J. Pharm. Biopharm. 163, 223–239. https://doi.org/10.1016/j.ejpb.2021.04.007.

Jacobus Berlitz, S., De Villa, D., Maschmann Inácio, L.A., Davies, S., Zatta, K.C., Guterres, S.S., Külkamp-Guerreiro, I.C., 2019. Azelaic acid-loaded nanoemulsion with hyaluronic acid - a new strategy to treat hyperpigmentary skin disorders. Drug Dev. Ind. Pharm. 45, 642–650. https://doi.org/10.1080/03639045.2019.1569032.

Jain, A.K., Jain, S., Abourehab, M.A.S., Mehta, P., Kesharwani, P., 2022. An insight on topically applied formulations for management of various skin disorders. J. Biomater. Sci. Polym. Ed. 1–27. https://doi.org/10.1080/09205063.2022.2103625.

Karimi-Maleh, H., Khataee, A., Karimi, F., Baghayeri, M., Fu, L., Rouhi, J., Karaman, C., Karaman, O., Boukherroub, R., 2022. A green and sensitive guanine-based DNA biosensor for idarubicin anticancer monitoring in biological samples: a simple and fast strategy for control of health quality in chemotherapy procedure confirmed by docking investigation. Chemosphere 291, 132928. https://doi.org/10.1016/J.CHEMOSPHERE.2021.132928.

Kasprzak, J.M., Xu, Y.G., 2015. Diagnosis and management of lentigo maligna: a review. Drugs Context 4. https://doi.org/10.7573/DIC.212281.
Kaur, H., Kesharwani, P., 2021. Advanced nanomedicine approaches applied for treatment of skin carcinoma. J. Control. Release 337, 589–611. https://doi.org/10.1016/J.JCONREL.2021.08.003.
Kazi, M., Alqahtani, A., Alharbi, M., Ahmad, A., Hussain, M.D., Alothaid, H., Aldughaim, M.S., 2023. The development and optimization of lipid-based self-nanoemulsifying drug delivery systems for the intravenous delivery of propofol. Molecules 28. https://doi.org/10.3390/molecules28031492.
Kesharwani, P., Jain, K., Jain, N.K., 2014. Dendrimer as nanocarrier for drug delivery. Prog. Polym. Sci. https://doi.org/10.1016/j.progpolymsci.2013.07.005.
Kesharwani, P., Ma, R., Sang, L., Fatima, M., Sheikh, A., Abourehab, M.A.S., Gupta, N., Chen, Z.-S., Zhou, Y., 2023a. Gold nanoparticles and gold nanorods in the landscape of cancer therapy. Mol. Cancer 221 (22), 1–31. https://doi.org/10.1186/S12943-023-01798-8, 2023a.
Kesharwani, P., Sheikh, A., Abourehab, M.A.S., Salve, R., Gajbhiye, V., 2023b. A combinatorial delivery of survivin targeted siRNA using cancer selective nanoparticles for triple negative breast cancer therapy. J. Drug Deliv. Sci. Technol. 80, 104164 https://doi.org/10.1016/J.JDDST.2023.104164.
Khan, M., Ali, M., Shah, W., Shah, A., Yasinzai, M.M., 2019. Curcumin-loaded self-emulsifying drug delivery system (cu-SEDDS): a promising approach for the control of primary pathogen and secondary bacterial infections in cutaneous leishmaniasis. Appl. Microbiol. Biotechnol. 10318 103, 7481–7490. https://doi.org/10.1007/S00253-019-09990-X, 2019.
Kumari, S., Choudhary, P.K., Shukla, R., Sahebkar, A., Kesharwani, P., 2022. Recent advances in nanotechnology based combination drug therapy for skin cancer. J. Biomater. Sci. Polym. Ed. 1–34. https://doi.org/10.1080/09205063.2022.2054399.
Marzuki, N.H.C., Wahab, R.A., Hamid, M.A., 2019. An overview of nanoemulsion: concepts of dev. cosmeceutical applications 33, 779–797. https://doi.org/10.1080/13102818.2019.1620124.
Md, S., Alhakamy, N.A., Aldawsari, H.M., Kotta, S., Ahmad, J., Akhter, S., Alam, M.S., Khan, M.A., Awan, Z., Sivakumar, P.M., 2020. Improved analgesic and anti-inflammatory effect of diclofenac sodium by topical nanoemulgel: formulation development—in vitro and in vivo studies. J. Chem. https://doi.org/10.1155/2020/4071818, 2020.
Mohammadpour, A., Karami, N., Zabihi, R., Fazeliyan, E., Abbasi, A., Karimi, S., Barbosa de Farias, M., Adeodato Vieira, M.G., Shahsavani, E., Mousavi Khaneghah, A., 2023. Green synthesis, characterization, and application of Fe3O4 nanoparticles for methylene blue removal: RSM optimization, kinetic, isothermal studies, and molecular simulation. Environ. Res. 225, 115507 https://doi.org/10.1016/J.ENVRES.2023.115507.
Nasr, A., Gardouh, A., Ghorab, M., 2016. Novel solid self-nanoemulsifying drug delivery system (S-SNEDDS) for oral delivery of olmesartan medoxomil: design, formulation, pharmacokinetic and bioavailability evaluation. Pharmaceutics 8. https://doi.org/10.3390/pharmaceutics8030020.
Nguyen, Q.H., Bui, T.P., 1995. Azelaic acid: pharmacokinetic and pharmacodynamic properties and its therapeutic role in hyperpigmentary disorders and acne. Int. J. Dermatol. 34, 75–84. https://doi.org/10.1111/J.1365-4362.1995.TB03583.X.
Nodehi, M., Baghayeri, M., Veisi, H., 2021. Preparation of GO/Fe3O4@PMDA/AuNPs nanocomposite for simultaneous determination of As3+ and Cu2+ by stripping voltammetry. Talanta 230, 122288. https://doi.org/10.1016/J.TALANTA.2021.122288.
Ojha, B., Jain, V.K., Gupta, S., Talegaonkar, S., Jain, K., 2022. Nanoemulgel: a promising novel formulation for treatment of skin ailments. Polym. Bull. 79, 4441–4465. https://doi.org/10.1007/S00289-021-03729-3/METRICS.
Parveen, N., Abourehab, M.A.S., Thanikachalam, P.V., Khar, R.K., Kesharwani, P., 2023a. Nanocrystals as an emerging nanocarrier for the management of dermatological diseases. Colloids Surf. B Biointerfaces 225, 113231. https://doi.org/10.1016/J.COLSURFB.2023.113231.
Parveen, N., Sheikh, A., Abourehab, M.A.S., Karwasra, R., Singh, S., Kesharwani, P., 2023b. Self-nanoemulsifying drug delivery system for pancreatic cancer. Eur. Polym. J. 190, 111993 https://doi.org/10.1016/J.EURPOLYMJ.2023.111993.
Passi, S., Picardo, M., Zompetta, C., Luca, C. de, Breathnach, A.S., Nazzaro-porro, M., 1991. The oxyradical-scavenging activity of azelaic acid in biological systems. Free Radic. Res. Commun. 15, 17–28. https://doi.org/10.3109/10715769109049121.
Patel, A.R., Vavia, P.R., 2007. Preparation and in vivo evaluation of SMEDDS (self-microemulsifying drug delivery system) containing fenofibrate. AAPS J. 9, E344–E352. https://doi.org/10.1208/aapsj0903041.
Ponto, T., Latter, G., Luna, G., Leite-Silva, V.R., Wright, A., Benson, H.A.E., 2021. Novel self-nano-emulsifying drug delivery systems containing astaxanthin for topical skin delivery. Pharmaceutics 13. https://doi.org/10.3390/PHARMACEUTICS13050649.
Pople, P.V., Singh, K.K., 2010. Targeting tacrolimus to deeper layers of skin with improved safety for treatment of atopic dermatitis. Int. J. Pharm. 398, 165–178. https://doi.org/10.1016/J.IJPHARM.2010.07.008.
Pratiwi, L., Fudholi, A., Martien, R., Pramono, S., 2017. Self-nanoemulsifying drug delivery system (snedds) for topical delivery of mangosteen peels (Garcinia mangostana L.,): formulation design and in vitro studies. J. Young Pharm. 9, 341–346. https://doi.org/10.5530/JYP.2017.9.68.
Qin, W., Chandra, J., Abourehab, M.A.S., Gupta, N., Chen, Z.S., Kesharwani, P., Cao, H. L., 2023. New opportunities for RGD-engineered metal nanoparticles in cancer. Mol. Cancer 22, 87. https://doi.org/10.1186/S12943-023-01784-0/FIGURES/8.
Rathore, C., Hemrajani, C., Sharma, A.K., Gupta, P.K., Jha, N.K., Aljabali, A.A.A., Gupta, G., Singh, S.K., Yang, J.C., Dwivedi, R.P., Dua, K., Chellappan, D.K., Negi, P., Tambuwala, M.M., 2023. Self-nanoemulsifying drug delivery system (SNEDDS) mediated improved oral bioavailability of thymoquinone: optimization, characterization, pharmacokinetic, and hepatotoxicity studies. Drug Deliv. Transl. Res. 13, 292–307. https://doi.org/10.1007/S13346-022-01193-8/FIGURES/12.
Safitri, F.I., Nawangsari, D., Febrina, D., 2021. Overview: Application of Carbopol 940 in Gel. https://doi.org/10.2991/AHSR.K.210127.018.
Salimi, A., Zadeh, B.S.M., Godazgari, S., Rahdar, A., 2020. Development and evaluation of azelaic acid-loaded microemulsion for transfollicular drug delivery through Guinea pig skin: a mechanistic study. Adv. Pharm. Bull. 10, 239–246. https://doi.org/10.34172/APB.2020.028.
Schäkel, K., Döbel, T., Bosselmann, I., 2014. Future treatment options for atopic dermatitis - small molecules and beyond. J. Dermatol. Sci. 73, 91–100. https://doi.org/10.1016/j.jdermsci.2013.11.009.
Schaller, M., Sebastian, M., Ress, C., Seidel, D., Hennig, M., 2016. A multicentre, randomized, single-blind, parallel-group study comparing the efficacy and tolerability of benzoyl peroxide 3%/clindamycin 1% with azelaic acid 20% in the topical treatment of mild-to-moderate acne vulgaris. J. Eur. Acad. Dermatology Venereol. 30, 966–973. https://doi.org/10.1111/jdv.13541.
Self-microemulsifying and microemulsion systems for transdermal delivery of indomethacin: Effect of Phase Transition - ScienceDirect [WWW Document], (n.d).
Shafiq, S., Shakeel, F., Talegaonkar, S., Ahmad, F.J., Khar, R.K., Ali, M., 2007. Development and bioavailability assessment of ramipril nanoemulsion formulation. Eur. J. Pharm. Biopharm. 66, 227–243. https://doi.org/10.1016/j.ejpb.2006.10.014.
Sharifi, F., Jahangiri, M., Nazir, I., Asim, M.H., Ebrahimnejad, P., Hupfauf, A., Gust, R., Bernkop-Schnürch, A., 2021. Zeta potential changing nanoemulsions based on a simple zwitterion. J. Colloid Interface Sci. 585, 126–137. https://doi.org/10.1016/J.JCIS.2020.11.054.
Silverberg, J.I., 2020. Atopic dermatitis in adults. Med. Clin. North Am. 104, 157–176. https://doi.org/10.1016/J.MCNA.2019.08.009.
Song, Z., Wen, Y., Teng, F., Wang, M., Liu, N., Feng, R., 2022. Carbopol 940 hydrogel containing curcumin-loaded micelles for skin delivery and application in inflammation treatment and wound healing. New J. Chem. 46, 3674–3686. https://doi.org/10.1039/D1NJ04719A.
Souto, E.B., Dias-Ferreira, J., Oliveira, J., Sanchez-Lopez, E., Lopez-Machado, A., Espina, M., Garcia, M.L., Souto, S.B., Martins-Gomes, C., Silva, A.M., 2019. Trends in atopic dermatitis—from standard pharmacotherapy to novel drug delivery systems, 2019 Int. J. Mol. Sci. 20. https://doi.org/10.3390/IJMS20225659, 5659 20, 5659.
Takiwaki, H., Tsuda, H., Arase, S., Takeichi, H., 2003. Differences between intrafollicular microorganism profiles in perioral and seborrhoeic dermatitis. Clin. Exp. Dermatol. 28, 531–534. https://doi.org/10.1046/J.1365-2230.2003.01349.X.
Thiboutot, D., 2008. Versatility of azelaic acid 15% gel in treatment of inflammatory acne vulgaris. J. Drugs Dermatology 7, 13–16.
Tiwari, N., Kumar, D., Priyadarshani, A., Jain, G.K., Mittal, G., Kesharwani, P., Aggarwal, G., 2023. Recent progress in polymeric biomaterials and their potential applications in skin regeneration and wound care management. J. Drug Deliv. Sci. Technol. 82, 104319 https://doi.org/10.1016/J.JDDST.2023.104319.
Try, C., Moulari, B., Béduneau, A., Fantini, O., Pin, D., Pellequer, Y., Lamprecht, A., 2016. Size dependent skin penetration of nanoparticles in murine and porcine dermatitis models. Eur. J. Pharm. Biopharm. 100, 101–108. https://doi.org/10.1016/J.EJPB.2016.01.002.
Ugur Kaplan, A.B., Cetin, M., Orgul, D., Taghizadehghalehjoughi, A., Hacımuftuoglu, A., Hekimoglu, S., 2019. Formulation and in vitro evaluation of topical nanoemulsion and nanoemulsion-based gels containing daidzein. J. Drug Deliv. Sci. Technol. 52, 189–203. https://doi.org/10.1016/J.JDDST.2019.04.027.
van Staden, D., du Plessis, J., Viljoen, J., 2020. Development of topical/transdermal self-emulsifying drug delivery systems, not as simple as expected, 2020 Sci. Pharm. 88, 17. https://doi.org/10.3390/SCIPHARM88020017, 17 88.
Xu, Z., Liu, G., Liu, P., Hu, Y., Chen, Y., Fang, Y., Sun, G., Huang, H., Wu, J., 2022. Hyaluronic acid-based glucose-responsive antioxidant hydrogel platform for enhanced diabetic wound repair. Acta Biomater. 147, 147–157. https://doi.org/10.1016/J.ACTBIO.2022.05.047.
Zeng, L., Gowda, B.H.J., Ahmed, M.G., Abourehab, M.A.S., Chen, Z.S., Zhang, C., Li, J., Kesharwani, P., 2023. Advancements in nanoparticle-based treatment approaches for skin cancer therapy. Mol. Cancer 1–50. https://doi.org/10.1186/S12943-022-01708-4, 2023 221 22.
Zhang, J., Shen, Q., Ma, Y., Liu, L., Jia, W., Chen, L., Xie, J., 2022. Calcium homeostasis in Parkinson's disease: from pathology to treatment. Neurosci. Bull. 38, 1267–1270. https://doi.org/10.1007/S12264-022-00899-6.
Zheng, J., Yue, R., Yang, R., Wu, Q., Wu, Y., Huang, M., Chen, Xu, Lin, W., Huang, J., Chen, Xiaodong, Jiang, Y., Yang, B., Liao, Y., 2022. Visualization of zika virus infection via a light-initiated bio-orthogonal cycloaddition labeling strategy. Front. Bioeng. Biotechnol. 10, 940511 https://doi.org/10.3389/FBIOE.2022.940511/BIBTEX.
Zhuo, F., Abourehab, M.A.S., Hussain, Z., 2018. Hyaluronic acid decorated tacrolimus-loaded nanoparticles: efficient approach to maximize dermal targeting and anti-dermatitis efficacy. Carbohydr. Polym. 197, 478–489. https://doi.org/10.1016/J.CARBPOL.2018.06.023.

Colloids and Surfaces B: Biointerfaces 234 (2024) 113728

Contents lists available at ScienceDirect

Colloids and Surfaces B: Biointerfaces

journal homepage: www.elsevier.com/locate/colsurfb

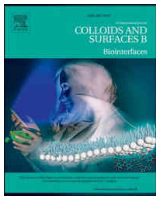

Hesperidin-loaded cubogel as a novel therapeutic armamentarium for full-thickness wound healing

Urushi Rehman [a], Afsana Sheikh [a], Abdulrhman Alsayari [b], Shadma Wahab [b], Prashant Kesharwani [a,*,1]

[a] Department of Pharmaceutics, School of Pharmaceutical Education and Research, Jamia Hamdard, New Delhi 110062, India
[b] Department of Pharmacognosy, College of Pharmacy, King Khalid University, Abha 61421, Saudi Arabia

ARTICLE INFO

Keywords:
Nanotechnology
Cubosomes
Wound healing
Hydrogel
Full-thickness wound

ABSTRACT

Wounds are a physical manifestation of injury to the skin causing it to rupture or tear. The process of wound healing naturally restores skin integrity while minimizing the extent of the damage. Hesperidin (HPN) is a natural polyphenolic flavonoid and is effective in treating wounds due to its ability to reduce inflammation and stimulate angiogenesis. However, its use is limited by its poor physicochemical attributes such as poor solubility in water. Recently, nanoparticles, particularly Cubosomes, are found to be promising candidates for advancing wound-healing therapies, owing to their unique properties. The present study was conducted to develop a hydrogel system based on Cubosomes encapsulating HPN (HPN-Cubogel), with the potential to mitigate full-thickness wounds. The therapeutic efficacy of the formulation assessed in the animal model showed that the HPN-Cubogel formulation group exhibited a wound closure rate of 98.96 ± 1.50% after 14 days post-wounding compared to 89.12 ± 2.6% in the control group suggesting superior wound contraction activity. Collagen synthesis was superior in the formulation compared to the control group, as determined through MT staining. In summary, the HPN-Cubogel formulation was found to be the most effective in enhancing full-thickness wound healing.

1. Introduction

The skin is a vital part of the human body that protects against a variety of biological and non-biological hazards such as damage; heat, cold, chronic illnesses, and infections [1–4]. Skin loss can occur due to a variety of factors, including trauma, surgery, burns, or serious wounds [5]. A wound is defined as an injury to living tissue or a tear in the top layer of the skin that disrupts the anatomical structure and function of the skin [6]. A full-thickness skin incision affects all skin layers, including subcutaneous tissue, and may reach muscle, soft tissue, or bone, resulting in a serious infection that offers considerable dangers [7]. Wound healing; is a complex process that is necessary for bodily homeostasis. Under normal conditions, the skin has self-healing properties, and lesions may be addressed with minimum scarring via four continuous phases: coagulation and hemostasis, inflammation, proliferation, and remodelling. Nonetheless, the wound-healing process can be influenced by a multitude of factors, such as age, sex hormones, auto-immune dysfunction, obesity, smoking, and various medical conditions. Additionally, environmental factors like heat, infections, and oxygen supply can impede the healing process [8–11]. Key players in the healing process include inflammatory cytokines, growth factors, extracellular matrix (ECM) components, and various cell types [12]. Skin wounds that are less than 1 mm in thickness can regenerate during the healing process. However, chronic wounds or full-thickness present formidable therapeutic challenges that can lead to persistent structural defects [13,14]. The amount of money spent on wound care, the loss of productivity for affected persons and their families, and their reduced quality of life all have a high societal cost [15]. It is estimated that 1–2% of the population in affluent nations suffer from chronic wounds at any time, and this number is projected to climb dramatically as the population ages [16]. The prevalence of chronic wounds is increasing, which is expected to significantly increase global wound care costs. The predicted cost is up to USD 18.7 billion by 2027, with chronic wound treatment receiving a sizable percentage of the healthcare budget [17].

* Corresponding author.
E-mail address: prashantdops@gmail.com (P. Kesharwani).
[1] https://scholar.google.com/citations?user=DJkvOAQAAAAJ&hl=en

https://doi.org/10.1016/j.colsurfb.2023.113728
Received 30 August 2023; Received in revised form 18 December 2023; Accepted 23 December 2023
Available online 26 December 2023
0927-7765/© 2023 Elsevier B.V. All rights reserved.

Skin grafting from xenograft, allograft, and autograft sources is being used to treat full-thickness wounds. Unfortunately, these procedures have drawbacks such as skin scarcity and graft rejection. Furthermore, conventional wound-care products face significant challenges, such as poor healing, insufficient scar formation, insufficient skin appendage formation, prolonged hospitalisation, and high manufacturing costs.

Therefore, complete wound healing is essential to offset the costs of wound healing treatments and prevent the progression of chronic wounds. Numerous studies have been conducted to identify effective approaches to accelerate the wound healing process [18]. Given the unique properties of nanoparticles, nanotechnology has emerged as a promising field for advancing wound-healing therapies [19–28]. Nanoparticles have sizes that typically fall within the range of 10 to 1000 nm [29]. Their biological properties are closely tied to their physical and chemical characteristics [30]. Integrating phytocompounds into nanocarriers is a novel technique to enhance their skin efficacy [31]. Because of their structure, biocompatibility, and resemblance to skin components, phospholipid vesicles are regarded as one of the most valuable and adaptable nanocarriers known, particularly for skin distribution [32,33]. Several studies have shown that compounds trapped in phospholipid vesicles have increased efficacy and can accumulate in deep skin layers when administered topically. To be helpful in wound healing, phytocompounds must infiltrate the skin adequately. Cubosomes, also known as cubic-phase nanoparticles, show considerable potential as an alternative to typical lipid vesicles, such as liposomes. These are lipid-based nanostructured aqueous dispersions generated by a highly organised spontaneous self-assembly process, resulting in dispersed particles ranging in size from 10–300 nm [34,35]. Owing to their unique geometry, cubosomes can effectively solubilize hydrophilic, hydrophobic, and amphiphilic drugs, making them promising candidates for drug nanocarriers. One of the most striking features of cubosomes is their bio-adhesive nature, which enhances their biocompatibility and reduces irritation. Furthermore, they are biodegradable in nature and exhibit remarkable thermodynamic stability over extended period [36]. By carefully selecting the right polymer, it is also possible to achieve controlled and targeted bioactive release from cubosomes [37]. Researchers have found similarities between the human skin bilayer and the cubic phase of the cubosome, which has led to improved lipid fluidity, enhanced drug skin permeability, and increased absorption and bioavailability [38]. Cubosomes, despite their promising attributes, come with certain drawbacks. The entrapment of water-soluble drugs is challenging due to the substantial water content within cubosomes. Large-scale production faces obstacles given their high viscosity, potentially leading to exorbitant viscosity during manufacturing. Moreover, there is a risk of leakage during storage or in vivo transmission. Exposure to the external environment may trigger a phase change in cubosomes. Additionally, if left undisturbed for an extended period, there is a possibility of particle growth. Notably, issues may arise in retaining polar drugs, underscoring the need for careful consideration of these limitations in the application of cubosomes [39–41]. In recent times, many natural compounds derived from plants have been utilized for treating various diseases. HPN is a natural polyphenolic flavonoid that occurs in citrus fruits like oranges and lemons. It possesses a range of therapeutic properties, such as anti-diabetic, anti-cancer, anti-inflammatory, and analgesic properties, among others. Several studies have shown that HPN can effectively treat wounds due to its anti-inflammatory, anti-bacterial, angiogenic, and antioxidant properties [42–44]. Nevertheless, its therapeutic use is restricted due to poor oral bioavailability (25%), poor solubility in water, and thermodynamic instability. As a result, topical application of HPN offers the advantage of targeted drug delivery, reduces total drug consumption, and improves therapeutic effectiveness by elevating and maintaining drug concentration at the site of action [45,46].

The optimal wound dressing should exhibit a trifecta of qualities - it must maintain moisture at the site, protect against infection, and expedite the recovery process [47]. Hydrogels are three-dimensional networks composed of hydrophilic polymers that expand and absorb when exposed to water. Owing to their flexibility, they create a protective barrier, assist in exudate removal, encapsulate bioactive compounds, and offer a moist milieu that promotes wound healing [48,49]. Hydrogels possess adjustable physical features, such as swelling and degradability, allowing them to control drug release rates, which makes them an advantageous vehicle for drug delivery in clinical settings [50–52]. In light of HPN's known properties, including its capacity to enhance collagen synthesis, prevent haemorrhages and infection, and exhibit anti-oxidative and anti-inflammatory characteristics, we aimed to develop a novel therapeutic approach by combining a hydrogel matrix with HPN-loaded cubosomes called as HPN-Cubogel. Through an in vivo evaluation, we examined the synergistic impact of this combination on the healing of full-thickness wounds. The key novelty of our research lies in investigating the topical application of HPN-Cubogel, in the context of wound healing studies. To the best of our knowledge, this specific approach has not been previously explored. Our study offers valuable insights into efficacy and potential application of this formulation for promoting full-thickness wound healing without any side effects.

2. Materials and methods

Please refer **supplementary file** for the detailed materials and methods.

3. Results and discussion

3.1. Preparation of HPN-cubosomes

A HPN-cubosome formulation was expertly prepared, incorporating Tween as a surfactant to coat the surface of the globules. This crucial step ensured that the droplets did not aggregate and were stabilized. In addition, the presence of Tween played a critical role as a stabilizer by creating particles that were readily dispersible in the aqueous medium. This is an essential characteristic that is often required in cubosomal dispersions to modify their surface properties and enhance their overall stability.

The prepared formulation was then integrated into a carbopol hydrogel, producing a homogenous HPN-Cubogel. This innovative hydrogel was designed to alleviate full-thickness wounds in an animal model. The loading of HPN into the Cubosomes was verified through multiple assessments, including entrapment efficiency, drug loading, and further analysis using Fourier Transform Infrared Spectroscopy (FTIR).

3.2. FTIR spectroscopy

The IR spectrum obtained of HPN in shown in Fig. 1-A. The FTIR spectra of pure drug HNP showed characteristic bands because of existence of different functional groups like, 3336, 2925, 1639, 1512, 1060 cm− 1 which could be attributed to O–H stretching vibration, C–H stretching, C═O stretching, C═C stretching and C–O stretching, respectively. The observed peak was found to be in close agreement with FTIR data reported earlier by Balakrishnan and colleagues [53]. The FT-IR spectra of the formulation displayed distinct absorption bands at various wavenumbers. The band observed at 2923 cm^{-1} corresponded to the C-H bending in the aromatic compound. The band at 1736.67 cm^{-1} indicated C═O stretching. Furthermore, the band observed at 1459.10 cm^{-1} was associated with the C-C stretching in the ring. The band at 1352.18 cm^{-1} resulted from O-H bending in the alcohol. Additionally, the 1086.30 cm^{-1} band represented C-O stretching in alkyl-substituted ether, while the 943.90 cm^{-1} band indicated C═C bending in alkene (Fig. 1-A). The FT-IR spectra of HPN-Cubosomes demonstrated that when HPN was made into Cubosomes, there was no substantial change in the functional groups or chemical structure. The

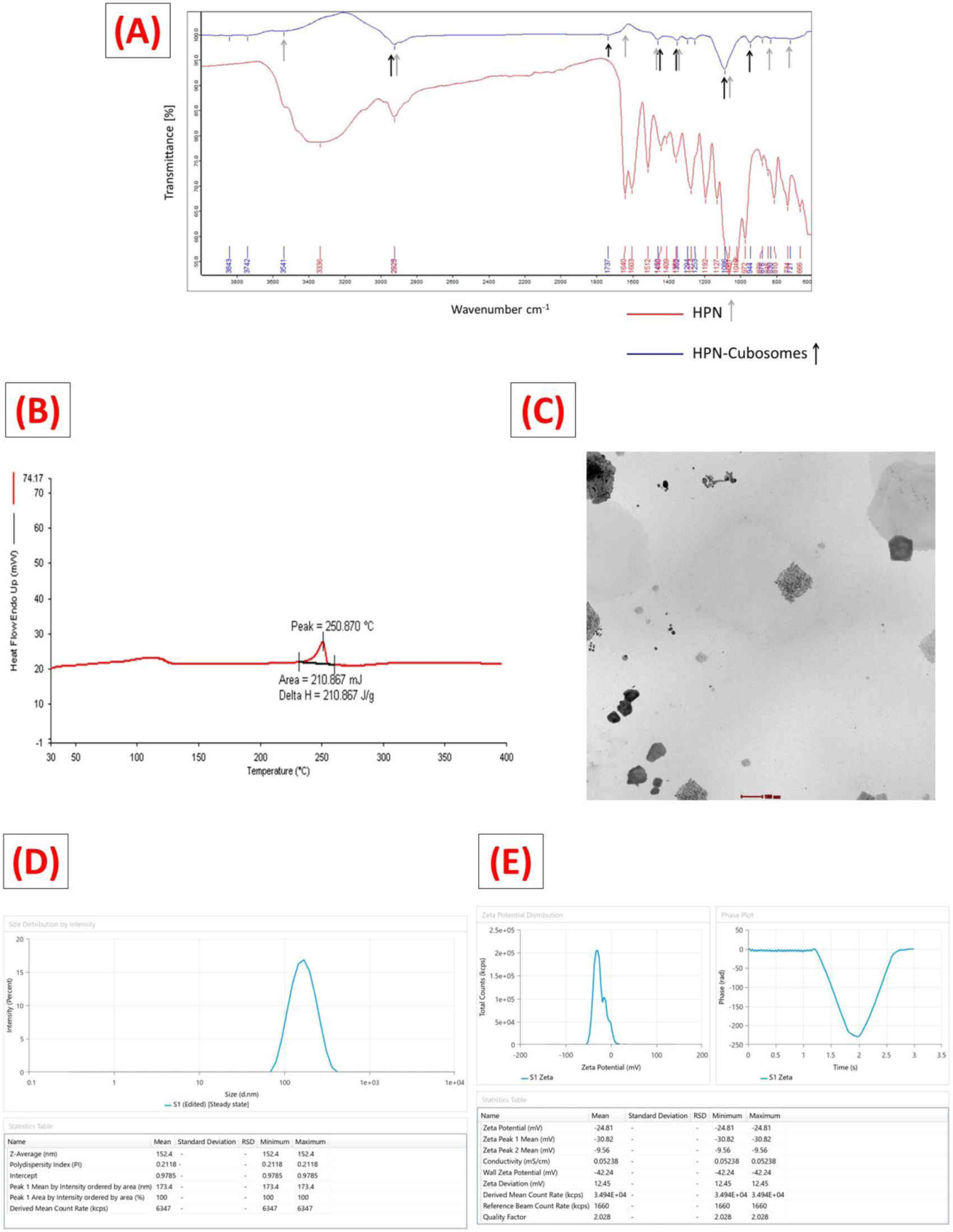

Fig. 1. (A) FTIR spectra of pure drug-Hesperidin and HPN-cubosomes, (B) DSC Thermogram of pure drug-Hesperidin, (C) TEM image showcasing particle morphology of HPN-cubosomes, (D) Mean Particle size and PDI of HPN-cubosomes and (E) Zeta Potential of HPN-cubosomes using Malvern Zetasizer.

existence of intermolecular hydrogen bonding might explain the minor discrepancy in wavenumber. This result indicates that no chemical interaction occurred between the drug and the excipients.

3.3. Differential Scanning Calorimetry (DSC)

The DSC thermogram of the drug sample displayed a sharp endothermic peak of at 250.870 °C with the enthalpy of 210.867 J/g. It proves that the sample provided is semi crystalline in nature as a sharp peak is obtained and close to reported value 250–255 °C reported in the literature [54]. Thus, it can be concluded that the sample of HPN was pure and authentic. The DSC thermogram of pure HPN is shown in the Fig. 1-B.

3.4. Characterization of the HPN-cubosomes

3.4.1. Transmission Electron Microscopy (TEM)

TEM analysis revealed cubic-shaped particles with zero mean curvature and a marginal population of hexagonal vesicles that is consistent with existing literature [55]. Nano-sized, isolated particles appeared dark due to drug solubilization in the lipid. Particle size determined by TEM matched Zetasizer results (Fig. 1-C).

3.4.2. Particle size, PDI and Zeta potential (ZP)

Particle size analysis of HPN-cubosome nanoparticles showed a nano-sized, monodisperse system with a particle size of 152.4 nm and PDI of 0.21 (Fig. 1-D). These findings support the formulation's suitability for topical delivery, aligning with literature recommendations for lipid-based formulations [56]. A PDI value of 0.21 indicated minimal particle size variation, ensuring a stable particulate system. The zeta potential of HPN-cubosomes was − 24.81 mV (Fig. 1-E), promoting stability and preventing particle agglomeration. This negative charge, resulting from the ionization of unbound oleic acid, enabled electrostatic repulsion and inhibited coalescence [57,58]. Recent research suggests that negatively charged particles can penetrate the skin through repulsive interactions with skin lipids [59].

3.4.3. Entrapment efficiency and drug loading

Cubosomes efficiently incorporated HPN into the liquid crystal structure of the particles, due to the strong affinity between HPN and GMO, resulting in a high entrapment efficiency of 92.85 ± 0.89% for the HPN-cubosomes. Thereby enabling a therapeutic effect with a smaller drug volume and secure inclusion inside the particles. The drug loading capacity for HPN was determined to be 9.34 ± 0.10%.

3.5. Characterization of the HPN-cubogel

3.5.1. Visual examination

Hydrogels are a remarkable class of materials consisting of cross-linked polymers that exhibit high water content. They can deliver therapeutic agents over a prolonged period and in a localized manner. Hydrogels fabricated from diverse synthetic materials, including carbopol 934, have been extensively studied for their controlled release of various treatments, exhibiting distinct mechanical properties and biological responses.

The HPN-Cubogel which was prepared meticulously, demonstrated homogeneity and clarity, without any rough or coarse lumps, forming three-dimensional networks of gel**.** This favourable characteristic is particularly useful in facilitating the monitoring of wound healing processes.

3.5.2. pH determination

It is imperative to take the pH level of a hydrogel intended for wound healing into account as it can significantly impact its efficacy in promoting wound healing. It is optimal for the pH level of the hydrogel to be within the typical pH range of the skin, which is slightly acidic, ranging from 4.5 to 5.5. The skin's pH plays a vital role in maintaining its natural barrier function, which shields the underlying tissues from external factors and pathogens. If the hydrogel's pH level is too low or high, it may cause irritation, and inflammation, and prolong the wound healing process [60]. In light of this, it is crucial to ensure that the pH level of the hydrogel falls within the optimal range. In this regard, the pH value of the HPN-Cubogel was assessed to be 6.0 ± 0.23, which is neutral and this suggests that the formulation is safe to apply to the skin, and there is no potential for irritation or adverse effects.

3.5.3. Swelling index

The ability of hydrogels to expand or swell is a crucial aspect in the development of wound dressings. This characteristic plays a significant role in determining a wound's capacity to withstand a certain amount of exudate while keeping a moist environment at the site of injury. In the case of the HPN-Cubogel, a swelling ratio of 18% was observed after a three-hour period, indicating that it can be deemed satisfactory for use in topical therapy as reported by previous literature [61]. It is worth noting that the swelling capacity of hydrogels is inversely related to their crosslinking density and is a measure of their hydrophilicity.

3.5.4. Spreadability measurement

The parameter of spreadability wields an immense influence on the even application of semi-solid dosage from onto the skin. The quality of the prepared formulation is reflected in the time it takes to spread, as well as in its overall credibility and spreadability. Spreadability is a crucial factor in ensuring that patients remain compliant with their medication regimen, as it promotes the uniform and thorough application of the gel to the skin. In the case of HPN-Cubogel, a spreadability value of 8.4 ± 0.07 was determined, indicating a commendable level of performance [62]. It should be noted that viscosity plays a significant role in determining the spreadability of the preparation. In essence, the thicker the preparation, the lower its spreadability, and conversely, the thinner the preparation, the higher its spreadability.

3.5.5. Viscosity

The rheological properties of a gel formulation play a pivotal role in determining the product's physical attributes, including its form, appearance, texture, and flow behaviour. In this regard, it is essential to pay close attention to these properties during the development and application of any gel product. In the case of HPN-Cubogel, it was found that the formulation exhibited a shear thinning flow pattern, as evidenced by the decrease in viscosity with an increasing shear rate, as depicted in (Table S1-(b), Fig. 2-A). The measured viscosity dropped from 936.28 ± 0.417 to 427.36 ± 0.321 cps, indicating that the product's consistency became less resistant to deformation as the rate of shear increased.

3.5.6. Texture profile analysis (TPA)

The mechanical properties of a substance, including hardness, cohesiveness, firmness, and consistency, are crucial factors that determine its suitability for a particular application. In the case of the HPN-Cubogel, these properties have been defined using TPA (texture profile analysis), with the resulting TPA graph and computed mechanical characteristics being presented in the accompanying Fig. 2-B and Table S1-**(c)**.

One of the key mechanical properties determined using TPA is hardness, which is calculated based on the maximal peak force during the first compression cycle. In the case of the HPN-cubogel, the hardness value was found to be 127.38 g, indicating that the gel can be easily applied to the skin. Furthermore, this value falls within the permitted limits for topical gel applications, ensuring that the gel is safe for use. TPA also provides insights into the cohesive properties of a substance, which are important for structural recovery following application. Cohesion is determined by analysing the ratio of the area under the force-time curve generated during the second compression cycle to that

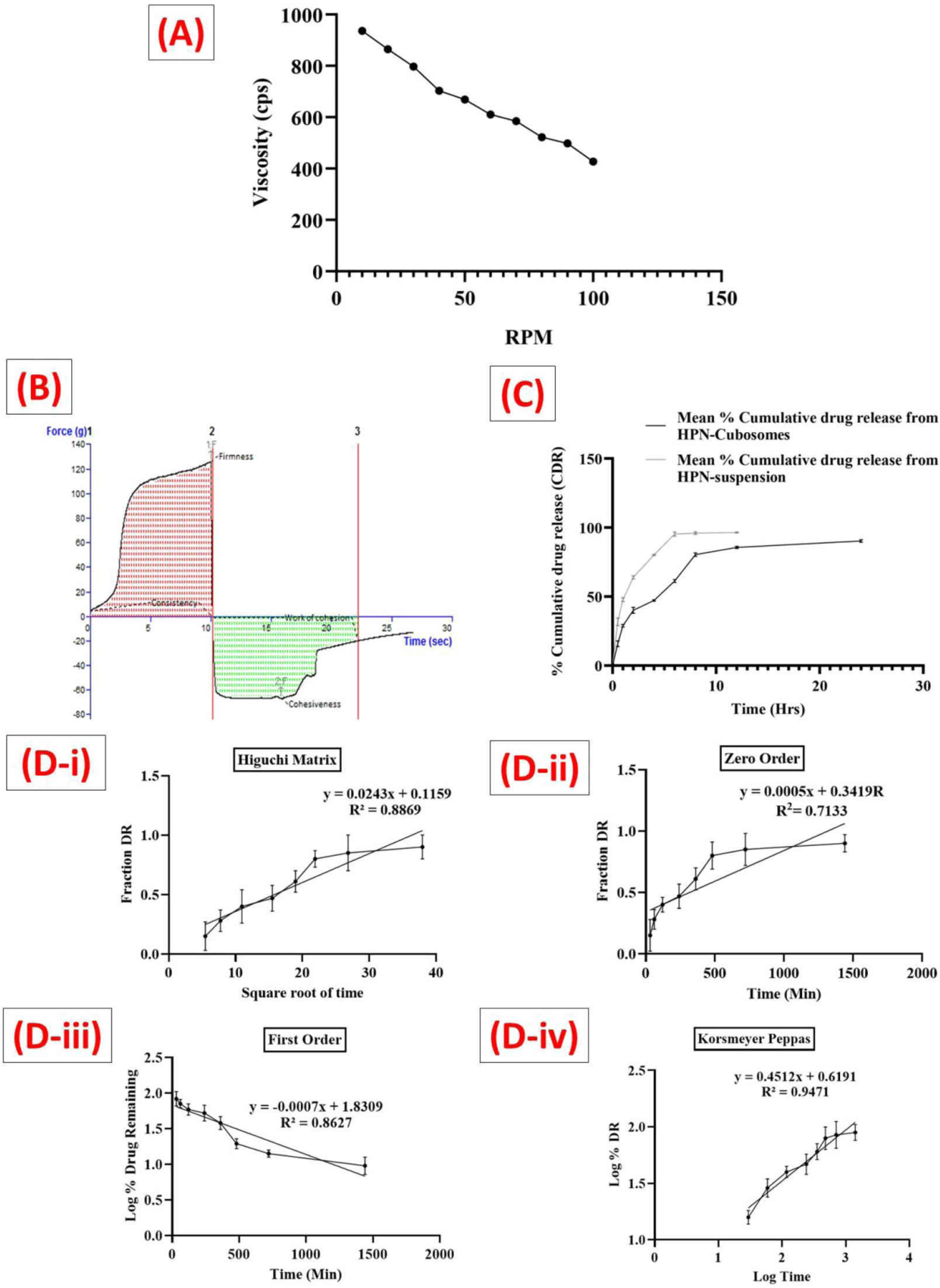

Fig. 2. : (A) The figure illustrates the shear thinning behaviour of the prepared HPN-Cubogel, as evidenced by the decrease in viscosity, (B) Texture Profile Analysis (TPA) Graph of HPN-Cubogel, (C) In-vitro drug release curve for HPN-cubosomes & HPN-suspension and (D) The release kinetic graphs of HPN-cubosomes depicting different models for HPN release kinetics: (i) the Higuchi model for HPN, (ii) the Zero order model for HPN, (iii) the First order model for HPN, and (iv) the Korsemeyer Peppas plot for HPN.

produced during the first compression cycle. In the case of the HPN-cubogel, the cohesiveness value was found to be − 67.09 g, which is considered nominal for topical applications. This high degree of cohesiveness ensures complete structural recovery following gel application.

Based on the TPA findings, it can be concluded that the HPN-Cubogel possesses adequate mechanical characteristics for topical application [63]. Its hardness and cohesiveness values fall within the permitted limits for such applications, indicating that the gel is suitable for use in this context.

3.6. In-Vitro drug release and release kinetic study

Comparative in vitro release studies were conducted to evaluate the difference in release behaviour between HPN-Suspension and the HPN-cubosomes formulation using UV spectrophotometry. The release profile of the HPN-cubosomes displayed a biphasic release pattern, with an initial burst release observed after 30 min, followed by a slower rate of release (as shown in the Fig. 2-C) ($p = 0.002$ in comparison to HPN-Suspension). This pattern of release aligns with previous reports by Boyd, who investigated the release of lipophilic drugs from cubosome particles [64]. The initial burst effect may be attributed the drug adsorbed on the cubosome surface while the comparatively slow rate of HPN release observed subsequently from the cubosomes might be due to the drug molecules' restricted diffusion inside the aqueous channels, which is regulated by the tortuousness and comparatively small pore size of the channels. Another aspect adding to the slow drug release from cubosomes is the inclusion of GMO as one of its key components, which may result in delayed drug partitioning from the oily to the aqueous phase.

Subsequently, the acquired in vitro release information was analyzed using various release kinetic models. The release kinetic analysis data for HPN-cubosomes is shown Fig. 2-D (i-iv). For the formulation, the Korsemeyer Peppas model was found to be the best-fitted model [as shown in Table S1-(d)], with the highest correlation coefficient value ($R^2 = 0.9471$). The release exponent "n" was found to be between 0.43 and 0.85 (0.45 for HPN), indicating non-Fickian diffusion-controlled release (anomalous) from a non-swellable matrix system.

3.7. DPPH assay

To determine the antioxidant potential of HPN inside the HPN-cubosomes, a comparison was made with the standard ascorbic acid solution. The results revealed that both ascorbic acid and the formulation exhibited high antioxidant activity, with percentages of 92.67 ± 0.06% and 88.34 ± 0.02%, respectively. This observation provides evidence of the strong antioxidant capability of HPN loaded in Cubosomes.

3.8. Hemocomptability study

It is crucial to ensure that a formulation is compatible with red blood cells, especially erythrocytes. Therefore, the hemolysis effect of both the prepared HPN-suspension and HPN-cubosomes were evaluated at different time intervals of 1, 2, and 4 h, with results of 0.12 ± 0.04%, 0.25 ± 0.01%, 0.45 ± 0.02%, and 0.14 ± 0.04%, 0.32 ± 0.01%, 0.50 ± 0.03%, respectively, as shown in Fig. 3-A and B. These values are within permitted limits, according to the ASTM E2524–08 standard, which specifies that a hemolytic value greater than 5% for studied nanoparticles can induce RBC hemolysis [65]. As a result, the produced formulation is hemocompatible, allowing it to be used in the body at lower doses. Fig. 3-C depicts the results of the light microscopy pictures of the HPN-suspension and HPN-cubosomes, which reveal that the hemolysis study did not affect the shape or morphology of the RBCs. As a result, the developed formulation is biocompatible and may be safely employed within the body.

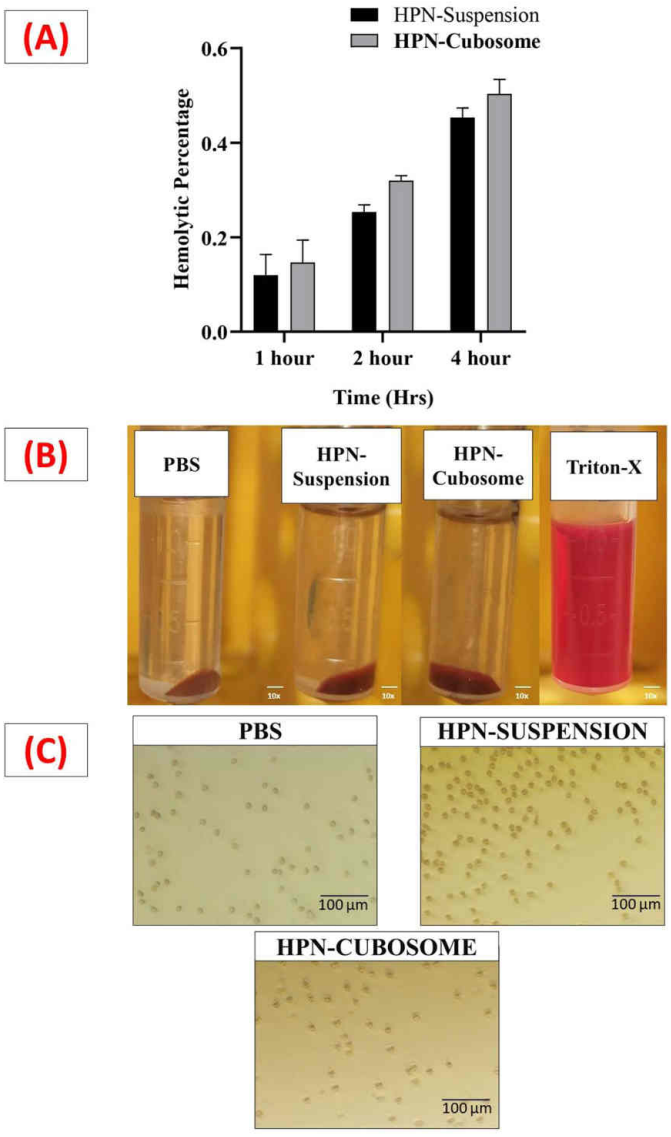

Fig. 3. Illustration of the percentage of hemolysis observed in (A) HPN suspension and HPN-cubosomes, (B) Comparison of hemolysis levels from left to right: PBS, treated with HPN suspension, HPN-cubosomes, and positive control, and (C) Optical microscopy images of RBCs treated with (i) PBS, (ii) HPN suspension, and (iii) HPN-cubosomes.

3.9. Ex - Vivo evaluation of formulation

3.9.1. Ex-vivo permeation studies on rat skin

In this experiment, we investigated the ex vivo drug permeation behaviour of HPN-Cubogel and HPN-Suspension by using rat skin as a model. The percentage of cumulative drug permeated after 24 h was calculated for both HPN-Cubogel and HPN-Suspension. Interestingly, the percentage of cumulative drug permeated was significantly higher for HPN-Cubogel, with a value of 97.21 ± 0.84%, compared to HPN-Suspension, which had a value of 71.20 ± 0.21%, indicating that HPN-Cubogel was more effective in facilitating drug permeation through the skin (Fig. 4-A).

In order to further examine the drug permeation behavior of the formulation, we conducted an assessment of the steady-state flux. Our results indicate that the HPN-Cubogel exhibited a steady-state flux of 93.94 µg/cm^2/h, while the steady-state flux of the HPN-Suspension was 85.09 µg/cm^2/h (as illustrated in Fig. 4-B). Furthermore, we also observed that the permeability coefficient (kp) values for HPN-Cubogel

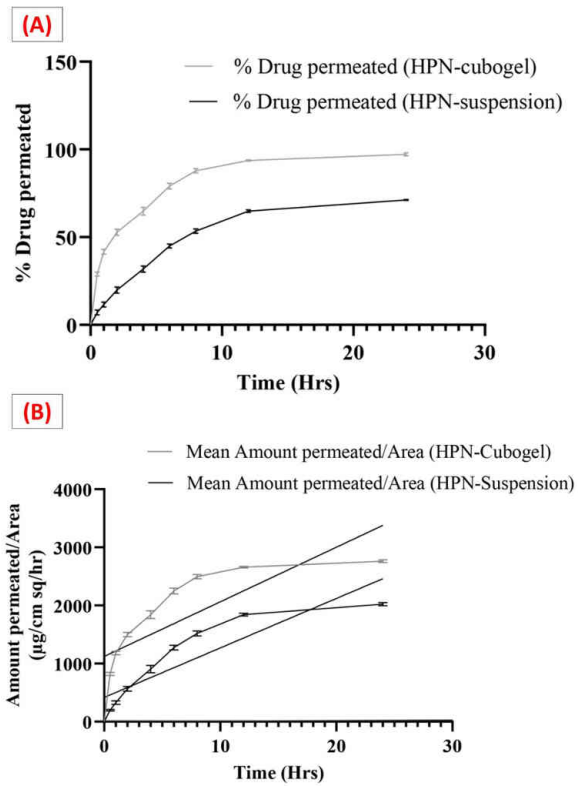

Fig. 4. (A) Ex-vivo permeation and (B) Flux of HPN-loaded Cubogel and Suspension.

and HPN-suspension were 18.788 cm/min and 17.018 cm/min, respectively [Table S2-(a)]. Overall, the enhanced flux observed for HPN-Cubogel suggests that the formulation has the potential to effectively permeate through the skin.

Taken together, our findings suggest that the HPN-Cubogel have a superior drug permeation behaviour compared to the HPN-suspension ($p = 0.06$), indicating that the use of Cubosomes as a drug delivery system can potentially enhance the efficacy of topical drug delivery.

3.9.2. *Ex-Vivo Confocal Laser Scanning Microscopy (CLSM) visualization*

To visualize the extent of HPN-cubosomes penetration through rat skin, Rhodamine B dye was incorporated into the lipid phase of the Cubosome. A methanolic solution of Rhodamine B dye and HPN-cubosomes was applied to the skin, and the penetration extent was measured using confocal laser scanning microscopy (CLSM). The results showed that HPN-cubosomes exhibited high penetration (up to 35 µm) through various layers of the rat skin, demonstrating significantly higher fluorescence intensity compared to HPN-suspension (penetrated up to 25 µm) and Control (up to 15 µm). As a result, the findings suggest that the drug could be efficiently absorbed between the epidermis and dermis layer, that is critical for treating full-thickness wounds (refer to Fig. 5).

3.10. *Skin permeation enhancement study*

Two analytical techniques were used to study the permeability of HPN from the HPN-Cubogel into the skin, as well as the underlying process of permeation. These techniques were FTIR and DSC.

The FTIR analysis of normal skin (depicted in Fig. 6-A) revealed that the absorption band from 3000 to 2800 cm^{-1} arose due to the C-H stretching motion of the alkyl group, which is present in both proteins and lipids. The asymmetric and symmetric C-H stretching in the lipids were observed at absorption bands 2921.41 and 2854.49 cm^{-1}, respectively. In addition, bands at 1645.36 and 1536.74 cm^{-1} were observed, which were attributed to the amide I and amide II stretching vibrations of the proteins. The amide I band is caused by C═O stretching vibration, whereas the amide II band is caused by C-N bending vibration. It is worth noting that the amide I band is made up of component bands that reflect the different keratin structures.

Upon examination of the HPN-Cubogel treated skin via FTIR, absorption bands at 3306.75, 3165.92, and 2902.72 cm^{-1} were observed, as illustrated in Fig. 6-B. The band at 2858.82 cm^{-1} represented C-H stretching (alkane), while the 1723.62 cm^{-1} band indicated C═O stretching, and the 1546.83 cm^{-1} band depicted C═C stretching (alkene). Furthermore, the absorption band at 1451.35 cm^{-1} showed C-H bending (alkane), the 1403.53 cm^{-1} band showed O-H bending, and the 942.92 cm^{-1} band represented C═C bending (alkene). It is worth noting that the spectra of the HPN-Cubogel and untreated rat skin exhibited comparable characteristic peaks, with slight differences. These variations in peaks could be attributed to the chemical interaction between the skin and HPN-Cubosomes.

The DSC thermograms of normal rat skin and skin treated with HPN-Cubogel were compared. The normal rat skin DSC thermogram indicated an endothermic peak at 174.998 °C, which was caused by protein denaturation. The DSC thermogram of the rat skin treated with the formulation (HPN-Cubogel), on the other hand, revealed a pronounced endothermic peak at 115.073 °C, as shown in Fig. 6- C, D. This change in the peak to a lower value shows intervention at the stratum corneum juncture, which is required for drug penetration.

3.11. *HET CAM assay*

The tolerability and irritability of the HPN-cubosomes and HPN-Cubogel were evaluated using the HET-CAM test and compared with both the negative control (0.9% w/v normal saline) and the positive control (0.1 N NaOH). The test samples (HPN-Cubosome and HPN-Cubogel) and the negative control were found to be non-irritating in contrast to the positive control, which yielded an average irritation score of 16.89 ± 0.03 indicating severe irritation. The mean irritation score for normal saline was 0.43 ± 0.01. These findings align with the study conducted by Sandeep and associates [66]. Furthermore, the HPN-Cubosome and HPN-Cubogel were found to be well-suited for topical administration, as evidenced by a mean irritation score of 0.58 ± 0.04 and 0.60 ± 0.02 respectively, while the drug suspension-treated CAM showed a mean irritation score of 0.62 ± 0.03. As shown in Fig. 6-E (i-v) the results indicate that the both HPN-Cubogel and HPN-Cubosome are non-toxic, non-irritating, and very well tolerated for topical administration.

3.12. *In-Vivo wound healing activity of formulation*

Determining the efficacy of a novel formulation is best achieved through its in-vivo performance evaluation. Typically, a formulation's effectiveness in vitro is not mirrored in vivo, necessitating testing in an appropriate animal model before moving on with marketing. In this regard, a study was conducted to investigate the impact of a formulation on the healing of incisional wounds in Wistar rats. Fig. 7-B depicts the percent decrease in wound site in the control (No treatment), placebo (Cubogel), blank (HPN-hydrogel), and treatment (HPN-Cubogel) groups. The study found that all wounds shrunk in size over time, irrespective of the group. The control and placebo groups, on the other hand, exhibited symptoms of inflammation and slower decrease in size of wound, indicating inadequate recovery. Conversely, groups treated with the HPN-Cubogel demonstrated superior outcomes compared to the control and placebo groups. Also, by the 14th day of the study, the HPN-hydrogel and HPN-Cubogel groups had completed wound closure, but the control and placebo groups had not. These findings suggest that HPN encapsulated inside cubosomes accelerated wound healing, resulting in better outcomes when compared to other groups.

According to existing literature, the wound-healing properties of HPN are largely attributed to its ability to elevate VEGF production,

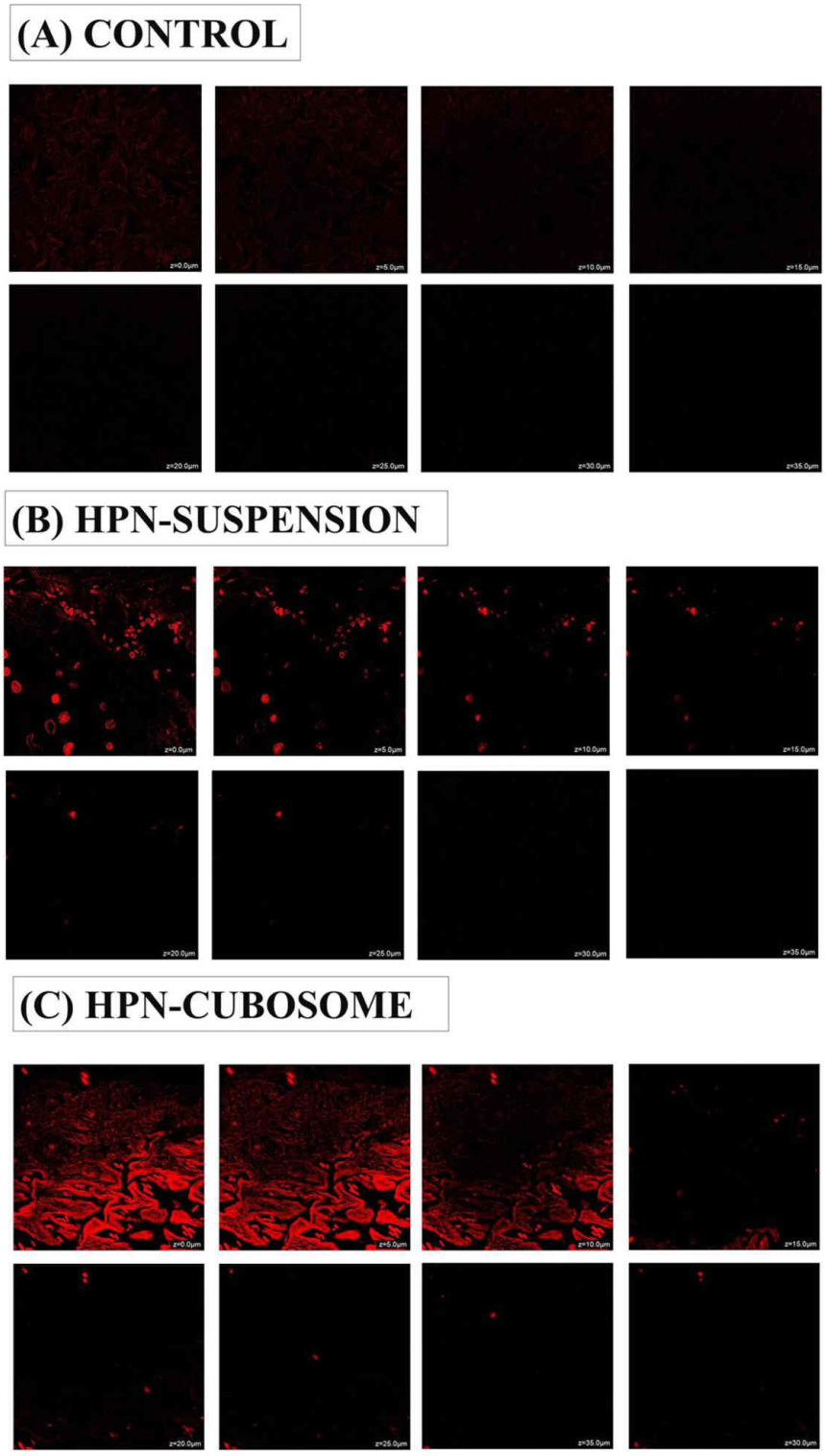

Fig. 5. Confocal microscopy images comparing the skin penetration of a (A) control, (B) HPN-Suspension, and (C) HPN-cubosomes. The control and HPN-Suspension groups showed limited penetration, with fluorescence intensity reaching depths of only 15 μm and 25 μm, respectively. In contrast, the HPN-cubosomes formulation exhibited significantly greater penetration, reaching a depth of 35 μm.

antioxidant enzymes, and anti-inflammatory actions. However, the clinical efficacy of HPN is limited by its poor bioavailability. Fortunately, the encapsulation of a drug within Cubosomes has been found to facilitate its permeation into the underlying skin layers of the wound, owing to its ability to fluidize the lipid membrane of the skin. Furthermore, Cubosomes offer a superior reservoir for poorly soluble drugs through their capacity for enhanced solubilisation. These findings suggest that the encapsulation of HPN within Cubosomes significantly improved its solubility, leading to accelerated wound healing.

A crucial requirement for effective wound healing is the provision of a moist and bacteria-free environment. Hydrogels offer several benefits in this regard, including the creation of a protective barrier, the removal

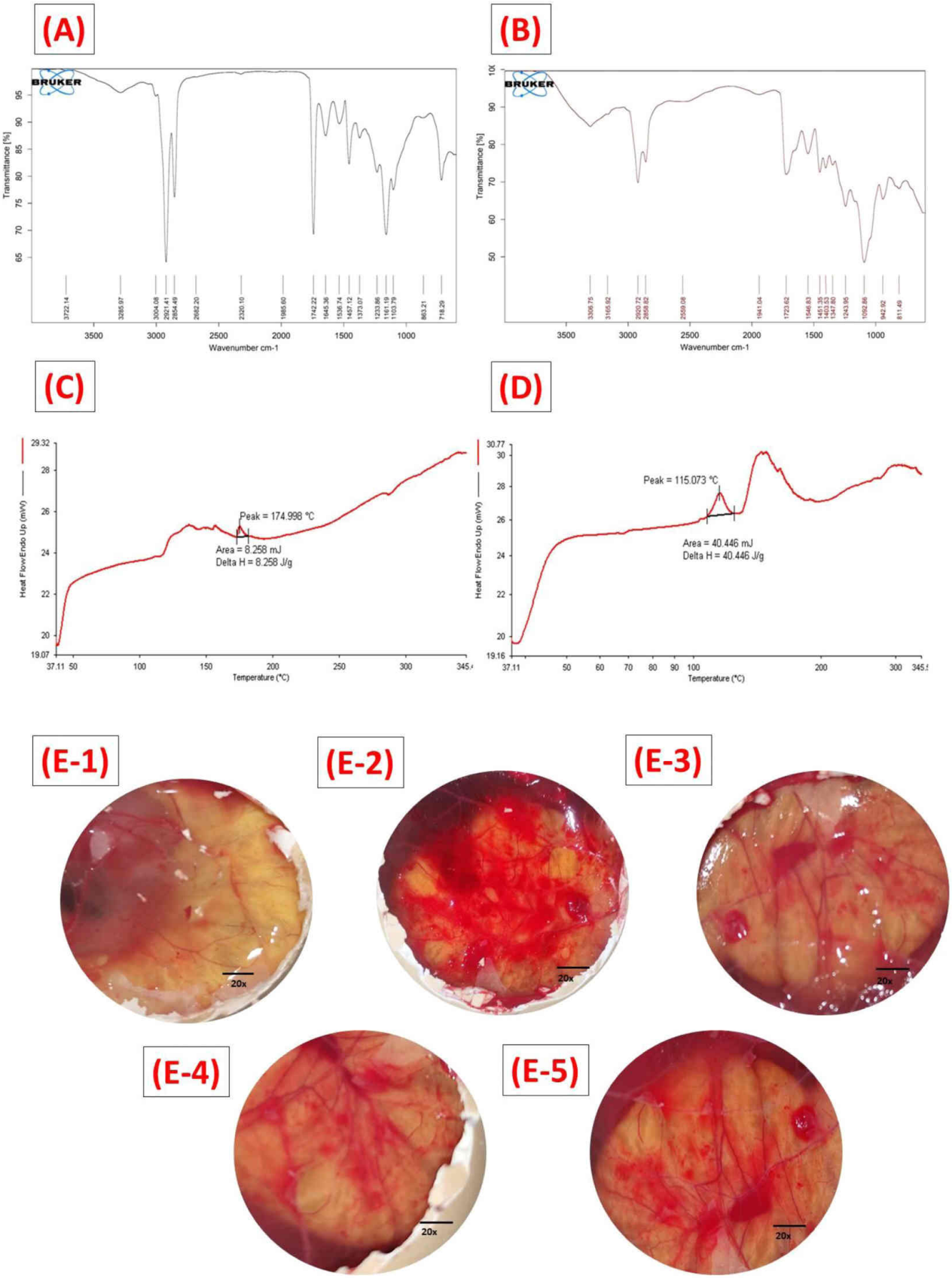

Fig. 6. Skin permeation enhancement investigation using FTIR of (A) normal skin and (B) HPN-Cubogel treated skin, DSC of (C) normal skin & (D) HPN-Cubogel treated skin and (E) Comparison between different treatments on a CAM (Chorioallantoic Membrane) model with (i) Normal Saline (0.9% NaCl), (ii) 0.1 N NaOH, (iii) HPN-cubosomes, (iv) HPN-Cubogel and (v) HPN-Suspension.

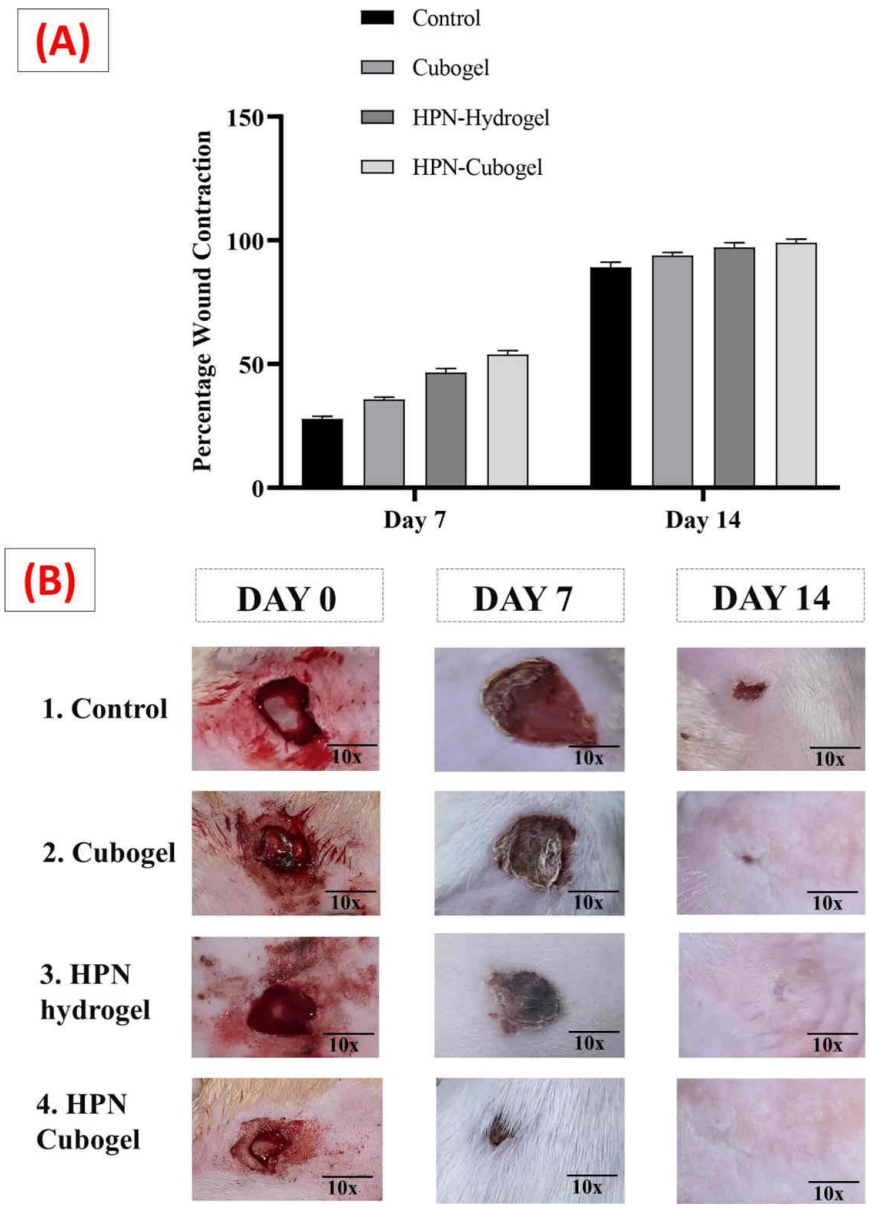

Fig. 7. A statistical and visual depiction of the healing process over time - (A) Percentage of wound contraction at 7 and 14 days post-treatment. (B) Wound healing progression from day 0 to day 14. Values represent the mean ± SD, n = 6, SD: standard deviation.

of exudates, the encapsulation of bioactive compounds, and the promotion of a moist milieu that facilitates wound healing. Considering HPN's ability to enhance collagen synthesis, prevent haemorrhages and infection, and its antioxidant and anti-inflammatory characteristics, the enhanced wound healing effect observed with the formulation can be attributed to the synergistic impact of the combination of hydrogel and HPN-Cubosomes.

To determine the extent of wound-healing progress, the percentage of wound contraction was evaluated and presented in Fig. 7-A. At 7- and 14-days post-wounding, the Control group had wound closure rates of 27.79 ± 1.13% and 89.12 ± 2.6%, respectively. The Placebo group, on the other hand, had wound closure rates of 35.68 ± 0.97% and 93.90 ± 1.17% after 7 and 14 days, respectively. Additionally, at 7- and 14-days post-wounding, the HPN-hydrogel group had wound closure rates of 46.54 ± 1.62% and 97.20 ± 1.84%, respectively. Control rats showed a delayed contraction rate of the wound when compared with the test formulation-treated animals as well as other groups. Notably, the Formulation treated group (HPN-Cubogel) demonstrated the most promising results, with a wound closure rate of 53.90 ± 1.54% and 98.96 ± 1.50% after 7- and 14-days post-wounding, respectively. Statistical analysis revealed that the wound contraction by HPN-Cubogel was found to be statistically significant when compared to the Control group ($p < 0.01$).

These findings demonstrate that the Formulation treated group exhibited a higher degree of wound contraction and quicker wound closure compared to the other groups, making it a more effective wound-healing option.

3.13. Histopathological study

Histologic section of normal skin are displayed in Fig. 8-A, while Fig. 8-B illustrates sections from the control and treatment groups. In the initial healing stages, the wounds in the Control, Cubogel and HPN-Hydrogel groups exhibited conspicuous infiltration of inflammatory cells (represented by black circles around them in Fig. 8-A), granulation tissue development, and epithelial proliferation. The epidermis was not restored in most regions of the control group, and the dermis had a fragmented and uneven structure with missing appendages and a

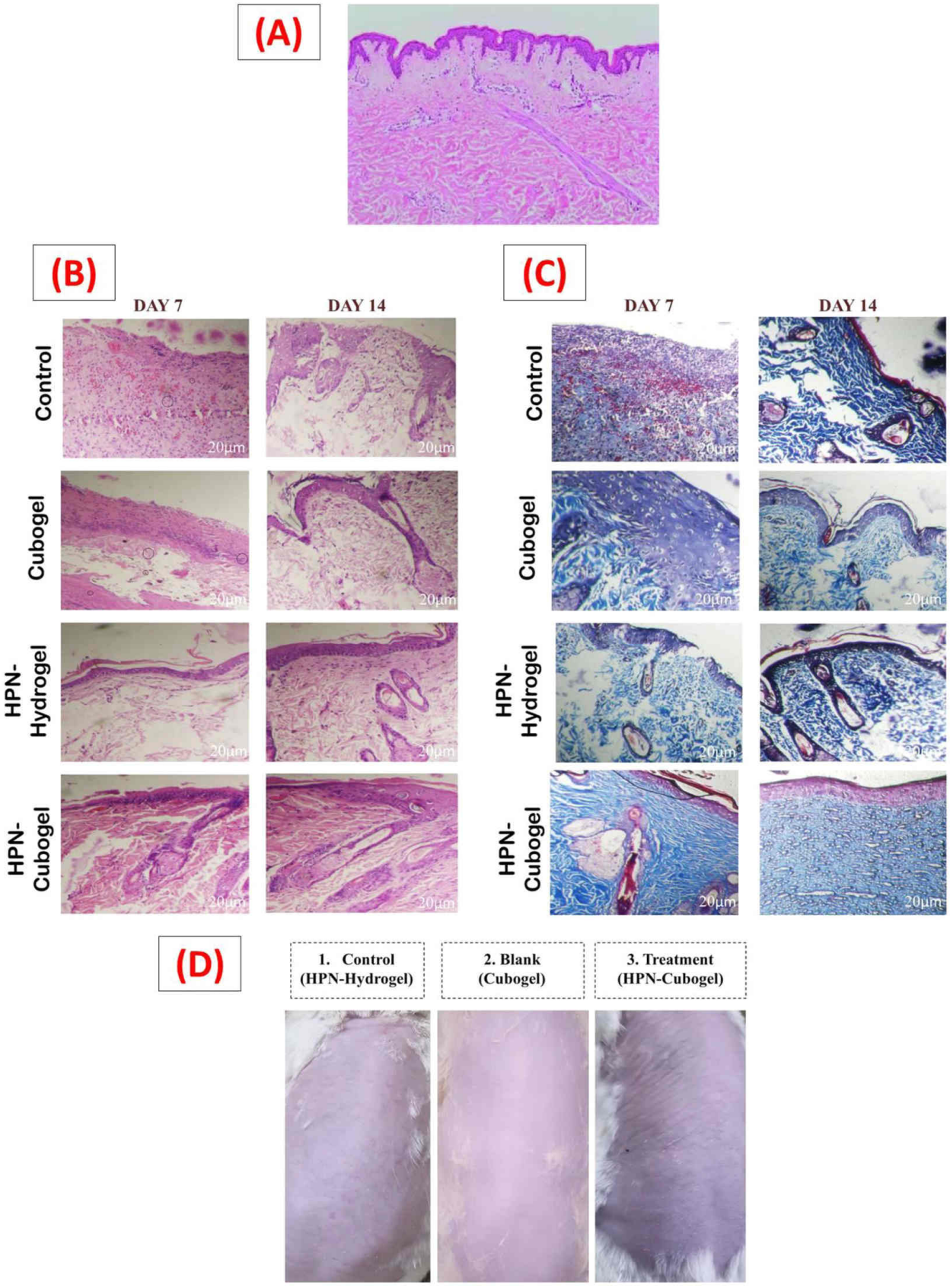

Fig. 8. (A) H&E stain of normal skin. There is a clear distinction between the dermis and epidermis. The epidermis shows keratin flaking from the surface. The dermo-epideroid junction is clearly defined and there are healthy rete pegs separating the papillary and reticular dermis [69], (B) & (C) Histological analysis of wound healing in each group at 7 and 14 days post-wounding and (D) Skin irritation test illustration following application of different hydrogels.

significant amount of infiltration of inflammatory cells. Conversely, the inflammatory cells and granulation tissue in the HPN-Cubogel group, faded rapidly, and new blood vessels and hair follicles commenced growing in this group ahead of the other groups. This can be attributed to the enhanced healing property of HPN, which is encapsulated inside the cubosomes. During the late stages of the healing process (Day 14), the HPN-Cubogel group exhibited the most striking similarity to normal skin and a thin epidermis with minimal hypertrophic scarring near the wounded area. The healing status of the HPN-Hydrogel group was similar to that of the HPN-Cubogel group on day 14, albeit with slow healing.

Collagen synthesis plays a pivotal role in the healing of wounds. To delve deeper into the impact in various groups, rat skin tissues were stained using Masson's trichrome staining (as shown in Fig. 8-C). This staining technique highlights collagen in blue, while red blood cells, muscle, and cytoplasm are stained red. By assessing the degree of deposition of collagen during granulation tissue growth and structural remodelling, the staining provides insight into the advancement of the healing process. The intensity of blue staining indicates the relative quantity of total collagen fibre deposited, reflecting the phases of synthesis, disintegration, and restoration. The results demonstrate that among the three groups, the HPN-Cubogel group had the highest synthesis of collagen. Conversely, the Control group exhibited the slowest and lowest rate and quantity of collagen formation.

3.14. Skin irritation study

HPN, being a phytoconstituent, is classified as non-irritant. However, the formulation prepared for topical delivery of HPN contains varying amounts of surfactants and other excipients. Therefore, a skin irritation study was deemed necessary (refer to Fig. 8-D). The study yielded a mean irritation score value of 0.14 for the HPN-Cubogel and 0.21 for Cubogel. Previous literature has reported that a score value ranging from 0–9 suggests non-irritant potential. Based on this data, we may infer that the proposed formulation is competent for topical application to the skin surface [67,68] [Table S2-(b)].

4. Conclusion

This study presents a novel approach to enhance the solubility and targeted distribution of HPN, aiming to accelerate wound healing. The formulation, HPN-Cubosome, was designed, formulated, and evaluated in a rat model to assess its efficacy in improving wound healing rates. Key findings indicate that HPN-cubosomes are biocompatible with red blood cells, suggesting suitability for treating full-thickness wounds without skin irritation or inflammation. In-vivo analysis demonstrated that HPN-Cubogel significantly outperformed other groups, stimulating angiogenesis, fibroblast and keratinocyte proliferation, leading to exceptional wound healing after 14 days—nearly 99%. The HPN-Cubosome system within the hydrogel exhibits a synergistic effect, showing promising potential for treating wounds and skin-related disorders. These results provide crucial insights into developing effective wound-healing therapies, paving the way for future research in this field.

Institutional Review Board Statement

The study was conducted in accordance with the Institutional Animal Ethics Committee (IAEC) of Jamia Hamdard (Protocol No. 1979, Date of approval: 21 December 2022) for studies involving animals.

CRediT authorship contribution statement

Sheikh Afsana: Writing – original draft. **Alsayari Abdulrhman:** Resources. **Wahab Shadma:** Resources. **Kesharwani Prashant:** Writing – review & editing. **Rehman Urushi:** Writing – original draft.

Declaration of Competing Interest

The authors declare that they have no known competing financial interests or personal relationships that could have appeared to influence the work reported in this paper.

Data availability

The data that has been used is confidential.

Acknowledgements

The authors (A. Alsayari and S. Wahab) extend their appreciation to the Deanship of Scientific Research at King Khalid University for funding this work through Large Research Groups Project under grant number (RGP.2/119/44). The author (P. Kesharwani) acknowledges the financial support from the Indian Council of Medical Research (ICMR), New Delhi, India, through Extramural Research Grants. The author acknowledges Department of Science and Technology (DST) for providing financial assistance under the special assistance Programme-II (SAP-II) and FIST Programme respectively to the department of Pharmaceutics, SPER, Jamia Hamdard.

Appendix A. Supporting information

Supplementary data associated with this article can be found in the online version at doi:10.1016/j.colsurfb.2023.113728.

References

[1] R.F. Pereira, P.J. Bártolo, Traditional therapies for skin wound healing, Adv. Wound Care. 5 (2016) 208, https://doi.org/10.1089/WOUND.2013.0506.
[2] N. Hasan, M. Imran, M. Nadeem, D. Jain, K. Haider, M. Moshahid Alam Rizvi, A. Sheikh, P. Kesharwani, G. Kumar jain, F. Jalees Ahmad, Formulation and development of novel lipid-based combinatorial advanced nanoformulation for effective treatment of non-melanoma skin cancer, Int. J. Pharm. 632 (2023) 122580, https://doi.org/10.1016/J.IJPHARM.2022.122580.
[3] A.K. Jain, S. Jain, M.A.S. Abourehab, P. Mehta, P. Kesharwani, An insight on topically applied formulations for management of various skin disorders, J. Biomater. Sci. Polym. Ed. (2022) 1–27, https://doi.org/10.1080/09205063.2022.2103625.
[4] R. Cassano, M. Cuconato, G. Calviello, S. Serini, S. Trombino, Recent Advances in Nanotechnology for the Treatment of Melanoma, Molecules 26 (2021) 785, https://doi.org/10.3390/molecules26040785.
[5] J. He, M. Shi, Y. Liang, B. Guo, Conductive adhesive self-healing nanocomposite hydrogel wound dressing for photothermal therapy of infected full-thickness skin wounds, Chem. Eng. J. 394 (2020) 124888, https://doi.org/10.1016/J.CEJ.2020.124888.
[6] R. Verma, P.P. Gupta, T. Satapathy, A. Roy, A review of wound healing activity on different wound models, J. Appl. Pharm. Res 7 (2019) 1–7, https://doi.org/10.18231/2348-0335.2018.0013.
[7] Partial & Full Thickness Wound Care | Omeza, (n.d.). ⟨https://omeza.com/partial-full-thickness-wound-care/⟩ (accessed September 23, 2022).
[8] S. El-Ashram, L.M. El-Samad, A.A. Basha, A. El Wakil, Naturally-derived targeted therapy for wound healing: Beyond classical strategies, Pharmacol. Res. 170 (2021), https://doi.org/10.1016/J.PHRS.2021.105749.
[9] P. Gupta, A. Sheikh, P. Kesharwani, M.A.S. Abourehab, M.A.S. Abourehab, Amelioration of Full-ThicknessWound Using Hesperidin Loaded Dendrimer-Based Hydrogel Bandages, Biosensors 12 (2022), https://doi.org/10.3390/bios12070462.
[10] B. Gorain, M. Pandey, N.H. Leng, C.W. Yan, K.W. Nie, S.J. Kaur, V. Marshall, S. P. Sisinthy, J. Panneerselvam, N. Molugulu, P. Kesharwani, H. Choudhury, Advanced drug delivery systems containing herbal components for wound healing, Int. J. Pharm. 617 (2022) 121617, https://doi.org/10.1016/J.IJPHARM.2022.121617.
[11] L. Gan, J. Jiang, J.W. Duan, X.J.Z. Wu, S. Zhang, X.R. Duan, J.Q. Song, H.X. Chen, Cold atmospheric plasma applications in dermatology: A systematic review, J. Biophotonics. (2020), https://doi.org/10.1002/jbio.202000415.
[12] D. Medina-Cruz, B. Saleh, A. Vernet-Crua, A. Ajo, A.K. Roy, T.J. Webster, Drug-delivery nanocarriers for skin wound-healing applications, Wound Heal. Tissue Repair, Regen. Diabetes (2020) 439–488, https://doi.org/10.1016/B978-0-12-816413-6.00022-8.
[13] A. Sheikh, S. Md, P. Kesharwani, Aptamer grafted nanoparticle as targeted therapeutic tool for the treatment of breast cancer, Biomed. Pharmacother. 146 (2022) 112530, https://doi.org/10.1016/J.BIOPHA.2021.112530.

[14] M.M. Wen, I.A. Abdelwahab, R.G. Aly, S.A. El-Zahaby, Nanophyto-gel against multi-drug resistant Pseudomonas aeruginosa burn wound infection, Drug Deliv. 28 (2021) 463, https://doi.org/10.1080/10717544.2021.1889720.
[15] A. Hjort, F. Gottrup, Cost of wound treatment to increase significantly in Denmark over the next decade, ⟨Https://Doi.Org/10.12968/Jowc.2010.19.5.48046⟩. 19, 2013: 173–184. https://doi.org/10.12968/JOWC.2010.19.5.48046.
[16] F. Gottrup, P. Holstein, B. Jørgensen, M. Lohmann, T. Karlsmark, A new concept of a multidisciplinary wound healing center and a national expert function of wound healing, Arch. Surg. 136 (2001) 765–772, https://doi.org/10.1001/ARCHSURG.136.7.765.
[17] D.A. Safta, C. Bogdan, M.L. Moldovan, Vesicular Nanocarriers for Phytocompounds in Wound Care: Preparation and Characterization, Pharm 14 (2022) 991, https://doi.org/10.3390/PHARMACEUTICS14050991.
[18] A.E. Nel, L. Mädler, D. Velegol, T. Xia, E.M.V. Hoek, P. Somasundaran, F. Klaessig, V. Castranova, M. Thompson, Understanding biophysicochemical interactions at the nano–bio interface, 2009 87, Nat. Mater. 8 (2009) 543–557, https://doi.org/10.1038/nmat2442.
[19] V. Saluja, Y. Mishra, V. Mishra, N. Giri, P. Nayak, Dendrimers based cancer nanotheranostics: An overview, Int. J. Pharm. 600 (2021) 120485, https://doi.org/10.1016/j.ijpharm.2021.120485.
[20] S. Aziz Hazari, H. Kaur, R. Karwasra, M.A.S. Abourehab, A. Ali Khan, P. Kesharwani, An overview of topical lipid-based and polymer-based nanocarriers for treatment of psoriasis, Int. J. Pharm. 638 (2023) 122938, https://doi.org/10.1016/J.IJPHARM.2023.122938.
[21] Z. Khan, A. Alhalmi, N. Tyagi, W.U. Khan, A. Sheikh, M.A.S. Abourehab, K. Kohli, P. Kesharwani, Folic acid engineered sulforaphane loaded microbeads for targeting breast cancer, ⟨Https://Doi.Org/10.1080/09205063.2022.2144692⟩. (2022) 1–20. https://doi.org/10.1080/09205063.2022.2144692.
[22] N. Parveen, A. Sheikh, M.A.S. Abourehab, R. Karwasra, S. Singh, P. Kesharwani, Self-nanoemulsifying drug delivery system for pancreatic cancer, Eur. Polym. J. 190 (2023) 111993, https://doi.org/10.1016/J.EURPOLYMJ.2023.111993.
[23] Z. Khan, M.A.S. Abourehab, N. Parveen, K. Kohli, P. Kesharwani, Recent advances in microbeads-based drug delivery system for achieving controlled drug release, ⟨Https://Doi.Org/10.1080/09205063.2022.2127237⟩. (2022) 1–28. https://doi.org/10.1080/09205063.2022.2127237.
[24] T.T. Dongsar, T.S. Dongsar, M.A.S. Abourehab, N. Gupta, P. Kesharwani, Emerging application of magnetic nanoparticles for breast cancer therapy, Eur. Polym. J. 187 (2023) 111898, https://doi.org/10.1016/J.EURPOLYMJ.2023.111898.
[25] A. Aziz, U. Rehman, A. Sheikh, M.A.S. Abourehab, P. Kesharwani, Lipid-based nanocarrier mediated CRISPR/Cas9 delivery for cancer therapy, ⟨Https://Doi.Org/10.1080/09205063.2022.2121592⟩. (2022). https://doi.org/10.1080/09205063.2022.2121592.
[26] P. Kesharwani, A. Sheikh, M.A.S. Abourehab, R. Salve, V. Gajbhiye, A combinatorial delivery of survivin targeted siRNA using cancer selective nanoparticles for triple negative breast cancer therapy, J. Drug Deliv. Sci. Technol. 80 (2023) 104164, https://doi.org/10.1016/J.JDDST.2023.104164.
[27] K. Zhang, M.A. Bhutto, L. Wang, K. Wang, J. Liu, W. Li, W. Cui, Q. Fu, Double-Layer Nanofibrous Sponge Tube via Electrospun Fiber and Yarn for Promoting Urethral Regeneration, Adv. Fiber Mater. 5 (2023) 662–680, https://doi.org/10.1007/S42765-022-00252-6/METRICS.
[28] L. Wang, K. Wang, M. Yang, X. Yang, D. Li, M. Liu, C. Niu, W. Zhao, W. Li, Q. Fu, K. Zhang, Urethral Microenvironment Adapted Sodium Alginate/Gelatin/Reduced Graphene Oxide Biomimetic Patch Improves Scarless Urethral Regeneration, Adv. Sci. (2023) 2302574, https://doi.org/10.1002/ADVS.202302574.
[29] K. McNamara, S.A.M. Tofail, Nanoparticles in biomedical applications, ⟨Http://Dx.Doi.Org/10.1080/23746149.2016.1254570⟩. 2 (2016) 54–88. https://doi.org/10.1080/23746149.2016.1254570.
[30] A. Sheikh, S. Md, N.A. Alhakamy, P. Kesharwani, Recent development of aptamer conjugated chitosan nanoparticles as cancer therapeutics, Int. J. Pharm. 620 (2022) 121751, https://doi.org/10.1016/J.IJPHARM.2022.121751.
[31] M. Allaw, M. Manconi, P. Caboni, G. Bacchetta, E. Escribano-Ferrer, J.E. Peris, A. Nacher, O. Diez-Sales, M.L. Manca, Formulation of liposomes loading lentisk oil to ameliorate topical delivery, attenuate oxidative stress damage and improve cell migration in scratch assay, Biomed. Pharmacother. 144 (2021) 112351, https://doi.org/10.1016/J.BIOPHA.2021.112351.
[32] M. Allaw, M.L. Manca, J.C. Gómez-Fernández, J.L. Pedraz, M.C. Terencio, O.D. Sales, A. Nacher, M. Manconi, Oleuropein multicompartment nanovesicles enriched with collagen as a natural strategy for the treatment of skin wounds connected with oxidative stress, ⟨Https://Doi.Org/10.2217/Nnm-2021–0197⟩. 16 (2021) 2363–2376. https://doi.org/10.2217/NNM-2021–0197.
[33] M. Allaw, M. Pleguezuelos-Villa, M.L. Manca, C. Caddeo, M. Aroffu, A. Nacher, O. Diez-Sales, A.R. Saurí, E.E. Ferrer, A.M. Fadda, M. Manconi, Innovative strategies to treat skin wounds with mangiferin: Fabrication of transfersomes modified with glycols and mucin, Nanomedicine 15 (2020) 1671–1685, https://doi.org/10.2217/NNM-2020-0116/ASSET/IMAGES/LARGE/FIGURE7.JPEG.
[34] A. Yaghmur, O. Glatter, Characterization and potential applications of nanostructured aqueous dispersions, Adv. Colloid Interface Sci. 147–148 (2009) 333–342, https://doi.org/10.1016/J.CIS.2008.07.007.
[35] A.M. Al-mahallawi, A.A. Abdelbary, S.A. El-Zahaby, Norfloxacin loaded nano-cubosomes for enhanced management of otitis externa: In vitro and in vivo evaluation, Int. J. Pharm. 600 (2021) 120490, https://doi.org/10.1016/J.IJPHARM.2021.120490.
[36] S.B. Rizwan, Y.D. Dong, B.J. Boyd, T. Rades, S. Hook, Characterisation of bicontinuous cubic liquid crystalline systems of phytantriol and water using cryo field emission scanning electron microscopy (cryo FESEM), Micron 38 (2007) 478–485, https://doi.org/10.1016/J.MICRON.2006.08.003.
[37] A.R. Tekade, G.D. Avhad, a Review on Cubosome: a Novel Approach for Drug Delivery, Int. J. Pharm. Sci. Res. 13 (2022) 579, https://doi.org/10.13040/IJPSR.0975-8232.13(2).579-588.
[38] L. Norlén, Skin Barrier Formation: The Membrane Folding Model, J. Invest. Dermatol. 117 (2001) 823–829, https://doi.org/10.1046/J.0022-202X.2001.01445.X.
[39] K. Singhal, N. Kaushik, A. Kumar, Cubosomes: Versatile Nanosized Formulation for Efficient Delivery of Therapeutics, Curr. Drug Deliv. 19 (2021) 644–657, https://doi.org/10.2174/1567201818666210708123855.
[40] D. Sivadasan, M.H. Sultan, S.S. Alqahtani, S. Javed, Cubosomes in Drug Delivery—A Comprehensive Review on Its Structural Components, Preparation Techniques and Therapeutic Applications, Biomedicines 11 (2023), https://doi.org/10.3390/BIOMEDICINES11041114.
[41] B. Siekmann, H. Bunjes, M.H.J. Koch, K. Westesen, Preparation and structural investigations of colloidal dispersions prepared from cubic monoglyceride-water phases, Int. J. Pharm. 244 (2002) 33–43, https://doi.org/10.1016/S0378-5173(02)00298-3.
[42] W. Li, A.D. Kandhare, A.A. Mukherjee, S.L. Bodhankar, Hesperidin, a plant flavonoid accelerated the cutaneous wound healing in streptozotocin-induced diabetic rats: Role of TGF-ß/Smads and Ang-1/Tie-2 signaling pathways, EXCLI J. 17 (2018) 399, https://doi.org/10.17179/EXCLI2018-1036.
[43] L. Wang, T. He, A. Fu, Z. Mao, L. Yi, S. Tang, J. Yang, Hesperidin enhances angiogenesis via modulating expression of growth and inflammatory factor in diabetic foot ulcer in rats, Eur. J. Inflamm. 16 (2018), https://doi.org/10.1177/2058739218775255/ASSET/IMAGES/LARGE/10.1177_2058739218775255-FIG2.JPEG.
[44] Z. Bagher, A. Ehterami, M.H. Safdel, H. Khastar, H. Semiari, A. Asefnejad, S. M. Davachi, M. Mirzaii, M. Salehi, Wound healing with alginate/chitosan hydrogel containing hesperidin in rat model, J. Drug Deliv. Sci. Technol. 55 (2020) 101379, https://doi.org/10.1016/j.jddst.2019.101379.
[45] M. Tsirigotis-Maniecka, R. Gancarz, K.A. Wilk, Polysaccharide hydrogel particles for enhanced delivery of hesperidin: Fabrication, characterization and in vitro evaluation, Colloids Surf. A Physicochem. Eng. Asp. 532 (2017) 48–56, https://doi.org/10.1016/J.COLSURFA.2017.07.001.
[46] S. Majumdar, R. Srirangam, Solubility, stability, physicochemical characteristics and in vitro ocular tissue permeability of hesperidin: a natural bioflavonoid, Pharm. Res. 26 (2009) 1217–1225, https://doi.org/10.1007/S11095-008-9729-6.
[47] M.H. Hettiaratchi, A. Schudel, T. Rouse, A.J. García, S.N. Thomas, R.E. Guldberg, T.C. McDevitt, A rapid method for determining protein diffusion through hydrogels for regenerative medicine applications, APL Bioeng. 2 (2018) 026110, https://doi.org/10.1063/1.4999925.
[48] A. Gupta, M. Kowalczuk, W. Heaselgrave, S.T. Britland, C. Martin, I. Radecka, The production and application of hydrogels for wound management: A review, Eur. Polym. J. 111 (2019) 134–151, https://doi.org/10.1016/J.EURPOLYMJ.2018.12.019.
[49] M.E. Aljghami, S. Saboor, S. Amini-Nik, Emerging Innovative Wound Dressings, 2019 473, Ann. Biomed. Eng. 47 (2018) 659–675, https://doi.org/10.1007/S10439-018-02186-W.
[50] J.S. Boateng, K.H. Matthews, H.N.E. Stevens, G.M. Eccleston, Wound healing dressings and drug delivery systems: a review, J. Pharm. Sci. 97 (2008) 2892–2923, https://doi.org/10.1002/JPS.21210.
[51] J.L. Drury, D.J. Mooney, Hydrogels for tissue engineering: scaffold design variables and applications, Biomaterials 24 (2003) 4337–4351, https://doi.org/10.1016/S0142-9612(03)00340-5.
[52] Y. Hua, K. Wang, Y. Huo, Y. Zhuang, Y. Wang, W. Fang, Y. Sun, G. Zhou, Q. Fu, W. Cui, K. Zhang, Four-dimensional hydrogel dressing adaptable to the urethral microenvironment for scarless urethral reconstruction, 2023 141, Nat. Commun. 14 (2023) 1–16, https://doi.org/10.1038/s41467-023-43421-w.
[53] K. Balakrishnan, S.C. Casimeer, A.Y. Ghidan, F.Y. Ghethan, K. Venkatachalam, A. Singaravelu, Bioformulated Hesperidin-Loaded PLGA Nanoparticles Counteract the Mitochondrial-Mediated Intrinsic Apoptotic Pathway in Cancer Cells, J. Inorg. Organomet. Polym. Mater. 31 (2021) 331–343, https://doi.org/10.1007/S10904-020-01746-9.
[54] F. Sansone, A. Rossi, P. Gaudio, F. Simone, R.P. Aquino, M.R. Lauro, Hesperidin gastroresistant microparticles by spray-drying: Preparation, characterization, and dissolution profiles, AAPS PharmSciTech 10 (2009) 391–401, https://doi.org/10.1208/S12249-009-9219-0.
[55] X. Peng, Y. Zhou, K. Han, L. Qin, L. Dian, G. Li, X. Pan, C. Wu, Characterization of cubosomes as a targeted and sustained transdermal delivery system for capsaicin, Drug Des. Devel. Ther. 9 (2015) 4209, https://doi.org/10.2147/DDDT.S86370.
[56] M. Danaei, M. Dehghankhold, S. Ataei, F. Hasanzadeh Davarani, R. Javanmard, A. Dokhani, S. Khorasani, M.R. Mozafari, Impact of Particle Size and Polydispersity Index on the Clinical Applications of Lipidic Nanocarrier Systems, Pharmaceutics 10 (2018), https://doi.org/10.3390/PHARMACEUTICS10020057.
[57] O. Svensson, K. Thuresson, T. Arnebran, Interactions between drug delivery particles and mucin in solution and at interfaces, Langmuir 24 (2008) 2573–2579, https://doi.org/10.1021/LA702680X.
[58] H.E. Teba, I.A. Khalil, H.M. El Sorogy, Novel cubosome based system for ocular delivery of acetazolamide, Drug Deliv. 28 (2021) 2177, https://doi.org/10.1080/10717544.2021.1989090.
[59] A.K. Kohli, H.O. Alpar, Potential use of nanoparticles for transcutaneous vaccine delivery: Effect of particle size and charge, Int. J. Pharm. 275 (2004) 13–17, https://doi.org/10.1016/j.ijpharm.2003.10.038.
[60] P.C. Molan, The role of honey in the management of wounds, J. Wound Care. 8 (1999) 415–418, https://doi.org/10.12968/JOWC.1999.8.8.25904.

[61] J.A. Hubbell, Hydrogel systems for barriers and local drug delivery in the control of wound healing, J. Control. Release 39 (1996) 305–313, https://doi.org/10.1016/0168-3659(95)00162-X.
[62] H.S. Elsewedy, N.S. Younis, T.M. Shehata, M.E. Mohamed, W.E. Soliman, Enhancement of Anti-Inflammatory Activity of Optimized Niosomal Colchicine Loaded into Jojoba Oil-Based Emulgel Using Response Surface Methodology, Gels 8 (2022), https://doi.org/10.3390/GELS8010016.
[63] F.C. Carvalho, G. Calixto, I.N. Hatakeyama, G.M. Luz, M.P.D. Gremião, M. Chorilli, Rheological, mechanical, and bioadhesive behavior of hydrogels to optimize skin delivery systems, Drug Dev. Ind. Pharm. 39 (2013) 1750–1757, https://doi.org/10.3109/03639045.2012.734510.
[64] B.J. Boyd, Characterisation of drug release from cubosomes using the pressure ultrafiltration method, Int. J. Pharm. 260 (2003) 239–247, https://doi.org/10.1016/S0378-5173(03)00262-X.
[65] J. Choi, V. Reipa, V.M. Hitchins, P.L. Goering, R.A. Malinauskas, Physicochemical Characterization and In Vitro Hemolysis Evaluation of Silver Nanoparticles, Toxicol. Sci. 123 (2011) 133–143, https://doi.org/10.1093/TOXSCI/KFR149.
[66] D.S. Sandeep, Development, Characterization, and In vitro Evaluation of Aceclofenac Emulgel, Asian J. Pharm. 14 (2020), https://doi.org/10.22377/AJP.V14I03.3681.
[67] J.R. Schwartz, R.A. Bacon, R. Shah, H. Mizoguchi, A. Tosti, Therapeutic efficacy of anti-dandruff shampoos: a randomized clinical trial comparing products based on potentiated zinc pyrithione and zinc pyrithione/climbazole, Int. J. Cosmet. Sci. 35 (2013) 381–387, https://doi.org/10.1111/ICS.12055.
[68] L. Thomas, F. Zakir, M.A. Mirza, M.K. Anwer, F.J. Ahmad, Z. Iqbal, Development of Curcumin loaded chitosan polymer based nanoemulsion gel: In vitro, ex vivo evaluation and in vivo wound healing studies, Int. J. Biol. Macromol. 101 (2017) 569–579, https://doi.org/10.1016/J.IJBIOMAC.2017.03.066.
[69] D. (PDF) Kamel, J. Frame, J.D. Frame, T. Harle, Histological findings from controlled application of a thermal plasma to human skin, Clin. Surg. 1 (2016) 1176. ⟨https://www.researchgate.net/publication/311934003_Kamel_D_Frame_J_Frame_JD_Harle_T_Histological_Findings_from_Controlled_Application_of_a_Thermal_Plasma_to_Human_Skin_Clin_Surg_2016_1_1176⟩ (accessed December 9, 2023).